## *Signals of Early-Universe Physics in Cosmology*

CHADBURN, SARAH,ELIZABETH

# Signals of Early-Universe Physics in Cosmology

**Sarah Chadburn**

A Thesis presented for the degree of
Doctor of Philosophy


Department of Mathematical Sciences
University of Durham
England

March 2013

# Signals of Early-Universe Physics in Cosmology

**Sarah Chadburn**

## Abstract

This is a thesis on theoretical cosmology. The first and largest part is a study of cosmic strings, in particular their dynamics and signals in higher dimensional spacetimes. The second part is a study of black holes in a quintessence background.

Cosmic strings are predicted by models of the early universe. They were thought to arise, originally, from Grand Unified Theories, and more recently from brane inflationary models based in string theory.

In Chapter 3 we find exact solutions for cosmic string loop trajectories in higher dimensions, and find the regions of parameter space for which cusps exist. We find that winding the internal dimensions slows the average velocity of string loops, and conjecture that the periodicity of internal space may contribute to self-intersections.

In Chapter 4, we calculate the gravitational wave signal from cosmic string cusps in higher dimensions, and find it is much reduced relative to the 4D case. The main reason for this is the large reduction in the probability of cusps occurring on loops in higher dimensions, as well as a slight reduction in signal from individual cusps.

In Chapter 5, we study cosmic string trajectories in warped spacetimes, such as may be found in realistic brane inflation models. We find that contrary to claims in the literature, the warping of the internal space does not prevent the internal motion of strings. The energy associated with the warping of spacetime means that the energy of a loop appears to change over time from our 4D perspective.

Finally, in Chapter 6, we find an analytic, general-relativistic solution describing a black hole in a quintessence universe. Quintessence is a model of late-time cosmic acceleration in which expansion is sourced by a scalar field. Our solution shows the interaction between this scalar field and a black hole. The scalar field is shown to continue its cosmological "rolling" behaviour everywhere, including on the black hole event horizon, and the black hole is shown slowly to accrete scalar field. This is a perturbative solution valid throughout all of space but only over a finite period of time.

# Declaration

The work in this thesis is based on research carried out at the Centre for Particle Theory, Department of Mathematical Sciences, Durham, England. No part of this thesis has been submitted elsewhere for any other degree or qualification and it is all my own work unless referenced to the contrary in the text.

Chapters 1 and 2 are review. The original work was undertaken in collaboration with my supervisor, Ruth Gregory. The work in Chapters 3 and 4 was for the most part a collaboration with Eimear O'Callaghan, Ghazal Geshnizjani and Ivonne Zavala. The work in Chapter 5 was the result of a collaboration with Tasos Avgoustidis. Some of the work in Chapter 3 is an extension of work submitted in my undergraduate degree, and where this is the case it is clearly stated.

# Acknowledgements

Of course my biggest thank you goes to Ruth, for inspiring, guiding and enabling this PhD to happen. You have allowed me to work on really interesting problems and to have a great experience of academic life. I have enjoyed the times when I have been able to "flap about in the bushes", and equally when we have worked together on a problem and made sudden leaps of progress. I really appreciate the time and care you have taken to make my PhD a good one.

Secondly I must thank my family, who gave me my first experiences of mathematics and science and have always supported me unconditionally. Mum, thank you for teaching me my times tables and that I should be myself. Dad, thank you for inspiring me to do a PhD (although I slightly upscaled the objects of study). Jenny, thank you for playing pretend school so much, and for work club, and for always having perspective when I panic about something.

Thank you to Mr. Elvidge for teaching me calculus and making me realise that maths is interesting. Thank you to my schoolfriends for showing me that maths is cool. Thank you to the books that inspired my career choice: Collins pocket guide to the Sea Shore, and The Elegant Universe.

I appreciate all the people I have talked to about physics while studying for this PhD, and especially Anne Davis and Jonathan Pearson, whose discussions have helped with the work in this thesis. I would like to thank Tasos in particular for the visit to Cambridge and the interesting conversations while working on our paper.

Thank you to James, my compatriot in PhD writing and in life, and on-hand LaTeX support. Thank you to my tea buddies, Jo and Nick (and James again). Thank you to all my friends who have made my time in Durham a happy one.

Lastly thank you to my much-valued proof readers, Ruth, Mum, Dad and James.

# Contents

# Chapter 1

# Introduction

Cosmology has come a long way since people first studied the night sky, and particularly so in the last hundred years. However, there is still much that is not understood. In this thesis we examine some of the areas in which we lack understanding. The main part of the thesis is about cosmic strings, a prediction of many popular models, which may have various different observational effects but which have not yet been detected. We study the impact of higher dimensions on the dynamics and signals of cosmic strings, including the effect of a warped internal space. In the second part we search for fully general-relativistic black hole solutions in a cosmological background, which have not been found analytically before. The particular background we look at is a universe filled with a rolling scalar field that causes an accelerated expansion.

First we will give a brief introduction to the standard cosmology, the problems it faces, and a few of the proposed alternatives to solve some of these problems. We will describe in some detail the string theory model of the universe. Then we will outline how the work in this thesis fits into the overall picture.

## 1.1 The standard cosmology

In the standard cosmological model, it is thought that the universe began from a single point (the nature of which is problematic and much debated, see for example [52, 97]), and underwent a rapid expansion. This is known as the big bang. It is the

generally accepted theory, based on the observation that the universe is expanding [156], extrapolated back in time. The theory was first proposed by Lemaitre in 1927 [114].

It is the energy of the matter in the universe that causes it to expand. Since the universe started off very small, in its initial stages the density of matter would have been extremely high, and so would the temperature and pressure. If we raise matter to very high energies in the lab, we see that firstly the electrons are removed from atoms, secondly nuclei break into their constituent protons and neutrons, and thirdly these particles break down further into quarks and gluons, forming a state known as a quark-gluon plasma. It is surmised, therefore, that this process would have happened in reverse in the universe's history as it expanded and cooled.

Thus in the early universe there are several distinct stages. The earliest stage for which we have some understanding is electroweak symmetry breaking. The electromagnetic and weak forces unite at high energies, and would have separated once the universe fell below a critical temperature when the Higgs field acquired a vacuum expectation value. After this had taken place, the plasma universe cooled sufficiently that quarks and gluons joined to form hadrons, such as protons and neutrons. Following this, most of the hadrons and anti-hadrons annihilated, and neutrinos decoupled, leaving a background dominated by leptons and anti-leptons (electrons, muons, etc.). When the temperature became low enough that new lepton–anti-lepton pairs were no longer produced, most of these annihilated too. Then the energy-density of the universe was dominated by photons. It was during this time that nucleosynthesis took place − the formation of light nuclei from their constituent protons and neutrons by nuclear fusion. The abundance of different nuclei predicted by theory match well with observations, a major success of the big bang model. Later the energy-density of the universe became dominated by matter rather than radiation. During this phase, recombination took place, in which electrons came to orbit nuclei and atoms were thus formed. At this point, about 380000 years after the big bang, the universe became transparent to light. Then the Cosmic Microwave Background (CMB) was formed, made up of the last photons that scattered before the universe became transparent. The CMB has been observed and recorded in detail (for ex-

ample WMAP [6]). It is of great interest as it offers insight into the early universe. The CMB was another successful prediction of the big bang theory.

Prior to these fairly well-understood stages of big bang cosmology, it is widely believed that the three "gauge forces": electromagnetism, the weak force and the strong force, were united into one [73]. This is known as a grand unified theory (GUT). At some point before the electroweak transition, the strong force would have decoupled from the electroweak, and later the electromagnetic and weak forces decoupled. These phase transitions happened via a process known as *symmetry breaking*, which will be discussed in detail in Section 2.1. Also prior to the electroweak phase transition, a process known as baryogenesis is thought to have occurred. Baryogenesis refers to some mechanism by which an asymmetry between baryons and anti-baryons is formed, since we see that our universe is full of matter and there must therefore have been somewhat more particles than antiparticles in the early universe. An exact mechanism for this process is not known.

Earlier still, it is thought that perhaps the strong and electroweak forces united with gravity into a single force, but we know so little about physics at these energies that it is very difficult to be definitive. In particular we do not know how to consistently combine a theory of gravity with quantum field theory, which is one of the biggest problems of modern physics and will be discussed in Section 1.2.

General relativity is the best model we have for the large-scale structure of the universe. In the standard cosmology the universe is modelled as homogeneous and isotropic. The most general metric that respects these symmetries is known as the Friedmann-Lemaitre-Robertson-Walker metric [71,139], for which the shorthand FRW is often used,

$$ds^2 = dt^2 - a(t)^2 \left( \frac{dr^2}{1-kr^2} + r^2 d\Omega_{II}^2 \right). \tag{1.1.1}$$

Here, $t$ is a timelike coordinate, $r$ is a radial coordinate and $d\Omega_{II}^2 = d\theta^2 + \sin^2\theta d\phi^2$ is the metric on a 2-sphere. Henceforth, dot represents differentiation with respect to $t$. Putting this metric into the Einstein equations (1.2.6) with a given matter content determines the unknown function $a(t)$. Assuming a perfect fluid with pressure $p$ and

energy density $\rho$ gives the Friedmann equations, which can be written as

$$H^2 = \frac{8\pi G\rho}{3} - \frac{k}{a^2} \tag{1.1.2}$$

$$\dot{\rho} = -3H(\rho + p), \tag{1.1.3}$$

where $H = \dot{a}/a$ is the Hubble parameter, and $k$ is the curvature of the universe. By rescaling $r$, $k$ may be set either to $\pm 1$, or zero. In order to close this system, a relation between $p$ and $\rho$ is required, which is often taken to be a simple proportionality relation given by the equation of state parameter, $\omega$, where

$$p = \omega\rho. \tag{1.1.4}$$

When the universe is filled with radiation, $\omega = 1/3$, which means that the scale factor, $a$, is proportional to $t^{1/2}$ and the energy density is proportional to $1/a^4$. For matter, on the other hand, $\omega = 0$, since it is treated as a non-interacting "dust" and therefore has no pressure. This means the scale factor is proportional to $t^{2/3}$, and the energy density simply decreases with the expansion of space as $1/a^3$. For a cosmological constant, $\Lambda$, we have $\omega = -1$. This means the scale factor is exponential, $a \propto e^{Ht}$, where $H = \sqrt{\Lambda/3}$ is a constant, and the energy density is constant (hence cosmological constant). This means that different components will dominate the universe at different times. Looking at the behaviour of the energy densities, that of radiation will be largest at the beginning, but will fall off the most quickly. This will be followed by an era of matter domination, and later, if there is a cosmological constant, once the matter and radiation densities have sufficiently reduced this small-but-constant density comes to dominate. We may in fact be in the cosmological constant era at the moment, as we will discuss below.

General relativity may describe the basic behaviour of the universe, but it generally breaks down on large scales. Even on the scale of a galaxy, behaviour does not match the expected gravitational effects from the observed matter, for example the orbits of outer stars are much faster than expected [141]. Such discrepancies occur in many places, but they can all be explained by the presence of some non-luminous matter labelled *dark matter*. As yet the nature of dark matter is unknown.

On very large scales, gravity appears not to work at all: we observe that the expansion of the universe is accelerating, galaxies are accelerating away from each

other as though there were some repulsive force on large scales. An accelerated expansion can in fact be explained very well within the framework of general relativity, by the addition of a cosmological constant. This model currently matches well with observations (see for example [108]). Theoretically, however, there is a problem. The measured cosmological constant takes a very unnatural value. From observations, $\Lambda \sim 10^{-120}$, whereas the predicted vaccuum energy from quantum field theory is between 60 and 120 orders of magnitude larger than this [37]. Various different theoretical origins of the acceleration of the universe, termed *dark energy*, have therefore been proposed and studied (see Section 1.3).

Two of the other cosmological problems, perhaps the most famous, are the "horizon" and "flatness" problems. The horizon problem stems from the fact that the universe (particularly the CMB) looks the same in all directions, but the photons come from different regions of space that have never been in causal contact. There is therefore no way for this homogeneity to be established. The flatness problem is essentially that we observe the curvature of space to be very close to zero ($k = 0$), and that since this is an unstable equilibrium point in cosmological evolution, it must have started off *extremely* close to being flat when the universe was formed. There is no known theoretical reason for this to happen. A proposed explanation is *inflation*, a paradigm in which the universe underwent a period of very rapid exponential growth in its early history. This solves the horizon problem by widely separating the regions that were previously in causal contact, and solves the flatness problem by "stretching out" any curvature that was initially present so that space looks locally flat. Inflation was proposed by Guth in 1981 [80], but does not yet have a solid theoretical foundation. It successfully predicts the form of the density perturbations in the early universe[1], which are observed in the CMB, making it an appealing model (see for example [129]). There has been much work towards establishing a possible mechanism for inflation. One possibility is discussed in the next section.

[1]Cosmic strings were initially suggested to play this role, but data favours inflation.

## 1.2 String cosmology

One of the great outstanding problems in physics is the apparent incompatibility of quantum field theory, our best description of small-scale phenomena, and gravity, our best description of the behaviour of the universe on large scales. String theory is currently the only candidate for a consistent quantum theory of gravity. It takes a lot of work to derive anything resembling the real world from string theory, or even to do any calculations within the theory, but being a theory of quantum gravity it is of great interest.

General relativity was proposed by Einstein [64], and is encapsulated by the action,

$$S = -\frac{1}{2\kappa}\int d^D x\sqrt{-g}(R - 2\kappa\mathcal{L}_M). \tag{1.2.5}$$

$\kappa = 8\pi G$, where $G$ is Newton's constant, and $\mathcal{L}_M$ is the matter Lagrangian. For our universe, space and time are modelled as a curved 4-dimensional manifold, described by a 4-dimensional metric, $g_{\mu\nu}$, and known collectively as spacetime. However, in general there may be an arbitrary number of dimensions, D. In the action, $R$ is the Ricci scalar and $g$ is the determinant of the metric. This gives the Einstein equations,

$$R_{\mu\nu} - \frac{1}{2}Rg_{\mu\nu} = 8\pi G T_{\mu\nu}. \tag{1.2.6}$$

Here, $T_{\mu\nu}$, the energy momentum tensor, describes the matter content of spacetime and is derived from the matter Lagrangian, $\mathcal{L}_M$, according to,

$$T_{\mu\nu} = \frac{2}{\sqrt{-g}}\frac{\delta(\sqrt{-g}\mathcal{L}_M)}{\delta g^{\mu\nu}}. \tag{1.2.7}$$

Note, throughout this work we use the metric signature $(+,-,-,..,-)$.

It we try to quantise gravity in the same way as the other interactions, it is found to be non-renormalisable. So while gravity works at large scales, and quantum mechanics works at small scales, when strong gravitational effects occur on a small scale, for example at the beginning of the universe, or in a black hole, we have no physical description. This is strong motivation to find a theory of quantum gravity.

A quantum theory of gravity will contain massless spin-2 particles known as gravitons, the quanta of the gravitational field. The principle of string theory is

that the fundamental constituents of the universe are 1-dimensional strings. On quantising these strings, generically a group of massless fields emerge, namely an anti-symmetric 2-form field, $B_{\mu\nu}$; a scalar field, $\Phi$, known as the dilaton; and most importantly a symmetric, traceless field, $g_{\mu\nu}$, which corresponds to a massless spin-2 particle. $g_{\mu\nu}$ may be identified with the metric of spacetime, and this makes string theory a theory of gravity.

*Superstring* theories include both bosons and fermions, which are related to each other via supersymmetry. These theories can only be consistently quantised in a spacetime with 10 dimensions (9 space and 1 time). This poses a problem if we want them to describe the real world. The solution to this is to have the extra spatial dimensions *compactified* at a scale that is as yet too small for us to detect. Potential effects of these extra dimensions will be considered in this thesis.

There are five different types of superstring theory, due to different choices that may be made when including fermions, namely Type I, Type IIA, Type IIB, Heterotic $SO(32)$ and Heterotic $E_8 \times E_8$. On top of the generic fields $B_{\mu\nu}$, $g_{\mu\nu}$ and $\Phi$, and massless fermions, there are extra massless bosonic fields that depend on which theory we consider. We will not go into string theory in much detail in this work, but it is worth noting that for the Type II theories, the extra massless bosonic fields are called Ramond-Ramond (R-R) fields (a 1-form and a 3-form for type IIA, and a scalar, 2-form and 4-form for IIB), and that $B_{\mu\nu}$ is known as the Neveu-Schwarz 2-form.

In 1989, *D-branes* in their present form were discovered [53] (earlier investigations of similar objects in bosonic string theory ran into problems, see for example [154]). Then, in the early 1990's, it began to emerge that the 5 different string theories are related by dualities, and may all be different cases of one overarching theory known as M-theory. It also became clear that various different D-branes would naturally arise in superstring theory and that these would be dynamical objects. This was the "second superstring revolution", and gave string theory a much richer phenomenology than previously thought.

A D-brane is an object on which open strings can end. One can have either open or closed strings in string theory. Open strings must have one of two types of

boundary condition on their endpoints: Neumann or Dirichlet. Dirichlet boundary conditions fix the position of the endpoints, and Neumann boundary conditions fix the derivative at the endpoint, but in this case it is free to move. A string may have different boundary conditions in different spatial directions, which means that its endpoints cannot move in any of the Dirichlet directions, but they are free to move on a hypersurface along the directions with Neumann boundary conditions. This hypersurface is a D-brane, or D$p$-brane, where $p$ is the number of spatial dimensions of the brane.

There has been much work towards constructing a model of the universe from string theory. This is of particular interest in the very early universe, where quantum-gravitational effects are important. A natural picture is that the standard model particles will be open strings living on a D3-brane, which is in some sense our 4D universe. This is a kind of braneworld model. Braneworlds were initially proposed earlier, outside of the context of string theory, because they solve the hierachy problem − the large hierachy of scales between gravity and the other forces is explained because gravity propagates throughout the whole of the spacetime (known as the bulk) whereas the standard model is confined to the brane, thus the effects of gravity are much weakened because it is "lost" into the extra dimensions. For an early proposal of such a model, see [140], and for a review see [33].

There are a number of massless scalar fields in string theory, known as moduli. These include the dilaton, as well as massless modes related to the volume and structure of the internal manifold. Since these fields are not observed, they must somehow acquire a mass, in a process known as moduli stabilisation. This can be acheived in set-ups called flux compactifications, in which the internal manifold contains some configuration of D-branes, which are a source of R-R fluxes. These fluxes give masses to the moduli, and induce a warped geometry, which allows the hierachy problem to be solved [74]. For a review of flux compactifications see [78]. A warped geometry is one in which the normalisation of the 4-dimensional part of the metric depends on the internal dimensions, so the metric will be of the form:

$$ds_{10}^2 = h^{-1/2} g_{\mu\nu} dx^\mu dx^\nu - h^{1/2} \tilde{g}_{mn} dy^m dy^n, \tag{1.2.8}$$

where $g_{\mu\nu}$ is the 4D metric, $\tilde{g}_{mn}$ is the compact internal metric, and $h(y^m)$ is known

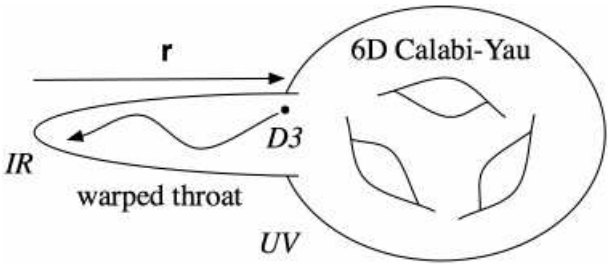


Figure 1.1: A schematic illustration of a warped compactification (from [63]). In a string theory universe the bulk geometry must take the form of a Calabi-Yau manifold, a particular type of manifold.

as the warp factor. It is expected in flux compactifications that there will be regions in the internal space known as warped throats, where the warp factor becomes very large as one moves towards the 'tip' of the throat, which is a region of low energy and towards which there is an attractive force. See Figure 1.1 for an illustration.

*Brane inflation* is a model of inflation that arises naturally in a warped compactification. It was first proposed in 1999 by Dvali and Tye [62], and the basic idea is that inflation is driven by a scalar field (the inflaton) corresponding to the position of a D-brane in the bulk. In a warped compactification where there are warped throats in the bulk, the warping allows a large number of e-foldings of inflation, as required to solve the horizon and flatness problems. A common set-up has a D3-brane and an anti-D3-brane, one of which sits at the tip of a warped throat and the other moves towards it due to the attractive force between the two branes. The inflaton field is the distance between the branes. Now the warp factor acts both to reduce the attractive force and to limit the speed of the brane moving down the throat, which allows inflation to go on for a suitably long time, before it ends with the annihilation of the two branes. A brane moving down a warped throat is illustrated on Figure 1.1.

A by-product of brane-inflation is the formation of cosmic superstrings, which will be a major topic in this thesis. More details are given in Chapter 2.

## 1.3 The recent universe

The universe as we see it now is populated by galaxies. Within these galaxies we find various interesting phenomena, and not the least of these are black holes. Black holes are localised objects in which a large mass is located within a very small volume, and has such a strong gravitational effect that the interior of a black hole is causally disconnected from the exterior. The first black hole solution in general relativity was found in 1916 by Schwarzschild [152], very soon after general relativity was proposed. However, it was a long time before it was fully established what the solution represented physically, and it wasn't until the late 1960's that the possibility of black holes existing in nature was taken seriously.

The gravitational attraction of a black hole is such that it is enclosed by a surface known as the event horizon, from which no matter or radiation can escape. Since massless particles, which travel at the speed of light, will be the last fields that are able to escape, the event horizon is a null surface. The simple black hole solution found by Schwarzschild is

$$ds^2 = \left(1 - \frac{r_s}{r}\right) dt^2 - \frac{dr^2}{1 - r_s/r} - r^2 d\Omega_{II}^2. \tag{1.3.9}$$

The event horizon is at $r = r_s = 2GM$, where $G$ is Newton's constant and $M$ is the mass of the black hole. There is a coordinate singularity here, which is clear from the fact that the denominator of the $dr^2$ term goes to zero. This is not a true singularity and can be removed by a suitable change of coordinates. However, the singularity at $r = 0$, at the centre of the black hole, is a physical singularity and the curvature of spacetime becomes singular here. At this point quantum gravity should have something to say.

Various different black hole solutions have since been found, including charged black holes (Reisner-Nordstrom), rotating black holes (Kerr), black holes in a space-time with non-zero cosmological constant, and, in higher dimensions, a wide variety of solutions including different topologies such as black rings [65]. However, none of the exact solutions very accurately model astrophysical black holes. One problem is that they are generally vacuum solutions. In this thesis we attempt to address this issue by looking for a black hole solution in a universe with matter.

Numerical simulations of black holes can be more realistic, modelling processes such as the gravitational collapse of matter to form a black hole, and the accretion of matter onto a black hole. For example in [16], the authors model the gravitational collapse of a neutron star to form a black hole, a realistic astrophysical scenario.

Individual galaxies are held together by gravity, but on intergalactic scales the universe is currently undergoing a phase of accelerated expansion [131, 137]. As mentioned in Section 1.1, the value of the cosmological constant is unnatural and there are many proposals for alternative physical explanations, which are grouped under the heading of dark energy (see [47] for a review). Gravity must somehow be modified on large scales so that it is no longer attractive, or at least counteracted by some other force, and therefore most dark energy models modify the gravitational action in some way. The simplest way to acheive this is to add in a scalar field minimally coupled to gravity. This is known as *Quintessence* and will be discussed in Chapter 6. One can also include interactions of a scalar field with gravity, with itself, or with matter. Such theories are collectively known as scalar-tensor theories. Another widely-used technique is to modify the form of the gravitational action itself so that it depends on the Ricci scalar, $R$, in a different way: these are known as $F(R)$ theories. There are too many possible modifications of gravity to list here, but a comprehensive review is found in [43].

Black hole solutions are subject to some famous conjectures known as the "no hair theorems" [142], which assert that all stationary, asymptotically flat black holes take the Kerr-Newman form, which is the exact solution for a charged and rotating black hole, and thus are classified by only 3 parameters: mass, charge and angular momentum (see for example [19, 20, 38]). This means one cannot have a non-trivial scalar field profile around a stationary black hole. The physical consequence of this is that any scalar matter in the vicinity of a black hole will be absorbed or radiated away in a finite amount of time, and indeed this is seen in numerical simulations, such as [81]. If, for example, a scalar field dark energy model such as Quintessence turns out to be a good description of the universe, it must somehow coexist with black holes. Therefore, in Chapter 6, we look for a black hole solution in a Quintessence background. The no hair theorems are circumvented in this case, as will be discussed

further in Section 6.1.1. There are other ways in which to circumvent the no hair theorems, including in the presence of a negative cosmological constant [107] and in higher dimensions [65].

In the universe today, as well as galaxies and black holes, there may also be relic topological defects. As mentioned in Section 1.1, these would have been formed in symmetry-breaking phase transitions in the early universe, and could therefore tell us about the universe at a much earlier time. The most likely objects to exist are cosmic strings, which can have distinctive observational signals. In Chapters 2-5 of this thesis we look at cosmic strings inspired by the string theory model of the universe, and consider the signals of high-energy physics that they could give us, in particular from extra dimensions and the warping of spacetime.

# Chapter 2

# The history of cosmic strings

In this chapter, we review past research into cosmic strings. Starting from their earliest days, we discuss in Section 2.1 how the idea of cosmic strings as topological defects from field theory was constructed. In Section 2.2, we review their study as the possible seeds of galaxy formation, and the eventual failure of this model. Section 2.3 gives more details of a field theory cosmic string, and shows how the effective zero-width action is derived from a finite-width topological defect solution. Then in Section 2.4 we review work on the behaviour of cosmological networks of strings.

In Section 2.5, we introduce the cosmic superstring. We go on to discuss the ways in which cosmic superstrings may differ from the original, field theory cosmic strings. In Section 2.6, we discuss networks of $(p, q)$-strings with a spectrum of different tensions, and in Section 2.7, we consider the fact that cosmic superstrings may not reconnect when they intersect, and the effect this can have on their dynamics. Finally, in Section 2.8, we outline the various different fields that cosmic strings and superstrings may emit.

## 2.1 The birth of symmetry breaking and defects

The original cosmic strings were conceived in the 1970's, as topological defects formed in the early universe. In this subsection we describe what topological defects are, how they would be formed, and thus how the idea of cosmic strings first came

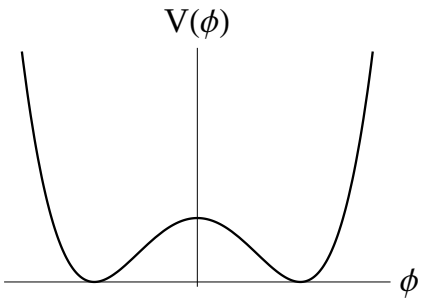


Figure 2.1: Potential for the $\phi^4$-kink.

about.

Topological defects are stable objects that arise in field theory, via a process known as symmetry breaking. This idea can be neatly illustrated by a simple model, known as the $\phi^4$-kink. For this we take the following lagrangian:

$$L = \frac{1}{2}\partial_\mu\phi\partial^\mu\phi - V(\phi), \tag{2.1.1}$$

where $\phi$ is a real scalar field, with the potential

$$V(\phi) = \frac{\lambda}{4}\left(\phi^2 - \eta^2\right)^2. \tag{2.1.2}$$

This potential is illustrated in Figure 2.1. $\lambda$ and $\eta$ are positive constants. The potential clearly has two minima, at $\phi = \pm\eta$. If a solution sits in one minimum in one region of space and the other minimum in another region, in order for the field to remain continuous there must be a region in which it crosses from one to the other, and does not lie at a minimum. The following solution to this system, shown on Figure 2.2, demonstrates this behaviour:

$$\phi = \eta \tanh\left(\sqrt{\frac{\lambda}{2}}\eta x\right). \tag{2.1.3}$$

While the energy of the field is zero when it sits in a minimum (known at the vacuum state), it is clearly non-zero in the central region as it passes over a "lump" in the potential (see Figure 2.1). The energy of the field is shown in Figure 2.3. The region of non-zero energy is localised and can therefore be thought of as an object, known as a topological defect.

Having all the field in the same potential minimum, i.e. a pure vacuum, would be a lower-energy state, but in order to reach such a state one would have to transfer

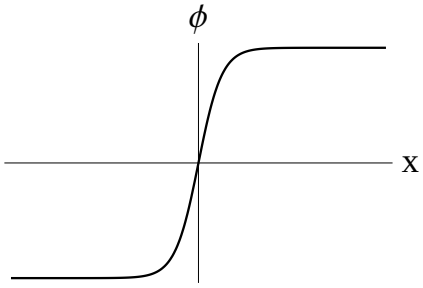


Figure 2.2: The $\phi^4$-kink.

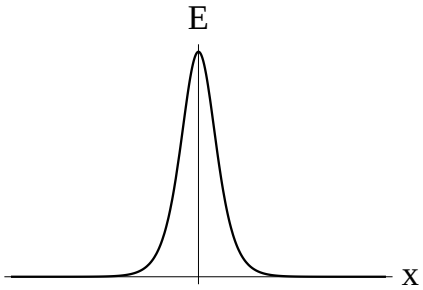


Figure 2.3: Energy density of the $\phi^4$-kink.

the whole of the field on one side of the defect into the other minimum, requiring an infinite amount of energy. Thus if a defect exists it cannot be removed, and they are stable objects. The obvious question, then, is how such a field configuration would arise in the first place.

The idea in cosmology is that defects would be formed by *symmetry breaking*. As an example, the theory described by equations (2.1.1) and (2.1.2), above, is $\mathbb{Z}_2$-symmetric. This symmetry would be manifest if the field took the value 0 everywhere, meaning it sat at the top of the "lump" in its potential (Figure 2.1). Were it to lose energy, it would drop down into one of the minima, which would break the symmetry. The key idea is that which minimum it lands in is random. If the field sat at zero across the whole of space, as it began to lose energy it would fall into different minima in different, causally disconnected, regions of space. Eventually regions of different vacua would meet, leaving finite-energy defects at their boundaries, like the one described above (Figure 2.2).

This idea is relevant for cosmology because the universe started off at a very high energy, and the fields in it would have undergone symmetry breaking as they lost energy in an expanding, cooling universe. The breaking of symmetries in the early

universe was first proposed in 1972 by Kirzhnits [103,104]. In 1974, the possibility of cosmological defects was first considered [181]. Before that, however, the process of symmetry breaking leading to defect formation had long been observed in condensed matter systems, where, for example, cooling a liquid to form a crystal results in defect lines between different grains of the crystal.

Defects are interesting because it is possible to have objects with different numbers of dimensions. A defect is normally classified by its *codimension*, the difference between the dimension of the defect and the dimensions of the space it is in. The $\phi^4$-kink, discussed above, is a codimension 1 defect. In the solution on Figure 2.2, we looked at it in a 1D space, where it was a 0D or pointlike object. We could imagine adding on another spatial dimension and extending this solution to form a 1D line-like object. Extending it again to 3D space, the $\phi^4$-kink becomes a 2D surface. The consistent quantity here is the codimension, which is always 1.

The key idea, proposed by Kibble in 1976 [98], is that the type of defects that are formed depend on the topology of the vacuum manifold. A codimension 1 defect, known as a *domain wall*, requires a disconnected vacuum manifold, such as in the $\phi^4$ theory above, where the vacuum manifold consists of 2 distinct points (the potential minima).

Defects of codimension 2 in our universe would be 1-dimensional objects, or strings. These were the original cosmic strings. A codimension 2 defect requires the vacuum manifold to contain non-trivial loops. A common example of such a theory has a potential known as the "mexican hat potential", shown on Figure 2.4, whose minimum, or vacuum, is a circle around a central maximum. In fact, this theory has the same potential as the $\phi^4$-kink, equation (2.1.2), but with $\phi$ now a complex scalar field. One also introduces a gauge field in order to have local symmetry[1].

That string-like defects can arise in such a theory was first shown by Nielsen and Olesen in 1973 [123], and this model of cosmic strings, known as the "Abelian-Higgs" model, is still used in simulations today [88,121,173]. The theory has a local rotational, or U(1), symmetry, and a field with high energy will sit in the centre of

[1]This removes massless goldstone bosons from the theory. See [85,86] for more details.

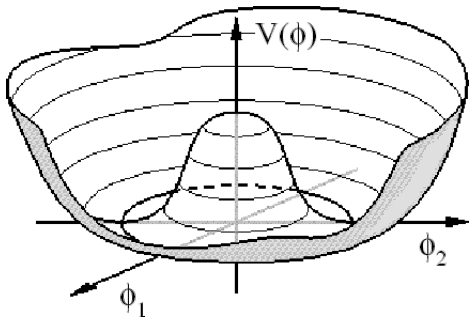


Figure 2.4: The "mexican hat" potential, which allows vortex solutions (from [169]).

the potential (see Figure 2.4) where this symmetry is manifest. At low energies, it drops down to a point on the circle of minima, breaking the symmetry. In different regions of space, the field may fall onto different points in the circle of minima, but in order to remain continuous it must change continuously between these values as one moves through space. Consider taking a circular path in space. For continuity, the field must make a whole number of loops of the vacuum manifold by the time the circle in space is completed. If it loops one or more times around the vacuum, known as *non-trivial winding*, a defect will be formed somewhere inside the circular path, since in order to remain continuous in the centre, the field must rise to the top of the potential (Figure 2.4), where its energy is finite. This argument implies that a defect will be found on any surface bounded by the circular path in space, so by considering a continuous deformation of such a surface it is clear that the defect formed will be an extended object, or string. These solutions are known in field theory as *vortices*.

Cosmic strings are by far the most interesting topological defects in cosmology, since they are the most likely both to exist and have observational effects. Two other possibilities are domain walls (2D objects) and *monopoles*, which are pointlike defects. Domain walls have a very strong gravitational effect, which essentially rules out the possibility of their existence [98, 181]. It was shown in [135, 180] that monopoles, if formed, would have too high a density to fit within observational bounds. The inflationary scenario [80] gets around this problem with the idea that monopoles would be formed before inflation, and be so highly diluted during inflation

that they would never be seen. This leaves only cosmic strings, populating the universe with a curious network of line-like objects, potentially affecting cosmology in many different ways. It was Kibble's paper in 1976 [98], discussing the different possible types of topological defects in cosmology and considering the behaviour of a network of strings, that initiated the study of cosmic strings and all of the research that was to follow.

## 2.2 The rise and fall of cosmic strings

The idea of symmetry breaking in the early universe is an important one because it led to the idea that the fundamental forces could be unified at high energies. Such a model is known as a Grand Unified Theory (GUT), and proposes that in the very early universe there was a larger symmetry group that broke down as the fields lost energy, leaving only that of the standard model today. It was the breaking of these symmetries that was assumed to lead to the formation of cosmic strings [101], thus the "original" cosmic strings are often referred to as GUT strings. This section outlines some of the major research into GUT cosmic strings.

One can calculate roughly the energy at which the symmetry breaking would have occurred, giving an estimate of the tension of GUT strings (see eg. [171]),

$$G\mu \sim 10^{-6} \tag{2.2.4}$$

Given the tension, one can predict the cosmological effects of cosmic strings and their possible observational signals. The idea was initially seized upon with enthusiasm, in a major part because cosmic strings could have seeded the density perturbations that eventually lead to galaxy formation, and their estimated tension was calculated to be of the right order of magnitude for this role [179]. They offered a neat explanation of one of the major unsolved problems in cosmology. This unfortunately turned out to be incorrect, but this was not known until much later.

It was proposed that cosmic strings would initially form as a network of "infinite" strings, stretching across the universe. One of their most important properties is their ability to form closed loops, first suggested in Kibble's original paper [98]. Loops could break off from the network when a pair of strings crossed. Field theory

simulations of vortices confirm that two crossing strings tend to "exchange partners", making loop formation likely [122, 153].

When cosmic strings were first considered as the seeds of galaxy formation, it was assumed that closed loops quickly collapsed and thus made a negligible contribution to the density perturbations [179]. Under this assumption, strings with GUT tensions do not provide sufficient density fluctuations. However, Vilenkin [171] suggested that loops could in fact have long lifetimes and thus make a much larger contribution. Taking this into account made the cosmic string model of galaxy formation fit very well with observations. It was even suggested that each galaxy would form around an oscillating loop of string, with different loop patterns leading to the differently shaped galaxies [164].

It remained to determine the likelihood of formation of long-lived loops. The main issue was that of *self-intersection*. If a loop folds back on itself and crosses over, it will break down into two smaller loops. If this happens many times, for example if the string is very wiggly, the loop will soon disintegrate. Over a period of a few years, dynamical loop solutions were found in which a significant proportion of the loops would never self-intersect. An initial family of solutions was found by Kibble and Turok [102], and extended to larger solution families by [164], [41] and [58] in turn. Copeland and Turok in 1986 [48] checked that the solution family in [164] was indeed stable to small perturbations.

All of these solutions describe loops that oscillate with only low harmonics. Higher harmonics, i.e. significant small-scale structure or wiggles, could lead to a much faster breakdown of loops and prevent stability. However, there are several possible sources of damping that, it was concluded, damp small-scale structure sufficiently that stable loops can be expected to form. The damping mechanisms are, firstly, friction from particles in the very early universe [99], secondly cosmological expansion, which stretches strings [170], and thirdly the emission of gravitational radiation [136]. Thus far, cosmic strings appeared to be a very good candidate for explaining galaxy formation.

There are many possible routes to observing cosmic strings, directly or indirectly. Calculating the observational signatures allowed constraints to be made on

the number and tension of cosmic strings that could exist, which ultimately ruled them out as the seeds of galaxy formation.

One way to detect a cosmic string is to observe the lensing effect as it passes in front of a star or galaxy, creating a double image. This effect was calculated in [77, 172] and there have been several possible detections, but all of these have turned out on closer observation not to be lensing events. See for example [147, 148] where two interacting galaxies were observed that produced an effect very similar to a double image.

Another possible detection method is to observe the signatures left by strings in the cosmic microwave background (CMB). Cosmic strings would leave distinctive step-like discontinuities in the temperature profile across the sky [31, 95]. This turned out to be a major part of their rejection as a theory, since no such pattern was observed in the CMB anisotropies, putting bounds on the cosmic string tension that were too low to make them viable candidates for galaxy formation. This was observed in the data from the COBE satellite [2] in 1997 [7], and again [178] in the higher resolution data from WMAP [6]. These more recent bounds indicate that $G\mu < 5 \times 10^{-7}$ and that cosmic strings could account for up to 7% of the observed CMB anisotropy. While this put paid to the cosmic string model of galaxy formation, there is always the possibility that strings with lower tension may yet be observed.

The third major signal from cosmic strings is their emission of gravitational waves [22, 89], which will be a theme in the work presented in this thesis. While gravitational waves have not yet been directly detected, it is possible to detect them indirectly by measuring the frequency of radio pulses from binary pulsars. The presence of a low-frequency gravitational wave background slightly modifies the frequency of arrival of pulses on earth, an effect that can be measured very accurately. In [163] the measured level of gravitational waves was compared with predictions for GUT cosmic strings [22, 89], giving the first indication that the galaxy formation model did not fit with observations. It may soon be possible to detect gravitational waves directly, with experiments such as the Laser Interferometer Gravitational Wave Observatory, or LIGO [4]. In 2001, Damour and Vilenkin recalculated the

expected gravitational wave background from cosmic strings, concluding that distinctive signatures could be observed by gravitational wave detectors [55]. Their recalculation also relaxed the bound on string tension from pulsar timing data.

The prospect for cosmic string detection is therefore not altogether bleak, but having lost their appealing ability to solve the problem of galaxy formation, the study of GUT cosmic strings fell out of favour in the mid 1990's. It is the advent of superstring theory, and the reinvention of the cosmic string as the cosmic *super*string, that has lead to a renaissance in recent years. Cosmic superstrings will be discussed in detail in Sections 2.5-2.8.

## 2.3 Effective action for a cosmic string

As discussed in Section 2.1, one of the most widely-used field theory models of cosmic strings is the Abelian-Higgs model [85], which includes string-like topological defect solutions. These solutions, known as Nielsen-Olesen vortices [123], are a good model for cosmic strings because they are codimension 2 objects, so in our 3D universe they appear as strings. It is also a simple model, so it is easy to work with, and the strings have no long-range interactions, as expected in nature.

The Abelian-Higgs model contains both a scalar and a gauge field, and a vortex solution appears as a finite-width "lump" of energy in both fields (see Figure 2.5, below). By identifying the centre, or *core* of the vortex profile as the location of the string, this solution can be thought of as a 1-dimensional object. On cosmological scales, the width of such a string is almost negligible, and when modelling the large scale dynamics we are not interested in the detailed structure of the vortex. We therefore approximate cosmic strings as purely 1-dimensional objects, and model them using an effective zero-width action known as the Nambu action [76].

In this section we first briefly describe the full field theory solution for a vortex string, and then show how the effective zero-width action can be derived from it. This action gives the simple equations of motion that we work with in the cosmological context.

The Abelian-Higgs model [85] includes a complex scalar field, $\phi$, and a gauge

field, $A_\mu$. The action is

$$S = \int d^4y \left( (\partial_\mu + ieA_\mu)\bar{\phi}(\partial^\mu - ieA^\mu)\phi - \frac{1}{4}F_{\mu\nu}F^{\mu\nu} - V(\phi) \right) \tag{2.3.5}$$

where

$$V(\phi) = \frac{1}{4}\lambda \left( |\phi|^2 - \eta^2 \right)^2, \tag{2.3.6}$$

which is the mexican hat potential (Figure 2.4). The first term in the action is a covariant derivative of $\phi$ and the second is a kinetic term for the gauge field,

$$F_{\mu\nu} = \partial_\mu A_\nu - \partial_\nu A_\mu. \tag{2.3.7}$$

The fields $\phi$ and $A_\mu$ transform under a gauge transformation (leaving the action invariant) as follows:

$$\phi(y) \to e^{i\alpha(y)}\phi(y) \; ; \quad A_\mu(y) \to A_\mu(y) + \frac{1}{e}\partial_\mu \alpha(y) \tag{2.3.8}$$

i.e. the symmetry of $\phi$ is a local U(1) symmetry.

From the action (2.3.5) it can be seen that the energy of a static vortex in 2 dimensions is

$$E = \int d^2y \left( |(\nabla - ie\boldsymbol{A})\phi|^2 + \frac{1}{2}\left( \boldsymbol{E}^2 + \boldsymbol{B}^2 \right) + V(\phi) \right). \tag{2.3.9}$$

For the energy to be finite, all terms in the integral must vanish at spatial infinity. The potential, $V(\phi)$, (2.3.6), vanishes for

$$|\phi| = \eta. \tag{2.3.10}$$

Since $\phi$ is a complex field it may lie anywhere on the circle of radius $\eta$ (the vacuum manifold) at infinity. Around a circular path in space, then, $\phi$ may wind around the vacuum manifold, producing a vortex in the centre of this circular path. Given (2.3.10), the first term in (2.3.9) vanishes if the gauge field, $A_\mu$, is a pure gauge rotation.

We consider a straight vortex lying along one direction in a 3D space, so the fields do not vary with this coordinate, and take the plane orthogonal to this coordinate in polar coordinates, $r$ and $\theta$. At large $r$ we must have

$$A_\theta = \frac{1}{e}\frac{d\alpha}{d\theta}, \tag{2.3.11}$$

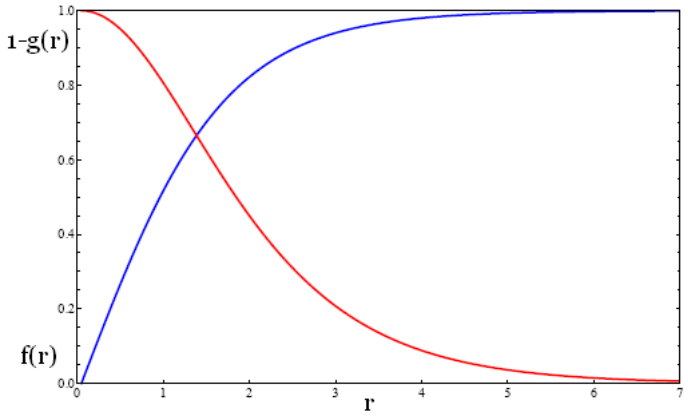


Figure 2.5: Field profiles for the Nielsen-Olesen vortex (from [79]).

where $\alpha$ is the phase of $\phi$. This allows the covariant derivative term in the energy (2.3.9) to vanish at infinity.

By rescaling the fields, $\eta$ can be set to 1. We then take the following ansatz:

$$\phi(\boldsymbol{y}) = e^{in\theta} f(r) \tag{2.3.12}$$

$$A_\theta(\boldsymbol{y}) = \frac{n}{e} g(r) \; ; \quad A_r(\boldsymbol{y}) = 0 \tag{2.3.13}$$

where $n$ is the winding number, $\boldsymbol{y} = (r, \theta)$, and we are using the coordinate basis for $A_\mu$. Requiring that

$$f(r) \to 1, r \to \infty \tag{2.3.14}$$

$$g(r) \to 1, r \to \infty \tag{2.3.15}$$

gives the correct asymptotic behaviour, (2.3.10) and (2.3.11). The field equations from the action (2.3.5) can be solved numerically for this ansatz, and the solution is illustrated in Figure 2.5 [79]. It is clear that the fields deviate from the vacuum in a region around $r = 0$, which is the location of the vortex. The non-zero field gradients in this region correspond to finite energy, which clearly occurs in a localised "lump" representing the cosmic string.

The zero-width action can be argued simply from physical considerations [75, 123], but can also be derived by integrating out the transverse degrees of freedom from (2.3.5) [69]. The resulting effective action is the Nambu (or Nambu-Goto) action [76],

$$S = -\mu \int d^2\zeta \sqrt{-\gamma}. \tag{2.3.16}$$

This action is proportional to the area of the *worldsheet* of the string. The worldsheet is a 2-dimensional surface representing the path of the string through space and time, parametrised by two coordinates $\zeta^a$, and with its geometry given by the 2D metric $\gamma_{ab}$. The factor of $\mu$ in front of the action (2.3.16) is the string energy per unit length (in the rest frame), which is given by (2.3.9).

In order to derive the Nambu action (2.3.16) from the Abelian-Higgs action (2.3.5), we take a coordinate system in 4D spacetime that breaks down into two worldsheet directions and two directions orthogonal to the worldsheet. The coordinates in the Abelian-Higgs action are $y^\mu$, and the new coordinates we call $\xi^\mu = (\zeta^a, \rho^A)$, where $a = 0, 1$ represent timelike and spacelike directions on the worldsheet, and the $\rho^A$, $A = 1, 2$, parametrise the 2 spacelike directions orthogonal to the string. The coordinate transformation can then be written as:

$$y^\mu(\xi) = x^\mu(\zeta) + \rho^A n^\mu_A(\zeta) \tag{2.3.17}$$

where $x^\mu$ describes the position of the worldsheet and the $n^\mu_A$ are normal vectors to the worldsheet (these depend on $\zeta$ as the normal will change as one moves around a curved worldsheet). This coordinate system will be single-valued as long as one does not move further from the string than its curvature radius, $R$. The normal vectors are chosen to be orthonormal, so they obey:

$$n^A_\mu x^\mu_{,a} = 0 \; ; \quad g^{\mu\nu} n^A_\mu n^B_\nu = -\delta^{AB}. \tag{2.3.18}$$

To make the transformation to the coordinates $\xi^\mu$, we must calculate the Jacobian

$$\sqrt{-g}\det\left(\frac{\partial y}{\partial \xi}\right) = \left(-\det\left(g_{\mu\nu}\frac{\partial y^\mu}{\partial \xi^\alpha}\frac{\partial y^\nu}{\partial \xi^\beta}\right)\right)^{1/2}. \tag{2.3.19}$$

We can see that

$$g_{\mu\nu}\frac{\partial y^\mu}{\partial \xi^\alpha}\frac{\partial y^\nu}{\partial \xi^\beta} = \mathrm{diag}\left(\gamma_{ab}, -\delta_{AB}\right) + \mathcal{O}\left(\frac{r}{R}\right) \tag{2.3.20}$$

where $\gamma_{ab} = g_{\mu\nu} x^\mu_{,a} x^\nu_{,b}$ is the worldsheet metric, and the correction term at the end comes from differentiating the normal vectors $n^\mu_A$ with respect to $\zeta$. Here $r = \sqrt{(\rho^1)^2 + (\rho^2)^2}$ is the radial distance from the worldsheet. Ignoring the correction term, the Jacobian is equal to $\sqrt{-\gamma}$ (where $\gamma$ is the determinant of $\gamma_{ab}$). Thus the coordinate transformed Abelian-Higgs action becomes,

$$S = \int d^2\zeta d^2\rho \sqrt{-\gamma}\left(|D_\mu\phi|^2 - \frac{1}{4}F_{\mu\nu}F^{\mu\nu} - V(\phi)\right). \tag{2.3.21}$$

The field configuration near the worldsheet will be approximately that of the static Nielsen-Olesen vortex, again with corrections $\mathcal{O}\left(\frac{r}{R}\right)$, so the fields $\phi$ and $A_\mu$ will depend almost entirely on the orthogonal coordinates, $\rho^A$. Integrating over $\rho^A$ therefore gives the negative of the energy per unit length, (2.3.9), or $-\mu$. (The first term in (2.3.21) is negative because the covariant derivative only has spatial parts.)

Because the field profiles drop off at order the string width, which we will call $\delta$, after integrating over the orthogonal directions the correction terms of order $r/R$ are cut off to order $\delta/R$, which in a cosmological context is tiny. Thus we have, to a good approximation, the Nambu action,

$$S = -\mu \int d^2\zeta \sqrt{-\gamma}. \tag{2.3.22}$$

From this effective action, the following equations of motion are derived:

$$\frac{1}{\sqrt{-\gamma}} \partial_a \left( \sqrt{-\gamma} \gamma^{ab} x^\mu_{,b} \right) + \Gamma^\mu_{\nu\sigma} \gamma^{ab} x^\nu_{,a} x^\sigma_{,b} = 0. \tag{2.3.23}$$

In flat spacetime these become very simple. This thesis contains a variety of work on the dynamics of cosmic strings using this Nambu description, both in flat and curved spacetimes.

A possible modification to the Nambu dynamics for GUT strings is the inclusion of a current on the string, allowing for superconducting strings. The possibility of superconducting strings was proposed by Witten in 1985 [176]. The modification to the Nambu action, derived in [49] is

$$S_{charged} = -\mu \int d^2\zeta \sqrt{-\gamma} \left(1 - \gamma^{ab} j_a j_b\right), \tag{2.3.24}$$

where $j_a$ is proportional to the conserved current along the string.

## 2.4 Evolution of a string network

This section reviews work on the dynamics of a network of GUT cosmic strings, which is very important for determining their overall cosmological effects. The properties of closed loops are also briefly discussed.

Starting with Kibble in 1985 [100], the evolution of a cosmological network of strings has been much studied. One of the most important quantities in the network

is its *correlation length*, $L$, which is the distance beyond which two different points on a long string are uncorrelated. It is reasonable to assume that there is approximately one string per correlation volume, $L^3$, of length $L$, which gives the energy density of cosmic strings as roughly

$$\rho = \frac{\mu}{L^2}, \tag{2.4.25}$$

where $\mu$ is the string tension. The evolution of $L$ thus determines the evolution of the energy density of cosmic strings, and hence whether they come to dominate the energy density of the universe, which would rule them out as a viable model.

Both in analytic models and numerical simulations, string networks consistently appear to reach a *scaling solution*, in which the correlation length of the network scales with the cosmological horizon: $L \propto t$. The advantage of this is that it does not come to dominate the energy density of the universe and is therefore cosmologically viable.

When performing numerical simulations, there are two main camps: those that use a full field-theory model such as Abelian-Higgs (2.3.5), and those that use the zero-width Nambu dynamics (2.3.23). The advantage of a field-theory model is that the interactions of strings are included in the model, whereas in a Nambu simulation, interactions are either not present or added by hand. Field-theory models also include the emission of radiation by the strings. The disadvantage of a field-theory model, however, is that it is much more computationally expensive. A consequence of this is that it is not possible to run a field-theory simulation in expanding space, as the string width quickly falls below the grid scale. Examples of field-theory simulations can be found in [88, 121, 173]. The first examples of Nambu simulations are found in [8,9,21], and more recent ones in [30,128,138]. Both types of simulation give broadly similar results and tend to reach scaling solutions, although the initial production of very small loops observed in Nambu simulations seems to be replaced by radiation of particles in the field theory case [88]. No numerical simulation yet includes gravitational backreaction. Figure 2.6 shows a Nambu-Goto simulation of a network and gives the reader an idea of the structure of a typical cosmic string network.

In order to model a network analytically, one must take into account both the

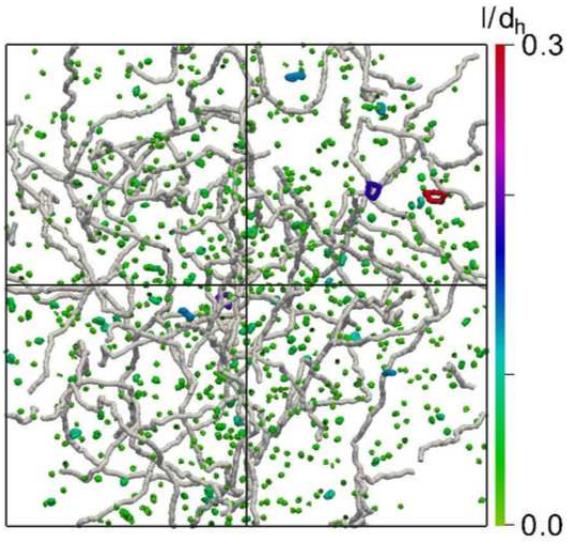


Figure 2.6: A network simulation (from [30]).

dynamics of the strings, given by the Nambu equations of motion (2.3.23), and loss of energy from the network due to the formation of loops. If loop formation is not included in the model, the network evolves to a state where strings are simply stretched by cosmological expansion, $L \sim a$, which gives that $\rho \sim 1/a^2$. Since this is a higher power of $a$ than the matter or radiation densities, the string network would come to dominate the energy density of the universe. Loop formation is therefore of key importance in reaching a scaling solution.

At formation there will be an initial correlation length, $L$, determined by the symmetry-breaking process that formed the cosmic strings. $L$ will then begin to grow over time. The first analytic model of network evolution, known as the one-scale model [100], has the correlation length, $L$, as the only parameter in the network. It determines the evolution of $L$ due to expansion of space (using the Nambu equations of motion in an expanding background) and loop production (using an unknown loop-production function to be determined by simulations). This model gives qualitative results, namely that the network reaches a scaling solution ($L \propto t$) if the rate of loop production is large enough. It includes the physical assumption that the average velocity of the strings is smaller when $L$ is a greater fraction of the horizon size, but has no exact model for this dependence.

The "velocity-dependent one-scale model" (VOS) [116] subsequently introduced

the r.m.s. (root mean square) string velocity, $v$, as another dynamical variable and modelled the evolution of both $L$ and $v$. This model uses the Nambu equations of motion (2.3.23) averaged over the length of the strings, as well as a similar loop-production term to that in the one-scale model. Its predictions match extremely well with behaviour observed in simulations [121], suggesting that the few features accounted for in this model are of key importance to the evolution of the network as a whole, and in reaching a scaling solution. There have been a few modifications to the model to account for smaller effects [117], but as an accurate description of the main features of network evolution it has not been superseded.

The loop-production term is added into analytic network models by hand, based on relatively simple assumptions. In order to calculate the rate of energy density loss to loops, one needs to know the average length of loop formed at string crossing, the string tension, $\mu$, and the average time between string crossings in a given volume. Assuming that there is approximately one string per correlation volume $L^3$, a string segment will have to travel roughly a distance $L$ before meeting another string. Thus the average time between string crossings will be approximately

$$t \simeq \frac{L}{v}, \tag{2.4.26}$$

where $v$ is the r.m.s. velocity of the strings. If the average length of loop produced at a string crossing is given by $l_{avg}$, the energy loss per loop will be $\mu l_{avg}$. Thus the rate of energy density lost to loops will be

$$\dot{\rho} \simeq \frac{\mu l_{avg}}{L^3}\frac{v}{L}. \tag{2.4.27}$$

The average loop length, $l_{avg}$, actually turns out to be quite close to $L$, and is written instead as $l_{avg} = \tilde{c}L$, where $\tilde{c}$ is close to unity and is in general determined numerically.

Once loops have broken off from a network, they become largely unimportant for the evolution of the network as a whole (unless they reconnect with it − a finite reconnection probability is normally included in analytic models). But on their own in space, loops begin to oscillate and to give off potentially important and interesting signals as they decay via gravitational radiation (see Section 4.1).

Closed loops of cosmic string will be discussed in detail in Chapter 3, but here we give a short introduction to their properties. There are three important features of cosmic string loop motion that are commonly studied. The first is the existence of *cusps*, which result in the emission of bursts of gravitational radiation. The second is the presence of sharp corners, known as *kinks*, which propagate around a string loop, again giving off gravitational radiation signals. The third feature is the tendency of a loop to break down into smaller loops by folding back on itself and *self-intersecting*.

A cusp is an event that occurs at a single point on a string, which instantaneously moves at the speed of light. This is due to constructive interference between left- and right-moving waves, and happens quite generically on string loops in 4D spacetime. Not surprisingly, cusps are powerful events, emitting a great deal of energy [168]. A kink is a long-lived feature of a loop, which can be formed at the point where a closed loop breaks off from a longer string, since the two segments of string generally meet at a non-zero angle. It is not as powerful as a cusp, but nonetheless emits a significant amount of energy. Cusps and kinks are mainly of interest due to their distinctive gravitational signals (see Section 4.1).

Self-intersections are important because a non-self-intersecting loop will be long-lived, and therefore of cosmological interest. The search for loops without self-intersections was reviewed in Section 2.2, and we will return to it later in the context of cosmic superstrings.

It is also possible (as mentioned at the end of Section 2.3) for cosmic strings to be superconducting. For such strings, the process of reconnection to form closed loops is similar to that for uncharged strings [111], and network scaling behaviour may also be very similar [34]. The main difference is some additional energy loss from the network due to radiation from the charged field. There is also the possibility that friction in the very early universe, when it is filled with plasma, may have a greater effect on superconducting strings, leading to a denser, slower-moving network containing strings with a smaller radius of curvature [42, 59]. In most scenarios, however, there is still a cosmologically acceptable scaling behaviour.

Ordinarily, closed loops will eventually radiate all their energy away via grav-

itational radiation, and disappear entirely from the string network. It is possible, however, that a superconducting loop may not be able to evaporate entirely, due to the repulsive force of its charge, and may form tiny magnetic dipoles. Such dipoles can be cosmologically problematic as they may have very long lifetimes, see for example [44, 49, 57, 83].

## 2.5 Cosmic superstrings

In Chapter 1, we described a model of cosmology based on string theory. A key feature of this model is its natural inflationary scenario, brane inflation [62]. Objects similar to the GUT cosmic strings, known as cosmic superstrings, are generically produced at the end of brane inflation, taking the form of fundamental strings or D-branes whose lengths are of cosmological scale. It was this discovery that reignited interest in cosmic strings after they were ruled out as the seeds of galaxy formation (see Section 2.2), since cosmic superstrings may provide an observational window into string theory.

As discussed in Chapter 1, the most popular brane inflationary scenario is that of a D3-brane moving down a warped throat towards an anti-D3-brane, their separation being the inflaton field [62]. Inflation ends when the two branes annihilate, and it is at this point that cosmic strings are produced. In the low-energy approximation of string theory, their production occurs by a very similar symmetry-breaking mechanism to the original cosmic strings (see Section 2.1). Each individual D3-brane has a U(1) gauge field living on it, and the annihilation of the two D3-branes breaks the U(1) symmetries, forming vortices. The breaking of a U(1) symmetry is exactly the mechanism of vortex formation in, for example, the Abelian-Higgs model (2.3.5). In this case, however, the resulting defects are fundamental string theory objects: cosmic F- and D-strings, of cosmological size.

A more general brane-inflation model may involve D$p$-branes, with $(p-3)$ directions wrapped in the internal dimensions. In such a scenario, cosmic superstrings are still formed, as discussed in [92]. The reason for this is that only branes with odd dimension, $p$, are stable, and the annihilation of D$p$-branes results in the formation

of D$(p-2n)$-branes, where $n$ is an integer. For branes of a given dimension, the RR-charges must total zero, which means that D$p$-branes with large dimension, $p$, tend to come in brane-antibrane pairs and therefore annihilate, leaving lower-dimensional branes in their place. In a realistic cosmological scenario, the compactification scale is generally smaller than the horizon size, so the defect formation process can take place only in the 3 large dimensions. Therefore in practice, a D$p$-brane with $(p-3)$ wrapped directions annihilates to form D$(p-2)$-branes, which are manifest as 1-dimensional cosmic strings in the non-compact directions, with the same $(p-3)$ wrapped internal directions.

Cosmic superstrings as by-products of brane inflation were first proposed in 2002 by Jones, Stoica and Tye [92], and have been much studied since. It is interesting to note that cosmologically problematic defects, such as monopoles or domain walls, are not produced. This is another appealing aspect of the brane inflation model.

The stability of cosmic superstrings was studied by Copeland, Myers and Polchinski [45]. They assert that, in general, long strings may be unstable to breakage if there are D-branes that fill the 4 large dimensions. D-branes represent the end-points of open strings, and therefore their presence allows a long string to break up into many open string quanta. Different types of strings and branes only end on D-branes of particular dimensions, thus in cosmological models where a particular type of D-brane is absent, stable cosmic superstrings can exist. Furthermore, if the D-brane on which the cosmic string would break does not fill the compact dimensions, the instability may be suppressed due to separation in the internal space. They conclude that cosmic superstrings can be stable in many models. Leblond and Tye [113] studied the stability of D1-strings within a D3-brane, which, given that our universe is thought to be located on a D3-brane, is a relevant set-up for cosmic strings, and found them to be stable. Thus, there are significant reasons to believe that long-lived cosmic superstrings could indeed be formed in brane inflation.

Cosmic superstrings, being fundamentally string theoretic objects, are quite different from the GUT strings discussed in this chapter so far. However, they may be modelled in very similar ways. In fact the Nambu-Goto action (equation 2.3.16) is generic in describing the dynamics of a string, and takes no account of the string's

internal structure. Both networks of string and individual loop dynamics may therefore be very similar to GUT strings (see Section 2.4, and later), as may gravitational wave signals, Section 4.1.

There are, however, some important differences and modifications. Some of these differences may be significant enough to be observable, and, should we observe cosmic strings in the future (see Section 2.2 for observational possibilities) this would provide evidence for or against the string-theory model of the universe.

The following sections outline the ways in which cosmic superstring motion and signals may differ from our standard field theory cosmic strings. Firstly, the idea of having multiple tensions and types of string is considered, which includes the possibility of forming 3-string junctions. This may have a significant effect on their dynamics and signals. Secondly, in Section 2.7, possible changes to the reconnection probability are discussed. This particularly affects the formation and stability of closed loops. Lastly, in Section 2.8, the somewhat controversial topic of whether cosmic superstrings may couple to, or emit, a wide variety of exotic fields is considered.

## 2.6 Multiple string-types and junctions

Unlike the original, GUT-scale strings, the tension of cosmic superstrings is not fixed by a known scale. Interestingly, it may be possible to have a network made up of several different string tensions and types. Cosmic superstrings may take the form of D-strings, F-strings, or a bound state of the two. In fact they can form any number of different composite strings known as $(p, q)$-strings, where $p$ and $q$ represent the number of F and D strings, respectively [151,177]. For stability $p$ and $q$ must be coprime. The stability of such strings on cosmological scales was studied in [45], where they were found to be stable in many models.

The tension of a $(p, q)$-string is given by

$$\mu_{(p,q)} = \mu_F \sqrt{p^2 + q^2/g_s^2}, \tag{2.6.28}$$

where $\mu_F$ is the fundamental string tension, so the higher $(p, q)$ numbers correspond to heavier strings.

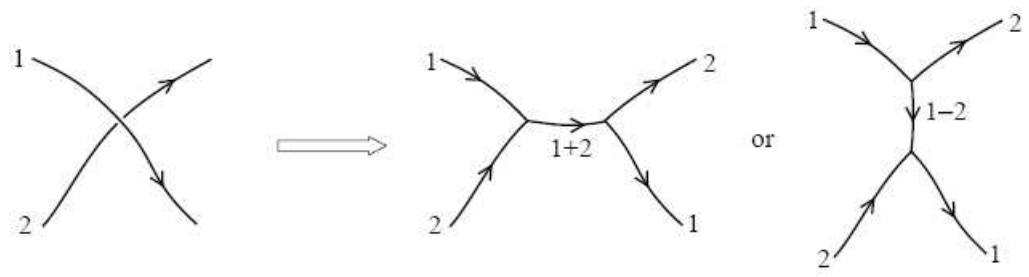


Figure 2.7: Formation of 3-string junctions (from [90]).

If two strings of different types collide they may join together to form a composite state, which requires them effectively to "zip" together, leaving Y-shaped junctions at the ends of the joined segment, made up of 3 different types of string (a schematic illustration of this process is shown in Figure 2.7). The formation of bound states is subject to various conditions. In [90], probabilities of different types of string joining to form bound states were considered, by looking at the microscopic properties of superstrings using string perturbation theory (their results depend of the details of the compactification). Later, Copeland, Kibble and Steer [51] looked at the kinematic constraints on bound state formation, finding that it depends on the angle and velocity at which strings collide, and also on their relative tensions. When the tensions are similar it becomes more likely that the strings may simply pass through each other without interacting.

As well as forming in a collision, bound states can break up again into two lighter strings by "unzipping". The dynamics of zipping and unzipping are important for determining the composition of the network in terms of the number densities of different types of string. It is found in [51] that states representing lighter strings tend to grow at the expense of heavier ones, suggesting that a $(p, q)$-string network will be dominated by the lighter cosmic superstrings. The dynamics of junction unzipping were studied in [67, 68], where it was shown dynamically that bound states are likely to unzip, again suggesting that lighter strings will dominate.

The studies of junction dynamics in [50,51,67] model the strings using the Nambu action (2.3.16), which is an effective zero-width action, valid when the radius of curvature of a string is much larger than its width. This action is therefore not valid at the junction itself, and cannot model the detailed process of junction formation.

The Nambu dynamics have been compared with field theory simulations in [23, 24, 146] in order to determine their accuracy. In [24] it was found that the probability of formation of a bound state when strings meet is only moderately well modelled, but that the later dynamics of a junction, should it form, are accurately captured by the Nambu description. [146] studied the formation of bound states, again finding some discrepancy with the Nambu case. The discrepancy was conjectured to coincide with the emission of radiation, which is not modelled by Nambu dynamics. This reduces the probability of forming a bound state as some of the energy that would go into forming the state is lost as radiation. In general, though, field theory simulations do not find a large radiative emission. In [23] it was found that a 3-string junction can sometimes be unstable to breakage into 3 individual junctions of lighter strings, and that on including this instability in Nambu simulations they matched very accurately with field theory models.

The evolution of networks of $(p, q)$-strings has been much studied. There were initially some suggestions that "network frustration" would prevent such a system reaching scaling [157], and therefore rule it out as cosmologically viable. This happens when the motion of the strings effectively comes to a halt, and therefore they no longer lose energy by breaking off closed loops. It is loss of energy in loops that prevents a cosmic string network coming to dominate the energy density of the universe, so it is important that this process can take place. The formation of bound states means that when strings collide, they may zip together rather than breaking off a closed loop, which not only prevents the loss of that loop from the network, but means that the strings cannot pass through each other and continue to move. Thus the network may eventually come to a halt, leaving no more opportunity for collision and loop formation.

However, analytic studies of $(p, q)$-string networks [12, 14, 115, 165], in which the velocity-dependent one scale model of Martins and Shellard [116] (see Section 2.4) is modified for a mixed network of $(p, q)$-strings, find that scaling behaviour is still generic in almost all cases. Field theory simulations of string networks with junctions have also been performed [46,87,145,167], and these too find scaling behaviour. Part of the reason for this is the dynamical tendency for bound states to unzip (see [67]),

meaning that their effect on the overall dynamics of a network is fairly small.

One interesting property of 3-string junctions is their effect on kinks. It is shown in [28] that a kink meeting a junction forms several daughter kinks, one on each leg of the junction. Often one of these is sharper than the original kink, and on closed loops this leads to proliferation of very sharp kinks. This in turn significantly enhances the gravitational wave signal [26]. Gravitational wave bursts from individual cusps or kinks are found to be largely unaffected by the presence of junctions [27], unless the cusp or kink is very close to a junction, in which case there are some extra, potentially detectable contributions to the gravitational wave signal. In [56], it is shown that strings with junctions generically have cusps, where they would not necessarily otherwise. This too means an enhancement of the gravitational wave signal, especially at early times.

Possible observational signatures of $(p, q)$-string networks also include changes to the CMB temperature and polarisation spectra. These changes are calculated in [134], where it is found that the dominant effect on these spectra may come either from light strings, or from the rarer heavy composites, depending on the value of the string coupling $g_s$.

## 2.7 Reconnection

An important difference between cosmic superstrings and standard, field theory strings is their interaction probability. A standard, field theory cosmic string in 4D spacetime, on meeting another such string, will almost always interact with it, the interaction being generally to exchange partners. Two cosmic superstrings, however, have a smaller interaction probability and thus a significant chance of simply passing through one another, should they meet. An important effect that contributes to this is the existence of extra spatial dimensions. This means that even if two strings appear to cross in the 3 large dimensions, the chances are that their locations in the internal dimensions do not coincide, and they will effectively miss each other. This makes a large effective reduction to the interaction probability. Then, in the event that two cosmic superstrings do meet, their interaction probability is further

lowered by their microscopic properties.

From [90], the interaction probability for F-strings is

$$P = g_s^2 \frac{V_{min}}{V_\perp} f(\theta, v). \tag{2.7.29}$$

Here, $V_{min}/V_\perp$ is a volume factor, the minimum volume, $V_{min}$, that strings must be within before they can interact, divided by the volume, $V_\perp$, of the internal space perpendicular to the strings. There is also a factor of $g_s^2$, the string coupling, which may be very small. This is the fundamental interaction probability of F-strings. $f$ is a kinematic factor, depending on the angle $\theta$, and velocity, $v$, at which the strings collide. Kinematic factors affect the standard, field theory cosmic strings in a similar way; generally at relativistic velocities, interaction becomes less likely. The probability, (2.7.29), is slightly modified for different types of cosmic superstring. However, quantitatively all that can be said is that there is some suppression to the probability relative to standard cosmic strings, so the details of different string interactions are not important for our discussion.

When crossing strings exchange partners, closed loops may be formed. As discussed in Section 2.4, the formation of closed loops is essential in allowing a string network to reach scaling. Loops are also of great interest in their own right, due to their distinctive gravitational wave signals (Chapter 4). The reduction in the probability of self-interaction for cosmic superstrings will make a great difference both to the formation and stability of closed loops.

If a loop self-intersects, it breaks down into smaller loops and is thus unstable. Only stable loops are long lived, and thus of cosmological interest, as discussed in Section 2.2. A smaller interaction probability makes loops less likely to break down when they apparently self-intersect in the 3 large dimensions, and therefore makes them more stable. It also, however, makes a loop less likely to break off from a network, and so fewer loops will be formed.

The effect of a lower rate of loop formation on networks of strings was first considered by Jones, Stoica and Tye [93], and a similar argument was made in [61]. Both consider the correlation length, $L$, and work with a simple physical argument that gives $L \propto P$, where $P$ is the reconnection probability. This means that a smaller reconnection probability enhances the density of a cosmic superstring network, since

there is on average one string per correlation volume, $L^3$. Intuitively, this makes sense as the formation of fewer loops means that less string is lost from the network.

Both [93] and [61] consider a scaling solution, in which the correlation length is proportional to time, $L \propto t$, since this is the cosmologically acceptable behaviour. The physical argument is that in a given time, $t$, a string will travel a distance of approximately $vt$, where $v$ is the r.m.s. velocity of the strings. It will encounter approximately one string per correlation distance, $L$, so the average number of "encounters" in a time, $t$, is

$$N \simeq \frac{vt}{L}. \tag{2.7.30}$$

In order to break off enough loops for a scaling solution, one requires these encounters to result in one or few reconnections in a Hubble time, so $NP \sim 1$, which gives

$$L \sim Pvt. \tag{2.7.31}$$

This dependence $L \propto P$, is, however, not reproduced by numerical simulations [144]. These simulations find a weaker dependence on the reconnection probability, $L \propto \sqrt{P}$. A possible explanation for this is the fact that a reduced reconnection probability results in an increase of small-scale wiggles, which would ordinarily break off as small loops. Small-scale structure increases the effective mass per unit length of a long string, and decreases its effective tension, resulting in a reduction of the r.m.s. velocity, $v$. However, it also means that each encounter between two long strings results in multiple chances for reconnection, which may effectively increase the probability of reconnection. So a reduction in $P$ may not have as much effect on a network as predicted in [61, 93].

Nonetheless, a reduced reconnection probability results in a significant enhancement to network density. It also significantly increases the stability of closed loops, a topic to which we will return in Chapter 3.

## 2.8 Emission of radiation and particles

Gravitational radiation is not the only form of radiation that may be emitted by cosmic strings, although it is the one of which we can be most certain. Even the original

field theory strings may give off various different signals. These include high-energy proton production by the collapse of closed loops [25], as well as proton, gamma ray and neutrino emission from long strings [175]. There are some claims that particle emission may be the main form of energy loss for cosmic strings [174], although this is not widely agreed upon. Making this assumption, in [175], observational bounds were placed on the allowed string tension.

Recently, in [94, 158] the emission of photons by cosmic strings was considered, and it was found that light from cosmic strings may be detectable by current experiments. This predicted emission is a quantum effect due to the time-dependent gravitational field of the cosmic string, which can cause pair-production of charged particles and antiparticles, in what is known as the "gravitational Aharonov-Bohm effect".

Superconducting cosmic strings may also emit electromagnetic radiation due to the currents they carry. The effects of this are considered in [42, 132, 161, 176]. In [132] the effect of the magnetic field of a superconducting string on the diffusion of cosmic rays was calculated, providing a means of experimental search. More recently, in [161], the effect of electromagnetic radiation from superconducting strings on the CMB was calculated, putting a bound on the allowed string current, which must be less than $\sim 10^7$ GeV to be compatible with observations.

Cosmic *super*strings have further possibilities for emission of radiation, due to the extra fields that exist in supergravity, namely R-R and NS-NS fluxes, and the dilaton (see Section 1.2). Similarly to the way that a point particle has electric charge from coupling to a 1-form gauge field, strings become charged by coupling to 2-form fields. For F-strings, this is the NS-NS 2-form, $B_{\mu\nu}$, and for D-strings it is the R-R 2-form $C_{\mu\nu}$. Thus it is thought that cosmic superstrings could emit these 2-form fields, and well as both dilaton and gravitational radiation.

As discussed in Section 1.2, the string theory model of cosmology has an internal geometry containing warped throats. The fact that cosmic superstrings live in a warped geometry can have a great effect on their properties. One of the effects that is easiest to identify is that warping suppresses the effective mass of an object, thus reducing gravitational interactions (see Section 5.1). It was therefore suggested

in [66] that the gravitational radiation from cosmic D-strings would be suppressed, and R-R radiation would be the dominant form of energy loss.

However, the effects of the warped compactification are more complicated than this. In [82], the authors note that in realistic compactifications, the R-R and NS-NS 2-forms are projected out, and there can be *no* massless radiation from either of these fields from cosmic F- or D1-strings. They do note that if a cosmic superstring is in fact a D3-brane with 2 of its directions wrapped in the internal space, it is possible to have some form of radiation. They were not, however, able to calculate this emission in detail.

Although the dilaton will acquire a mass in moduli stabilisation (see Section 1.2), it will also have its mass suppressed by the warped geometry [70], so it is possible that dilaton emission may be significant. There are also many other massive moduli from the compactification, which may also be emitted. In [15,54,130], fairly stringent observational constraints on either the cosmic string tension or the dilaton mass are calculated, based on the fact that cosmic strings would emit such scalar fields. These calculations do not, however, account for the effects of a warped geometry. In [143] warped compactifications are considered, where moduli masses are suppressed and their coupling to matter is stronger. They find that, if the coupling is very strong, a high level of radiation from these moduli fields makes the loop lifetime much shorter, and the moduli lifetime much shorter too, and hence the cosmological constraints can be significantly relaxed.

One quite generic possibility for the production of moduli by cosmic superstrings is that their coupling to the 10D metric allows them to emit Kaluza-Klein radiation [60]. While these are massive modes and thus would decay over cosmological scales, it is possible, as suggested in [60], that the fact that their mass is suppressed due to the warped geometry means that they may have observational effects. Such emissions are certainly worthy of serious consideration, along with emissions of the dilaton and other massive moduli fields.

The detailed properties of cosmic superstrings, as with most realistic calculations in string theory, are at present conjectured with limited certainty. A possible issue with the argument that massive modes have their masses suppressed by the warped

geometry and are therefore emitted in larger quantities is that the cosmic string tension is similarly suppressed, and thus its emission of particles is correspondingly suppressed as well. Looking at the 10D perspective, the masses of strings and particles are unchanged: the suppression due to warping is simply a suppression of the *effective* 4D masses. This suggests that the actual production of particles may be unchanged by this effect.

In this thesis we mostly consider the classical dynamics of cosmic strings using the Nambu action (2.3.16), and their emission of gravitational radiation, but it is worth bearing in mind that emission of other fields can also affect their motion and observational signals. These emissions are extremely model-dependent and in this section we have outlined only some of the possibilities.

# Chapter 3

# String loop dynamics in higher dimensions

One of the major difference between cosmic superstrings and GUT cosmic strings is that string theory lives in 10-dimensional spacetime, where 6 of the spatial dimensions are small and compact, but nonetheless present. It is therefore important to consider the impact of these extra dimensions on the dynamics of cosmic strings. Higher dimensions are relevant not only for cosmic superstrings, which live in a 10-dimensional string theory universe, but also in other models such as braneworlds (see Chapter 1). In this Chapter we look at cosmic string loops in higher dimensional flat space, and discuss their dynamics. We begin in Section 3.1 with a review of loop dynamics in 4D spacetime, and go on to look at the general effects of extra dimensions on this behaviour in Section 3.2. We then derive some exact solutions for loops in 5D spacetime, given in Section 3.3, and look at some properties of these solutions in Section 3.4.

## 3.1 Loops in 4D flat space

A loop of cosmic string can be modelled with the equations of motion (2.3.23) derived from the Nambu action (2.3.16). This section reviews solutions to these equations that have been found in 4-dimensional flat space.

The equations of motion, (2.3.23), are written in terms of the 2-dimensional

metric on the worldsheet of the string, $\gamma_{ab}$. $a, b = 0, 1$ refer to timelike and spacelike coordinates on the worldsheet ($\zeta^0$ and $\zeta^1$). The worldsheet metric is defined as the pullback of the spacetime metric,

$$\gamma_{ab} = g_{\mu\nu}\frac{\partial x^\mu}{\partial \zeta^a}\frac{\partial x^\nu}{\partial \zeta^b}. \tag{3.1.1}$$

We may therefore write it as

$$\gamma_{ab} = \begin{pmatrix} \dot{x}^2 & \dot{x}^\mu x'_\mu \\ \dot{x}^\mu x'_\mu & x'^2 \end{pmatrix}, \tag{3.1.2}$$

where dot and prime represent differentiation with respect to $\zeta^0$ and $\zeta^1$, respectively, and we have suppressed indices in squared quantities so, for example, $\dot{x}^2 = \dot{x}^\mu \dot{x}_\mu$.

Now, in any spacetime two gauge choices may be made. There are several different possibilities for this choice, but a common one, and the one that will be used in this work, is called the transverse temporal gauge. Firstly, $\gamma_{ab}$ is chosen to be diagonal, and secondly the timelike coordinate on the string worldsheet, $\zeta^0$, is equated with the timelike coordinate in space-time. First consider making $\gamma_{ab}$ diagonal. This is equivalent to setting

$$\dot{x}^\mu x'_\mu = 0. \tag{3.1.3}$$

The equation of motion, (2.3.23), then becomes

$$\left(\sqrt{\frac{-x'^2}{\dot{x}^2}}\dot{x}^\mu\right)^{\cdot} - \left(\sqrt{\frac{\dot{x}^2}{-x'^2}}x'^\mu\right)' + \Gamma^\mu_{\nu\sigma}\left(\sqrt{\frac{-x'^2}{\dot{x}^2}}\dot{x}^\nu\dot{x}^\sigma - \sqrt{\frac{\dot{x}^2}{-x'^2}}x'^\nu x'^\sigma\right) = 0. \tag{3.1.4}$$

In order to look at the second gauge condition - setting worldsheet time equal to coordinate time - we split our coordinates, $x^\mu$, into a timelike coordinate, $t$, and spacelike coordinates, $\mathbf{x} = (x^1, x^2, x^3)$. As mentioned above, this section concerns work on solutions in 4-dimensional Minkowski space, so we take the metric,

$$ds^2 = dt^2 - \left(dx^1\right)^2 - \left(dx^2\right)^2 - \left(dx^3\right)^2. \tag{3.1.5}$$

We therefore set $\zeta^0 = t$ and now refer to $\zeta^1 \equiv \zeta$. This second gauge choice simplifies the equations further, and the Christoffel symbols of the metric (3.1.5) are all zero, so the equations of motion (3.1.4) become:

$$\frac{\partial}{\partial t}\left(\sqrt{\frac{-x'^2}{\dot{x}^2}}\right) \equiv \frac{\partial}{\partial t}\left(\sqrt{\frac{\mathbf{x}'^2}{1-\dot{\mathbf{x}}^2}}\right) = 0, \tag{3.1.6}$$

$$\left(\sqrt{\frac{\mathbf{x}'^2}{1-\dot{\mathbf{x}}^2}}\dot{\mathbf{x}}\right)^{\cdot} - \left(\sqrt{\frac{1-\dot{\mathbf{x}}^2}{\mathbf{x}'^2}}\mathbf{x}'\right)' = 0. \tag{3.1.7}$$

In flat space-time an additional, third gauge choice may be made, known as the conformal gauge,

$$\dot{x}^2 + x'^2 = 0, \tag{3.1.8}$$

or

$$\dot{\mathbf{x}}^2 + \mathbf{x}'^2 = 1. \tag{3.1.9}$$

This simplifies things even further. Applying it to the zeroth equation of motion, (3.1.6), we see that the term in brackets is equal to 1 and so this equation is automatically satisfied when the gauge choice (3.1.8) is made. The quantity $\sqrt{-x'^2/\dot{x}^2}$ is proportional to the conserved energy of the string loop, which essentially may be set to 1 because for a single loop in flat space there are no other energy scales in the system.

Putting the gauge choice (3.1.9) into (3.1.7) results in a simple wave equation:

$$\ddot{\mathbf{x}} - \mathbf{x}'' = 0. \tag{3.1.10}$$

This has well-known analytic solutions. The full solution for a loop can be written as a sum of left- and right-moving modes,

$$\mathbf{x} = \frac{1}{2}\left(\mathbf{a}(t-\zeta) + \mathbf{b}(t+\zeta)\right). \tag{3.1.11}$$

The solution must be periodic in $\zeta$ for a closed loop. This is equivalent to having

$$\int_0^l \mathbf{x}' d\zeta = \int_0^l (\mathbf{b}' - \mathbf{a}') d\zeta = 0, \tag{3.1.12}$$

where $l$ is the period of $\zeta$, which may be thought of as the length of the loop, and for $\mathbf{a}$ and $\mathbf{b}$, prime represents differentiation of each function by its respective argument. If we choose also to be in the centre of mass frame of the loop, we have

$$\int_0^l \dot{\mathbf{x}} d\zeta = \int_0^l (\mathbf{b}' + \mathbf{a}') d\zeta = 0. \tag{3.1.13}$$

These two conditions combine to give

$$\int_0^l \mathbf{b}' d\zeta = \int_0^l \mathbf{a}' d\zeta = 0 \tag{3.1.14}$$

and thus the functions $\mathbf{a}(t-\zeta)$ and $\mathbf{b}(t+\zeta)$ must be individually periodic. This then means the motion of a closed loop will be periodic in time. In fact, the period of the motion is half of the loop length, $l$. This can be seen by adding $l/2$ to $t$, which gives $\mathbf{a}(t+l/2-\zeta)$ and $\mathbf{b}(t+l/2+\zeta)$. Then a shift of $l/2$ in $\zeta$, which does not change the loop at all, gives $\mathbf{a}(t-\zeta)$ and $\mathbf{b}(t+\zeta+l) \equiv \mathbf{b}(t+\zeta)$.

The gauge conditions (3.1.3,3.1.9) give the following constraints on the functions $\mathbf{a}$ and $\mathbf{b}$:

$$\mathbf{a}'^2 = \mathbf{b}'^2 = 1. \tag{3.1.15}$$

Any periodic functions satisfying this constraint form a valid cosmic string loop solution.

The most common way of solving equation (3.1.15) is to expand the functions $\mathbf{a}$ and $\mathbf{b}$ as Fourier series and solve for a finite number of harmonics. The argument for cutting off the higher harmonics comes from the idea that they will be damped by the expansion of space and the emission of gravitational radiation. They are commonly written as follows,

$$\mathbf{a}(\zeta_-) = \sum_n \frac{1}{n}\left(\mathbf{a}_n \sin(n\zeta_-) + \boldsymbol{\alpha}_n \cos(n\zeta_-)\right) \tag{3.1.16}$$

$$\mathbf{b}(\zeta_+) = \sum_n \frac{1}{n}\left(\mathbf{b}_n \sin(n\zeta_+) + \boldsymbol{\beta}_n \cos(n\zeta_+)\right), \tag{3.1.17}$$

where $\zeta_- = t-\zeta$ and $\zeta_+ = t+\zeta$, and the $\mathbf{a}_n$, $\boldsymbol{\alpha}_n$, etc are constant 3-vectors. For simplicity, $\zeta$ has been rescaled so that its period is $2\pi$.

The first loop solutions were found in 1982 [102], and had a single harmonic only, so just included the first term from the sum (3.1.17). In 1984 [164] Turok then found solutions for a 2-harmonic cosmic string. Larger portions of the solution space for a 2-harmonic string were uncovered by [41, 58]. The first thing that becomes clear when adding in a second frequency is that, if the lowest harmonic is $n = 1$, the only other single frequency that can be added is $n = 3$. To see this, we look at the harmonics 1 and $m$, and calculate the required form of $\mathbf{a}$, where

$$\mathbf{a} = \mathbf{a}_1 \sin(\zeta_-) + \boldsymbol{\alpha}_1 \cos(\zeta_-) + \frac{1}{m}\mathbf{a}_m \sin(m\zeta_-) + \frac{1}{m}\boldsymbol{\alpha}_m \cos(m\zeta_-). \tag{3.1.18}$$

Calculating $\mathbf{a}'^2$ in order to impose the constraint $\mathbf{a}'^2 = 1$ gives terms with harmonics 0, 2, $2m$, $m+1$ and $m-1$. This gives a total of 9 constraints, including both sine

and cosine terms from each non-zero harmonic:

$$0 \;:\; \frac{\mathbf{a}_1^2}{2} + \frac{\boldsymbol{\alpha}_1^2}{2} + \frac{\mathbf{a}_3^2}{2} + \frac{\boldsymbol{\alpha}_3^2}{2} = 1 \tag{3.1.19}$$

$$2 \;:\; \mathbf{a}_1^2 - \boldsymbol{\alpha}_1^2 = 0 \quad ; \quad \mathbf{a}_1.\boldsymbol{\alpha}_1 = 0 \tag{3.1.20}$$

$$2m \;:\; \mathbf{a}_m^2 - \boldsymbol{\alpha}_m^2 = 0 \quad ; \quad \mathbf{a}_m.\boldsymbol{\alpha}_m = 0 \tag{3.1.21}$$

$$m+1 \;:\; \mathbf{a}_1.\mathbf{a}_m - \boldsymbol{\alpha}_1.\boldsymbol{\alpha}_m = 0 \quad ; \quad \boldsymbol{\alpha}_1.\mathbf{a}_m + \mathbf{a}_1.\boldsymbol{\alpha}_m = 0 \tag{3.1.22}$$

$$m-1 \;:\; \mathbf{a}_1.\mathbf{a}_m + \boldsymbol{\alpha}_1.\boldsymbol{\alpha}_m = 0 \quad ; \quad \boldsymbol{\alpha}_1.\mathbf{a}_m - \mathbf{a}_1.\boldsymbol{\alpha}_m = 0. \tag{3.1.23}$$

The constraints from frequencies $(m+1)$ and $(m-1)$ can be rearranged to give:

$$\mathbf{a}_1.\mathbf{a}_m = \boldsymbol{\alpha}_1.\boldsymbol{\alpha}_m = \boldsymbol{\alpha}_1.\mathbf{a}_m = \mathbf{a}_1.\boldsymbol{\alpha}_m = 0. \tag{3.1.24}$$

Thus the conditions imply that the four vectors must be mutually orthogonal. In 3D space this is clearly impossible, so one of the vectors must be set to zero. From equations (3.1.21) and (3.1.20), that frequency will then drop out entirely. It is only in the case where $m = 3$, so $m - 1 = 2$ and thus the equations (3.1.20) and (3.1.23) combine together, that the system becomes soluble.

We will now outline the derivation of a solution to this system, using a method from [58], as an analogous method will be used in the work later on. The solution is chosen to have a single harmonic in $\mathbf{b}$, and the first and third harmonics in $\mathbf{a}$, so

$$\mathbf{a} = \mathbf{a}_1 \sin(\zeta_-) + \boldsymbol{\alpha}_1 \cos(\zeta_-) + \frac{1}{3}\mathbf{a}_3 \sin(3\zeta_-) + \frac{1}{3}\boldsymbol{\alpha}_3 \cos(3\zeta_-), \tag{3.1.25}$$

$$\mathbf{b} = \mathbf{b}_1 \sin(\zeta_+) + \boldsymbol{\beta}_1 \cos(\zeta_+). \tag{3.1.26}$$

The full solution is then proportional to the sum of the two. The gauge condition, (3.1.15), gives the following constraints:

$$\mathbf{a}_3^2 - \boldsymbol{\alpha}_3^2 = 0 \quad ; \quad \mathbf{a}_3.\boldsymbol{\alpha}_3 = 0 \tag{3.1.27}$$

$$\mathbf{a}_1.\mathbf{a}_3 - \boldsymbol{\alpha}_1.\boldsymbol{\alpha}_3 = 0 \quad ; \quad \boldsymbol{\alpha}_1.\mathbf{a}_3 + \mathbf{a}_1.\boldsymbol{\alpha}_3 = 0 \tag{3.1.28}$$

$$\frac{\mathbf{a}_1^2}{2} - \frac{\boldsymbol{\alpha}_1^2}{2} + \mathbf{a}_1.\mathbf{a}_3 + \boldsymbol{\alpha}_1.\boldsymbol{\alpha}_3 = 0 \tag{3.1.29}$$

$$-\mathbf{a}_1.\boldsymbol{\alpha}_1 + \boldsymbol{\alpha}_1.\mathbf{a}_3 - \mathbf{a}_1.\boldsymbol{\alpha}_3 = 0 \tag{3.1.30}$$

$$\frac{\mathbf{a}_1^2}{2} + \frac{\boldsymbol{\alpha}_1^2}{2} + \frac{\mathbf{a}_3^2}{2} + \frac{\boldsymbol{\alpha}_3^2}{2} = 1 \tag{3.1.31}$$

$$\mathbf{b}_1.\boldsymbol{\beta}_1 = 0 \;\; ; \quad \mathbf{b}_1^2 = \boldsymbol{\beta}_1^2 \;\; ; \quad \frac{1}{2}\left(\mathbf{b}_1^2 + \boldsymbol{\beta}_1^2\right) = 1. \tag{3.1.32}$$

There are six 3-vectors to find, making an initial total of 18 components. Some can be removed immediately by an appropriate choice of axes. We will call the axes $x$, $y$ and $z$ for clarity. Firstly, the $x$-axis is chosen to lie along the direction $\mathbf{a}'(0)$. This gives

$$\mathbf{a}_1 + \mathbf{a}_3 = (1, 0, 0). \tag{3.1.33}$$

We now rotate around the $x$-axis until the $z$-component of $\mathbf{a}_3$ vanishes, which fixes the axes completely. We can then write in full generality:

$$\mathbf{a}_3 = c(\sin\phi, -\cos\phi, 0) \;\; ; \;\; \mathbf{a}_1 = (1 - c\sin\phi, c\cos\phi, 0). \tag{3.1.34}$$

Next, the first constraint (3.1.27), that $\boldsymbol{\alpha}_3$ and $\mathbf{a}_3$ must be perpendicular and the same length, may now be applied, giving

$$\boldsymbol{\alpha}_3 = c(\sin\theta\cos\phi, \sin\theta\sin\phi, \cos\theta). \tag{3.1.35}$$

This leaves five equations for $\mathbf{a}$, (3.1.28-3.1.31), of which four are independent. This allows one to solve for the 3 components of $\boldsymbol{\alpha_1}$, and the fourth equation gives a constraint on the parameters $c$, $\phi$ and $\theta$, leaving effectively two free parameters in the solution. Eventually the result is,

$$\boldsymbol{\alpha}_1 = \left(-3c\sin\theta\cos\phi, \sin\theta(1 - 3c\sin\phi), \cos\theta\sin\phi - \frac{c}{\cos\theta}(1 - 3\sin^2\theta)\right), \tag{3.1.36}$$

$$c = \frac{1}{2}\cos^2\theta\,(\sin\phi \pm 1)\,. \tag{3.1.37}$$

This completes the solution for $\mathbf{a}$. When finding $\mathbf{b}$, none of the freedom of axis-choice remains. However, there will generically be a point at which $\mathbf{a}'$ and $\mathbf{b}'$ are equal (see below), and this may be chosen as the point $\mathbf{a}'(0) = \mathbf{b}'(0) = (1, 0, 0)$. This fixes the origins of $\zeta$ and $t$, and means that

$$\mathbf{b}_1 = (1, 0, 0). \tag{3.1.38}$$

The constraints (3.1.32) clearly imply that $\mathbf{b}_1$ and $\boldsymbol{\beta}_1$ must be orthogonal unit vectors. Thus $\boldsymbol{\beta}_1$ is simply a unit vector in the $y$-$z$ plane,

$$\boldsymbol{\beta}_1 = (0, \cos\lambda, \sin\lambda). \tag{3.1.39}$$

The full solution can then be constructed from the 3-vectors, according to (3.1.25,3.1.26), and has 3 free parameters: $\theta$, $\phi$ and $\lambda$, so it is a 3D space of solutions.

In Section 2.4, 3 important features of cosmic string loop behaviour were described, namely cusps, self-intersections and kinks. We now discuss these properties in greater depth. Self-intersections and cusps will also be investigated in the higher-dimensional context in Sections 3.2.1 and 3.4.

In order to discuss cusps it is useful to consider the meaning of the constraint on $\mathbf{a}'$ and $\mathbf{b}'$ (equation 3.1.15). The constraint implies that $\mathbf{a}'$ and $\mathbf{b}'$ are unit vectors, and it is therefore helpful to think of them as lying on the unit sphere[1]. Since they are each a function of one variable ($\zeta_+$ and $\zeta_-$) each represents some 1-dimensional curve on the unit 2-sphere. They are thus 1-dimensional lines on a 2-dimensional surface, and two such lines, if random, have a finite probability of crossing. In fact when we are in the centre of mass frame, (3.1.14) implies that the average position of $\mathbf{a}'$ and $\mathbf{b}'$ is the origin, and so they cover both halves of the sphere equally and will therefore generically cross.

The point where $\mathbf{a}'$ and $\mathbf{b}'$ intersect corresponds to the rather special event known as a cusp, where a single point on the string instantaneously moves at the speed of light. This is easy to see by calculating the velocity of the string,

$$\mathbf{x} = \frac{1}{2}\left(\mathbf{a}(t-\zeta) + \mathbf{b}(t+\zeta)\right) \tag{3.1.40}$$

$$\Rightarrow \dot{\mathbf{x}} = \frac{1}{2}\left(\mathbf{a}' + \mathbf{b}'\right). \tag{3.1.41}$$

Thus if $\mathbf{a}' = \mathbf{b}'$,

$$|\dot{\mathbf{x}}| = |\mathbf{a}'| = 1, \tag{3.1.42}$$

meaning the string travels at the speed of light at this point. The speed of the string in general is

$$|\dot{\mathbf{x}}| = \frac{1}{2}\sqrt{\mathbf{a}'^2 + \mathbf{b}'^2 + 2\mathbf{a}'.\mathbf{b}'}, \tag{3.1.43}$$

which clearly is less than 1 unless $\mathbf{a}'$ and $\mathbf{b}'$ exactly align. Such an alignment occurs at specific values of both $\zeta_+$ and $\zeta_-$, and therefore specific values of $t$ and $\zeta$. This means

[1]This is known as a Kibble-Turok sphere, as they were the first people to look at cosmic string loop solutions in this way [102]

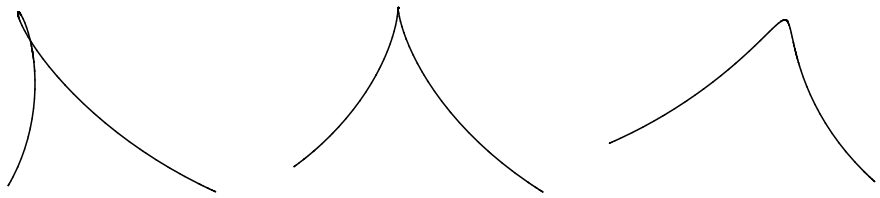

Figure 3.1: A cusp. Left to right: $t = -0.15$, $t = 0$, $t = 0.15$.

it is instantaneous and at a single point on the string, but is nonetheless significant. This is a moment at which the Nambu approximation to some extent breaks down. The finite width of the string and its self-interaction mean that a cosmic string would not travel at *exactly* the speed of light in reality, but nevertheless it would closely approach this limit, making a cusp a powerful and distinctive event.

In the solution (3.1.25,3.1.26), the crossing point of $\mathbf{a}'$ and $\mathbf{b}'$ was chosen to be at $\zeta_+ = \zeta_- = 0$. This effectively fixes the origin of $\zeta_\pm$ or equivalently $\zeta$ and $t$. So at this particular point in the periodic motion of the loop, every time its motion repeats, a cusp occurs. For illustration, snapshots of the string at the moment of the cusp, as well as shortly before and afterwards, are shown in Figure 3.1. A sharp point is seen to form momentarily.

The second important property of a loop solution is whether or not it self-intersects during its period of motion. A loop that self-intersects will break down into smaller loops, while one that does not will be stable and therefore of cosmological interest, since it may be long-lived. To determine whether a given solution self-intersects, values $\zeta_1$, $\zeta_2$, and $t$ must be found such that

$$\mathbf{x}(\zeta_1, t) = \mathbf{x}(\zeta_2, t), \tag{3.1.44}$$

$$\zeta_1 \neq \zeta_2 + 2n\pi. \tag{3.1.45}$$

This will in general be difficult to solve. Given a space of solutions, the general idea is to determine which portions of solution space admit a non-trivial solution to (3.1.44), which indicates the proportion of such loops that will be stable. The first cosmic string loop solutions, found in [102], which contain a single frequency, are shown in this paper to have no self-intersections. The more complex 2-harmonic

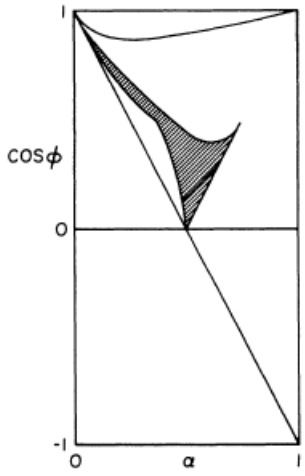


Figure 3.2: Self-intersections for a 2-parameter family of loops (from [41]).

loop solutions are shown to have self-intersections in a finite portion of the solution space, indicating that there are significant proportions of non-self-intersecting and therefore stable loops.

Taking a 2-parameter subset of the solution (3.1.25,3.1.26), to illustrate the point, Figure 3.2 shows a plot of the self-intersection of that family of string loops, produced by Chen, DiCarlo and Hotes [41]. Here the parameter $\phi$ on the plot is equivalent to $\lambda$ from (3.1.39). We set the parameter $\phi$ from the solution (3.1.34,3.1.35,3.1.36) to $\pi/2$, and then rotate in the $y-z$ plane by an angle $x = \theta + \pi/2$. This leaves the form of $\mathbf{b}$ unchanged, and then $\alpha$ in Figure 3.2 is given by $\alpha = c = \cos^2\theta$. It is clear that a large portion of the parameter space has no self-intersection.

Another significant feature that cosmic string loops may possess is a kink. This effectively appears as a sharp corner that propagates along the string, representing a discontinuity in $\mathbf{a}'$ or $\mathbf{b}'$. The string loops discussed so far have all been smooth, but a non-smooth solution is also certainly possible. In reality, such a feature naturally arises when a loop is formed. The loop breaks off from a longer string when two segments of this string cross over and exchange partners, where they will have a non-zero angle and thus form a corner-like feature on the loop. It is possible for such solutions not to have cusps, since a discontinuity in either $\mathbf{a}'$ or $\mathbf{b}'$ allows a solution for which $\mathbf{a}'$ and $\mathbf{b}'$ do not intersect. This can be understood again by thinking of $\mathbf{a}'$ and $\mathbf{b}'$ as curves on the unit sphere. A discontinuity means that there

will be a gap in one of the curves, which can clearly allow a configuration in which the two curves miss each other.

Kinks, as well as cusps, emit a distinctive gravitational wave signal. It is, however, not as strong as the cusp signal, so in the discussion of gravitational wave emission in Chapter 4, the focus will be on cusps. The signal from kinks may however be more important in higher-dimensional scenarios (see Section 4.2.3).

## 3.2 General properties of higher dimensional loops

Now we will look at loops in higher dimensional space, which are relevant in the string theory model of the universe in which spacetime is 10-dimensional, as well as in other models such as braneworlds. In this chapter we consider loops in higher-dimensional flat space, so we use the following simple extension of the Minkowski metric, (3.1.5), to arbitrary dimension, $D$:

$$\eta_{\mu\nu} = diag(1, -1, -1, ..., -1). \tag{3.2.46}$$

In order to be realistic, $(D-4)$ spatial dimensions must somehow be compactified or otherwise hidden. A flat metric allows a toroidal compactification, where the internal dimensions are simply taken to be periodic, so for example we make the identification

$$x^i + \omega = x^i, \tag{3.2.47}$$

where $\omega$ is a constant representing the size of the dimension, and $i > 3$.

The equation of motion, (3.1.10), and its solutions are unchanged except that the spatial vectors $\mathbf{a}$ and $\mathbf{b}$ now have $(D-1)$ components, so the solution is, as before

$$\mathbf{x} = \frac{1}{2}\left(\mathbf{a}(\zeta_-) + \mathbf{b}(\zeta_+)\right), \tag{3.2.48}$$

with

$$|\mathbf{a}'| = |\mathbf{b}'| = 1. \tag{3.2.49}$$

Some of the work presented here is review material from an MSci project [39], and some is new work. The first section discusses the differences in cusps and self-intersections for higher-dimensional loops.

### 3.2.1 Cusps and self-intersections

In this subsection we discuss the qualitative effect of higher dimensional motion on some of the features of loop motion. Much of this is taken from [39].

From Section 3.1, a cusp occurs when the left- and right-moving unit vectors $\mathbf{a}'$ and $\mathbf{b}'$ align. In higher dimensional space, $\mathbf{a}'$ and $\mathbf{b}'$ become unit $(D-1)$-vectors, so we may now consider them to trace out curves on a unit $(D-2)$-sphere. They are thus now 1-dimensional curves in a $(D-2)$-dimensional space, with $(D-2) > 2$, and therefore generically do not intersect. This means that cusps are no longer a generic feature of loops in higher dimensions. In fact, the solutions for which cusps occur will form a set of measure zero in the full space of possible solutions, which would lead to the conclusion that, in reality, cusps would never occur.

This effect has been noted in [39, 125, 162]. However, the reality is that if the curves $\mathbf{a}'$ and $\mathbf{b}'$ come very close to one another, something very like a cusp, which we label a *near cusp event* (NCE), will occur. It is defined as

$$|\mathbf{a}' - \mathbf{b}'| < 2\Delta, \tag{3.2.50}$$

where $\Delta$ is some small parameter. The choice of $\Delta$ simply determines how strong an event we wish to consider. As $\Delta \to 1$, the probability, $P_{NCE}$, of such an event becomes equal to 1, since $\mathbf{a}'$ and $\mathbf{b}'$ are unit vectors and therefore their difference cannot be larger than 2.

Now, in this discussion we consider two different spaces. Firstly, there is the $(D-2)$-dimensional space in which $\mathbf{a}'$ and $\mathbf{b}'$ lie, and for a given loop solution (i.e. a given configuration of $\mathbf{a}'$ and $\mathbf{b}'$), there will be some minimum value of $|\mathbf{a}' - \mathbf{b}'|$ in this space, which determines whether or not a NCE occurs on the loop. Secondly, there is a parameter space of different loop solutions, within which there is some region for which NCE's occur.

The parameter space of solutions may have any number of dimensions. The key feature is the *codimension* of the subset of loops that have exact cusps. For 3 spatial dimensions, all (smooth) loops have cusps, so this "subset" is the whole parameter space. Now consider adding another spatial dimension. Looking at the space in which $\mathbf{a}'$ and $\mathbf{b}'$ lie: they are now, in general, separated along one axis. A shift

in either $\mathbf{a}'$ or $\mathbf{b}'$ along this axis can change a general loop solution to one with a cusp. Such a shift may be described by a shift in a single parameter in solution space. Thus, the solutions with cusps are a codimension-1 subspace of the total parameter space of loops. Similarly, adding another extra dimension means a shift in two parameters is generally required to bring $\mathbf{a}'$ and $\mathbf{b}'$ together, so with two extra dimensions, the codimension of solution space with cusps is 2, and in general, the codimension is the number of extra dimensions, $(D-4)$.

The set of loops that contain NCE's may be pictured as a thickening of the set that contains exact cusps, so it is now a region of finite volume in the parameter space of loops. If $\epsilon$ is the thickness of the region, for a codimension-$n$ subspace of loops with exact cusps, the volume of the region of NCE's will be proportional to $\epsilon^n$, or in our case, $\epsilon^{D-4}$.

We make the assumption that a shift in the minimum distance $|\mathbf{a}' - \mathbf{b}'|$ corresponds linearly to a shift in the parameter space of solutions. Then $\epsilon$ is proportional to $\Delta$, the cut-off for a NCE. This should generally (although not certainly) be possible to engineer by changing the parameters used to describe the solutions. Then we expect that the probability of a loop containing an NCE goes like $P_{NCE} \propto \Delta^{D-4}$.

The constant of proportionality can be estimated by measuring the cusp event parameter for a set of randomly generated loop solutions [39], and also by following a few different paths in parameter space and plotting $\Delta$ along these paths [126]. Although these methods depend on the parameter choices, different parametrisations were used in each case and the proportionality was consistently found to be of order 1, so we have

$$P_{NCE} \simeq \Delta^{D-4}. \tag{3.2.51}$$

The way in which the gravitational wave signal from an NCE differs from that of an exact cusp is described in Chapter 4. The difference in the appearance of the actual string is shown in Figure 3.3. Here $|\mathbf{a}' - \mathbf{b}'| = 0.01$. The NCE corresponds to a slight "rounding" of the exact cusp.

As discussed in Section 2.7, the existence of extra dimensions means that two segments of string that appear to intersect in 3D may in fact miss each other in the internal space. If one considers the width of the string to be negligible compared

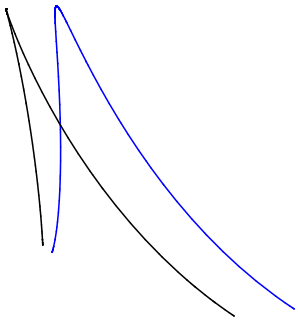

Figure 3.3: An exact cusp (black) and a near cusp event (blue), where the difference corresponds to a slight parameter shift away from a 3D solution.

with the size of the internal space, the probability of a string self-intersecting is also negligible. However, taking into account the finite width of the string, the probability of self-intersection is suppressed by a volume factor (see equation (2.7.29)),

$$\frac{V_{min}}{V_\perp}, \tag{3.2.52}$$

where $V_{min} \sim \delta^n$ is the space that two strings must come within in order to interact, and $V_\perp \sim \omega^n$ is the volume of the internal space. Here $\delta$ is the string width, $\omega$ is the width of the internal dimensions, and $n$ is the number of internal dimensions, $n = (D-4)$.

Note that the existence of kinks, which correspond to discontinuities in $\mathbf{a}'$ or $\mathbf{b}'$, is not fundamentally affected by the higher-dimensional nature of the motion.

### 3.2.2 Winding

This subsection contains new work on the effect of internal winding on loops of cosmic string.

With toroidally compactified internal dimensions, (3.2.47), there is the possibility that a string may extend a long way "into" the internal dimensions. Once its length extends further than the width of the extra dimension, it simply comes back to where it started, but there is no reason it shouldn't continue, and wrap around the internal space many times. One result of this is to increase its chances to self-intersect, which, if it wraps enough times, will eventually result in the string intercommuting and

breaking off, providing an approximate restriction on the possible internal extent of the string.

There is also the possibility that a string may wrap the internal dimensions in such a way that it cannot be unwound. This is known as a non-trivial *winding*. The effect of this is to reduce the average velocity of the string compared with the un-wound case. This can be thought of as reducing the kinetic energy of the string by trapping some of its energy in the internal length.

For a solution without winding we can write $\mathbf{a}$ and $\mathbf{b}$ as a sum of harmonics

$$\mathbf{a} = \sum_n \left(\mathbf{a}_n \sin(n\zeta_-) + \boldsymbol{\alpha}_n \cos(n\zeta_-)\right) \frac{1}{n}, \tag{3.2.53}$$

$$\mathbf{b} = \sum_n \left(\mathbf{b}_n \sin(n\zeta_+) + \boldsymbol{\beta}_n \cos(n\zeta_+)\right) \frac{1}{n}. \tag{3.2.54}$$

In order to include winding we choose one component of $\mathbf{a}$ and $\mathbf{b}$ not to be periodic (say the 4th component) but to transform as follows:

$$a^4(\zeta_- - 2\pi) = a^4(\zeta_-) + \omega, \tag{3.2.55}$$

$$b^4(\zeta_+ + 2\pi) = b^4(\zeta_+) + \omega, \tag{3.2.56}$$

where $\omega$ represents the size of the extra dimension. Again, the period of $\zeta$ has been rescaled to $2\pi$. In order to achieve this we include the following term in the 4th component (as well as the harmonics, (3.2.53,3.2.54)),

$$\frac{\omega(\zeta \mp t)}{2\pi} = \mp \frac{\omega\zeta_\mp}{2\pi}. \tag{3.2.57}$$

The presence of such a term reduces the average speed of the string, as follows. The velocity is

$$\dot{\mathbf{x}} = \frac{1}{2}\left(\mathbf{a}'(\zeta_-) + \mathbf{b}'(\zeta_+)\right) \tag{3.2.58}$$

$$\Rightarrow \dot{\mathbf{x}}^2 = \frac{1}{4}\left(\mathbf{a}'^2 + \mathbf{b}'^2 + 2\mathbf{a}'.\mathbf{b}'\right) = \frac{1}{2} + \frac{1}{2}\mathbf{a}'.\mathbf{b}'. \tag{3.2.59}$$

If there is no winding, $\mathbf{a}'$ and $\mathbf{b}'$ are entirely composed of harmonics in $\zeta_-$ and $\zeta_+$, repsectively. In order to find the average velocity we integrate over both of these variables, from 0 to $2\pi$, and divide by $(2\pi)^2$. This causes these harmonic terms to disappear and leaves the average velocity squared as

$$\bar{\dot{\mathbf{x}}}^2 = \frac{1}{2}. \tag{3.2.60}$$

However, the inclusion of winding terms adds a constant term to the 4th components of $\mathbf{a}'$ and $\mathbf{b}'$, giving us

$$\dot{\mathbf{x}}^2 = \frac{1}{2} + \frac{1}{2}\mathbf{a}'.\mathbf{b}' = \frac{1}{2} - \frac{1}{2}\left(\frac{\omega}{2\pi}\right)^2 + harmonics. \tag{3.2.61}$$

The average of this is now

$$\bar{\dot{\mathbf{x}}}^2_{wind} = \frac{1}{2}\left(1 - \left(\frac{\omega}{2\pi}\right)^2\right). \tag{3.2.62}$$

i.e. the average velocity squared, and therefore the velocity itself, is smaller when the string is wound. It decreases with the size of the extra dimension, which can be thought of as part of the energy being "trapped" in the extra dimension due to the winding of the string, and therefore the larger the extra dimension the more energy is trapped there. The velocity reaches a limit of zero when $\omega = 2\pi$, which corresponds to a stationary trapped loop. Such loops may be a dark matter candidate or a cosmological problem [11].

The gauge choices made in flat spacetime actually fix the total energy of the loop, but this becomes ambiguous now we have introduced another scale, $\omega$. It might be better to think of $\omega$ as being related to the ratio of the size of the wound dimension to the energy of the loop. So when a loop has a high energy, $\omega$ is small, meaning that the part of the length trapped in winding is less significant.

A simple loop solution with winding will be derived in the next section, along with some other exact solutions. The properties of these solutions will be discussed in Section 3.4.

## 3.3 Exact higher-dimensional loop solutions

In this section we derive exact loop solutions in 5-dimensional flat spacetime. The solutions in Sections 3.3.1 and 3.3.2 are based on those of [39], but modify and improve the form of the solutions.

In higher dimensions a wider range of different behaviours become possible than are found in 3 spatial dimensions (by analogy, consider the restriction to the possible dynamics if we reduce a 3D space down to a 2D plane). We choose to add only 1 extra dimension to the 4-dimensional spacetime considered previously, since this is the

simplest case and captures the essential differences in behaviour. The spatial vector containing the dynamics of a cosmic string is a spatial 4-vector, $\mathbf{x} = (x^1, x^2, x^3, x^4)$. We will look at two different string solutions, each containing 2 harmonics, and a third solution in which the string wraps the internal dimension.

We look first at two-harmonic loops, which have been widely studied in the 4D case, for example in [41, 58, 164]. As discussed in Section 3.1, the equation (3.1.24) cannot be solved for unit vectors in 3 spatial dimensions, since it requires that the 4 vectors be mutually orthogonal. In 4 spatial dimensions, however, it is possible to have 4 mutually orthogonal vectors, which means that we may have a two-harmonic loop solution containing any two harmonics. As before, the case where the harmonics are 1 and 3 (or multiples thereof) is qualitatively different from any other combination, since two of the constraints combine, resulting in a different set of equations (3.1.27-3.1.32). This situation may be solved in 3 spatial dimensions, and the derivation of the solution is outlined in Section 3.1. The analogue in 4 spatial dimensions will be derived in a similar fashion in Section 3.3.2, and we will see that it reduces to the 3D solution when the extra dimension is removed.

We take the following ansatz:

$$\mathbf{a}(\zeta_-) = \mathbf{a}_1 \sin(\zeta_-) + \boldsymbol{\alpha}_1 \cos(\zeta_-) + \mathbf{a}_n \frac{1}{n} \sin(n\zeta_-) + \boldsymbol{\alpha}_n \frac{1}{n} \cos(n\zeta_-) \tag{3.3.63}$$

$$\mathbf{b}(\zeta_+) = \mathbf{b}_1 \sin(\zeta_+) + \boldsymbol{\beta}_1 \cos(\zeta_+), \tag{3.3.64}$$

and we shall look first at the case where $n \neq 3$. We label this a "(1,n)(1)" string, where the left bracket gives the harmonics that appear in $\mathbf{a}$ and the right bracket gives the harmonics in $\mathbf{b}$.

### 3.3.1 The case where $n \neq 3$, the (1,n)(1) loop.

Inserting the ansatz, (3.3.63,3.3.64), into the gauge condition (3.1.15), gives a sum of terms in the harmonics 0, 2, $(n-1)$, $(n+1)$ and $2n$. By imposing that the condition must hold for any arbitrary values of $\zeta_-$ and $\zeta_+$, we have, as in Section 3.1,

$$\mathbf{a}_n^2 - \boldsymbol{\alpha}_n^2 = 0 \quad ; \quad \mathbf{a}_1^2 - \boldsymbol{\alpha}_1^2 = 0 \tag{3.3.65}$$

$$\mathbf{a}_1^2 + \boldsymbol{\alpha}_n^2 = 1 \tag{3.3.66}$$

$$\mathbf{a}_1.\mathbf{a}_n = \boldsymbol{\alpha}_1.\boldsymbol{\alpha}_n = \boldsymbol{\alpha}_1.\mathbf{a}_n = \mathbf{a}_1.\boldsymbol{\alpha}_n = \mathbf{a}_n.\boldsymbol{\alpha}_n = \mathbf{a}_1.\boldsymbol{\alpha}_1 = 0 \tag{3.3.67}$$

$$\mathbf{b}_1^2 = \boldsymbol{\beta}_1^2 = 1 \quad ; \quad \mathbf{b}_1.\boldsymbol{\beta}_1 = 0. \tag{3.3.68}$$

At the outset, the $\mathbf{a}$'s, $\boldsymbol{\alpha}$'s, $\mathbf{b}$'s and $\boldsymbol{\beta}$'s contain a total of 24 free parameters. (3.3.65)-(3.3.68) give a total of 12 constraints, reducing the number of free parameters to 12. Choosing the axes removes 6 more parameters, and fixing the origins of $\zeta_+$ and $\zeta_-$ reduces the number by a further 2, leaving the final solution with 4 free parameters. The fact that choosing 4 axes reduces the number of free parameters by 6 stems from the fact that SO(4) has 6 generators.

It is clear from (3.3.67) that the 4 vectors $\mathbf{a}_1$, $\mathbf{a}_n$, $\boldsymbol{\alpha}_1$ and $\boldsymbol{\alpha}_n$ are mutually orthogonal. It seems sensible, then, to pick the axes such that each vector lies along an axis. The remaining constraints, (3.3.65) and (3.3.66) are then easily satisfied. The solution is as follows, with one free parameter, $p$,

$$\mathbf{a}_1 = \begin{pmatrix} \cos p \\ 0 \\ 0 \\ 0 \end{pmatrix} \qquad \boldsymbol{\alpha}_1 = \begin{pmatrix} 0 \\ \cos p \\ 0 \\ 0 \end{pmatrix}, \tag{3.3.69}$$

$$\mathbf{a}_n = \begin{pmatrix} 0 \\ 0 \\ \sin p \\ 0 \end{pmatrix} \qquad \boldsymbol{\alpha}_n = \begin{pmatrix} 0 \\ 0 \\ 0 \\ \sin p \end{pmatrix}. \tag{3.3.70}$$

And so

$$\mathbf{a} = \begin{pmatrix} \cos p \sin(\zeta_-) \\ \cos p \cos(\zeta_-) \\ \frac{1}{n} \sin p \sin(n\zeta_-) \\ \frac{1}{n} \sin p \cos(n\zeta_-) \end{pmatrix}. \tag{3.3.71}$$

As can be seen from (3.3.68), $\mathbf{b}_1$ and $\boldsymbol{\beta}_1$ should be orthogonal unit vectors. The situation is complicated a little by the fact that we have already picked all the axes, so they should point in arbitrary directions. We can achieve this by starting off with $\mathbf{b}$ pointing along the $x^1$-axis, and $\boldsymbol{\beta}$ as the most generic unit vector orthogonal to

it, and then rotating both of them until $\mathbf{b}$ points in an arbitrary direction. So we begin with the following

$$\mathbf{b}_{1,0} = \begin{pmatrix} 1 \\ 0 \\ 0 \\ 0 \end{pmatrix} \quad ; \quad \boldsymbol{\beta}_{1,0} = \begin{pmatrix} 0 \\ \sin\theta\sin\phi \\ \sin\theta\cos\phi \\ \cos\theta \end{pmatrix}. \tag{3.3.72}$$

Rotating $\mathbf{b}_1$ to point in an arbitrary direction requires 3 rotations, resulting in 5 free parameters in the solution, as follows:

$$\mathbf{b} = \begin{pmatrix} \cos\psi\cos\chi \\ \cos\psi\sin\chi \\ \sin\psi\cos\xi \\ \sin\psi\sin\xi \end{pmatrix} \sin(\zeta_+) + \begin{pmatrix} -\cos\chi\sin\psi\sin\theta\cos\phi - \sin\chi\sin\theta\sin\phi \\ -\sin\chi\sin\psi\sin\theta\cos\phi + \cos\chi\sin\theta\sin\phi \\ \cos\xi\cos\psi\sin\theta\cos\phi - \sin\xi\cos\theta \\ \sin\xi\cos\psi\sin\theta\cos\phi + \cos\xi\cos\theta \end{pmatrix} \cos(\zeta_+). \tag{3.3.73}$$

It remains to fix the origins of $\zeta_+$ and $\zeta_-$. As mentioned above, this removes two further degrees of freedom. The origin of $\zeta_+$ may be fixed by choosing a component of either $\mathbf{b}_1$ or $\boldsymbol{\beta}_1$ to be zero. This is clearer if it is done before solving the constraints, so first take $\mathbf{b}$ to be entirely general:

$$\mathbf{b} = \begin{pmatrix} a \\ b \\ c \\ d \end{pmatrix} \sin\zeta_+ + \begin{pmatrix} e \\ f \\ g \\ h \end{pmatrix} \cos\zeta_+. \tag{3.3.74}$$

Consider, for example, the 4th component. A constant shift in the origin of $\zeta_+$, so that $\zeta_+ \to \zeta_+ + \gamma$, transforms the 4th component as follows:

$$d\sin\zeta_+ + h\cos\zeta_+ \to (d\cos\gamma - h\sin\gamma)\sin\zeta_+ + (d\sin\gamma + h\cos\gamma)\cos\zeta_+. \tag{3.3.75}$$

We may then choose $\gamma$ such that either the coefficient of $\sin\zeta_+$ or $\cos\zeta_+$ is zero, which reduces the number of free parameters by 1.[2] For our solution we choose the

[2]Note, we cannot use the same technique with $\mathbf{a}$, because fixing the axes has set the maximum number of parameters to zero already.

4th component of $\mathbf{b}_1$ to be zero, which leaves the most general solution for $\mathbf{b}$ as

$$\mathbf{b} = \begin{pmatrix} \cos\psi\cos\chi \\ \cos\psi\sin\chi \\ \sin\psi \\ 0 \end{pmatrix} \sin\zeta_+ + \begin{pmatrix} -\cos\chi\sin\psi\sin\theta\cos\phi - \sin\chi\sin\theta\sin\phi \\ -\sin\chi\sin\psi\sin\theta\cos\phi + \cos\chi\sin\theta\sin\phi \\ \cos\psi\sin\theta\cos\phi \\ \cos\theta \end{pmatrix} \cos\zeta_+. \tag{3.3.76}$$

Unfortunately it is not known at present how to fix the origin of $\zeta_-$. Note, however, from the solution for $\mathbf{a}$, (3.3.71), that changing the origin of $\zeta_-$ corresponds to an arbitrary rotation in the $(x^1, x^2)$ plane, which also rotates the $(x^3, x^4)$ plane. This may be seen by making the shift, $\zeta_- \to \zeta_- + \lambda$, so that

$$\mathbf{a} = \begin{pmatrix} \cos p(\cos\lambda\sin\zeta_- + \sin\lambda\cos\zeta_-) \\ \cos p(\cos\lambda\cos\zeta_- - \sin\lambda\sin\zeta_-) \\ \frac{1}{n}\sin p(\cos(n\lambda)\sin(n\zeta_-) + \sin(n\lambda)\cos(n\zeta_-)) \\ \frac{1}{n}\sin p(\cos(n\lambda)\cos(n\zeta_-) - \sin(n\lambda)\sin(n\zeta_-)) \end{pmatrix}. \tag{3.3.77}$$

This may provide a clue as to how to remove the final degree of freedom from the solution, for example by a rotation of $\mathbf{b}$, but it is not yet clear how this would be achieved.

### 3.3.2 The case where $n = 3$, the (1,3)(1) loop.

The gauge condition, (3.1.15), gives a sum of terms in the harmonics 0, 2, $(n-1)$, $(n+1)$ and $2n$, but in the case where $n = 3$, two of these are clearly degenerate. This gives us the following set of constraints:

$$\mathbf{a}_3^2 - \boldsymbol{\alpha}_3^2 = 0 \quad ; \quad \mathbf{a}_3.\boldsymbol{\alpha}_3 = 0 \tag{3.3.78}$$

$$\mathbf{a}_1.\mathbf{a}_3 - \boldsymbol{\alpha}_1.\boldsymbol{\alpha}_3 = 0 \quad ; \quad \boldsymbol{\alpha}_1.\mathbf{a}_3 + \mathbf{a}_1.\boldsymbol{\alpha}_3 = 0 \tag{3.3.79}$$

$$\frac{\mathbf{a}_1^2}{2} - \frac{\boldsymbol{\alpha}_1^2}{2} + \mathbf{a}_1.\mathbf{a}_3 + \boldsymbol{\alpha}_1.\boldsymbol{\alpha}_3 = 0 \quad ; \quad -\mathbf{a}_1.\boldsymbol{\alpha}_1 + \boldsymbol{\alpha}_1.\mathbf{a}_3 - \mathbf{a}_1.\boldsymbol{\alpha}_3 = 0 \tag{3.3.80}$$

$$\frac{\mathbf{a}_1^2}{2} + \frac{\boldsymbol{\alpha}_1^2}{2} + \frac{\mathbf{a}_3^2}{2} + \frac{\boldsymbol{\alpha}_3^2}{2} = 1. \tag{3.3.81}$$

Here there are 7 constraints whereas in the $n \neq 3$ case there were 9, so there will be 6 free parameters in the final solution, as opposed to 4. The conditions for $\mathbf{b}$ are

of course unchanged, so we may take the same solution as before in Section 3.3.1, equation (3.3.76). We will now derive a solution for $\mathbf{a}$.

First, orient the $x^1$ axis with the direction of $\mathbf{a}'(0)$, i.e. $\mathbf{a}_1 + \mathbf{a}_3 = (1, 0, 0, 0)$, and then choose the $x^2$ axis to orient $\mathbf{a}_1$ and $\mathbf{a}_3$ in the $(x^1, x^2)$ plane, i.e.

$$\mathbf{a}_1 = (1 - c\sin\alpha, c\cos\alpha, 0, 0) \qquad \mathbf{a}_3 = c\,(\sin\alpha, -\cos\alpha, 0, 0) \tag{3.3.82}$$

We can fix the final two axes by orienting $\boldsymbol{\alpha}_3$ to have a zero $x^4$ component. $\boldsymbol{\alpha}_3$ has to be the same length as and orthogonal to $\mathbf{a}_3$, which means it is

$$\boldsymbol{\alpha}_3 = c\,(\sin\beta\cos\alpha, \sin\beta\sin\alpha, \cos\beta, 0)\,. \tag{3.3.83}$$

Putting this together with the constraints, and writing

$$c = \frac{1}{2}\cos^2\beta(\sin\alpha + \cos\delta) \tag{3.3.84}$$

gives

$$\begin{aligned}
\mathbf{a} \;=\; & \begin{pmatrix} 1 - \frac{1}{2}\cos^2\beta\sin\alpha(\sin\alpha + \cos\delta) \\ \frac{1}{2}\cos^2\beta\cos\alpha(\sin\alpha + \cos\delta) \\ 0 \\ 0 \end{pmatrix} \sin\zeta_- + \\
& \begin{pmatrix} -\frac{3}{2}\cos^2\beta\cos\alpha\sin\beta(\sin\alpha + \cos\delta) \\ \sin\beta(1 - \frac{3}{2}\cos^2\beta\sin\alpha(\sin\alpha + \cos\delta)) \\ \cos\beta\left[\sin\alpha - \frac{1}{2}(\sin\alpha + \cos\delta)(1 - 3\sin^2\beta)\right] \\ \cos\beta\sin\delta \end{pmatrix} \cos\zeta_- + \\
& \frac{1}{6}\cos^2\beta(\sin\alpha+\cos\delta)\begin{pmatrix} \sin\alpha \\ -\cos\alpha \\ 0 \\ 0 \end{pmatrix}\sin 3\zeta_- + \frac{1}{6}\cos^2\beta(\sin\alpha+\cos\delta)\begin{pmatrix} \sin\beta\cos\alpha \\ \sin\beta\sin\alpha \\ \cos\beta \\ 0 \end{pmatrix}\cos 3\zeta_-.
\end{aligned} \tag{3.3.85}$$

The reduction of this back to the 3D solution, (3.1.34,3.1.35,3.1.36,3.1.37), can easily be seen by setting, firstly, $\sin\delta = 0$, which implies that $\cos\delta = \pm 1$. Then making the identifications $\beta \equiv \theta$ and $\alpha \equiv \phi$ (where $\theta$ and $\phi$ are the free parameters in the 3D solution), the solutions are identical. The solution for $\mathbf{b}$ can be identified with

the 3D case, (3.1.38,3.1.39), by setting $\chi = 0$, $\psi = 0$, $\theta = \pi/2$ and $\phi \equiv \lambda$ in equation (3.3.76).

Rotating the 4D solution for $\mathbf{a}$, (3.3.85), by $\alpha$ in the $(x^1, x^2)$ plane leaves the form of $\mathbf{b}$ unchanged, but makes $\mathbf{a}$ a little simpler,

$$\begin{aligned}
\mathbf{a} \;=\; & \begin{pmatrix} \cos\alpha \\ \frac{1}{2}\cos^2\beta(\sin\alpha + \cos\delta) - \sin\alpha \\ 0 \\ 0 \end{pmatrix} \sin\zeta_- + \\
& \begin{pmatrix} \sin\beta(\sin\alpha - \frac{3}{2}\cos^2\beta(\sin\alpha + \cos\delta)) \\ \sin\beta\cos\alpha \\ \cos\beta\left[\sin\alpha - \frac{1}{2}(\sin\alpha + \cos\delta)(1 - 3\sin^2\beta)\right] \\ \cos\beta\sin\delta \end{pmatrix} \cos\zeta_- + \\
& \frac{1}{6}\cos^2\beta(\sin\alpha + \cos\delta) \begin{pmatrix} 0 \\ -1 \\ 0 \\ 0 \end{pmatrix} \sin 3\zeta_- + \frac{1}{6}\cos^2\beta(\sin\alpha + \cos\delta) \begin{pmatrix} \sin\beta \\ 0 \\ \cos\beta \\ 0 \end{pmatrix} \cos 3\zeta_-.
\end{aligned} \tag{3.3.86}$$

As before, it is at present not clear how to fix the origin of $\zeta_-$. The origin of $\zeta_+$ has been fixed in the solution for $\mathbf{b}$, (3.3.76).

### 3.3.3 A loop with winding

Here we consider a loop that winds the internal dimension, where, as discussed in Section 3.2.2, we add the following terms to the 4th components of $\mathbf{a}$ and $\mathbf{b}$,

$$\mp\frac{\omega\zeta_\mp}{2\pi}. \tag{3.3.87}$$

There are of course many possibilities for low harmonic solutions. For simplicity we assume only the first harmonic is present in $\mathbf{b}$, and we will show that in this case the 4th component can contain only the winding term, $\frac{\omega\zeta_+}{2\pi}$. In $\mathbf{a}$, one option is to have the 1st and 5th harmonics appearing in the first 3 components, and the 2nd

harmonic appearing in the 4th component, as follows,

$$\mathbf{a} = \begin{pmatrix} \vec{a}_1 \sin(\zeta_-) + \vec{\alpha}_1 \cos(\zeta_-) + \frac{1}{5}\vec{a}_5 \sin(5\zeta_-) + \frac{1}{5}\vec{\alpha}_5 \cos(5\zeta_-) \\ \frac{1}{2}a_2 \sin(2\zeta_-) + \frac{1}{2}\alpha_2 \cos(2\zeta_-) - \frac{\omega\zeta_-}{2\pi} \end{pmatrix}. \tag{3.3.88}$$

Here, $\vec{a}_1$, $\vec{\alpha}_1$, $\vec{a}_5$ and $\vec{\alpha}_5$ are 3-vectors. Substituting this into the condition $\mathbf{a}'^2 = 1$ gives the following constraints,

$$\frac{1}{2}\vec{a}_1^2 + \frac{1}{2}\vec{\alpha}_1^2 + \frac{1}{2}\vec{a}_5^2 + \frac{1}{2}\vec{\alpha}_5^2 + \frac{1}{2}a_2^2 + \frac{1}{2}\alpha_2^2 = 1 - \left(\tfrac{\omega}{2\pi}\right)^2 \equiv l^2 \tag{3.3.89}$$

$$\vec{a}_5^2 = \vec{\alpha}_5^2 \quad ; \quad \vec{a}_5.\vec{\alpha}_5 = 0 \tag{3.3.90}$$

$$\vec{a}_1.\vec{a}_5 - \vec{\alpha}_1.\vec{\alpha}_5 = 0 \quad ; \quad \vec{a}_1.\vec{\alpha}_5 + \vec{\alpha}_1.\vec{a}_5 = 0 \tag{3.3.91}$$

$$\vec{a}_1^2 - \vec{\alpha}_1^2 + \frac{2\omega}{\pi}a_2 = 0 \quad ; \quad \vec{a}_1.\vec{\alpha}_1 + \frac{\omega}{\pi}\alpha_2 = 0 \tag{3.3.92}$$

$$\vec{a}_1.\vec{a}_5 + \vec{\alpha}_1.\vec{\alpha}_5 + \frac{1}{2}\left(a_2^2 - \alpha_2^2\right) = 0 \quad ; \quad -\vec{a}_1.\vec{\alpha}_5 + \vec{\alpha}_1.\vec{a}_5 - a_2\alpha_2 = 0. \tag{3.3.93}$$

We have already chosen the $x^4$-axis, so it remains to choose the other 3, which we specify by choosing the orthogonal vectors $\vec{a}_5$ and $\vec{\alpha}_5$ to lie in the $x^1$ and $x^2$ directions. Then the constraints give the following solution,

$$\vec{a}_1 = \begin{pmatrix} -\left(\frac{\omega}{\pi}\right)^2 \frac{B^2\cos(2\theta)}{2lk} \\ \left(\frac{\omega}{\pi}\right)^2 \frac{B^2\sin(2\theta)}{2lk} \\ \frac{\omega}{\pi}\sqrt{2B}\sin(\frac{\theta}{2}) \end{pmatrix} \quad ; \quad \vec{\alpha}_1 = \begin{pmatrix} -\left(\frac{\omega}{\pi}\right)^2 \frac{B^2\sin(2\theta)}{2lk} \\ -\left(\frac{\omega}{\pi}\right)^2 \frac{B^2\cos(2\theta)}{2lk} \\ \frac{\omega}{\pi}\sqrt{2B}\cos(\frac{\theta}{2}) \end{pmatrix} \tag{3.3.94}$$

$$\vec{a}_5 = \begin{pmatrix} \frac{lk}{2} \\ 0 \\ 0 \end{pmatrix} \quad ; \quad \vec{\alpha}_5 \begin{pmatrix} 0 \\ \frac{lk}{2} \\ 0 \end{pmatrix} \tag{3.3.95}$$

$$a_2 = -\frac{\omega}{\pi}B\cos\theta \quad ; \quad \alpha_2 = \frac{\omega}{\pi}B\sin\theta. \tag{3.3.96}$$

Here $k = \sqrt{1 - \left(\frac{\omega}{\pi l}\right)^2 B} \pm \sqrt{1 - \left(\frac{\omega}{\pi l}\right)^2 (B + B^2)}$, and $B$ and $\theta$ are free parameters giving the space of solutions. $B$ is positive, and its upper limit is determined by the second term in $k$ (by requiring it to be real).

The left-moving half of the string, $\mathbf{b}$, with one harmonic, can be written as follows:

$$\mathbf{b} = \mathbf{b}_1 \sin\zeta_+ + \boldsymbol{\beta}_1 \cos\zeta_+ + \begin{pmatrix} 0 \\ 0 \\ 0 \\ \frac{\omega\zeta_+}{2\pi} \end{pmatrix}. \tag{3.3.97}$$

From this we find $\mathbf{b}'^2$

$$\begin{aligned}\mathbf{b}'^2 &= \frac{1}{2}\mathbf{b}_1^2(1+\cos(2\zeta_+)) + \frac{1}{2}\boldsymbol{\beta}_1^2(1-\cos(2\zeta_+)) - \mathbf{b}_1.\boldsymbol{\beta}_1\sin(2\zeta_+) \\ &\quad +2\mathbf{b}_{1,4}\cos(\zeta_+)\frac{\omega}{2\pi} - 2\boldsymbol{\beta}_{1,4}\sin(\zeta_+)\frac{\omega}{2\pi} + \frac{\omega^2}{(2\pi)^2} \\ &= 1, \end{aligned} \tag{3.3.98}$$

from which it is clear that the 4th components of $\mathbf{b}_1$ and $\boldsymbol{\beta}_1$ must be zero, and the remaining 3-vectors must be orthogonal, with length $l$. It is also possible to fix the origin of $\zeta_+$ by choosing one of the components of $\mathbf{b}_1$ to be zero (see Section 3.3.2). So we have

$$\mathbf{b} = \begin{pmatrix} l\cos\psi\sin(\zeta_+) - l\sin\psi\cos\phi\cos(\zeta_+) \\ l\sin\psi\sin(\zeta_+) + l\cos\psi\cos\phi\cos(\zeta_+) \\ l\sin\phi\cos(\zeta_+) \\ \frac{\omega\zeta_+}{2\pi} \end{pmatrix}, \tag{3.3.99}$$

where $\phi$ and $\psi$ are free parameters.

## 3.4 Cusps on the exact solutions

In this section we examine some of the properties of the solutions derived in Section 3.3. We will look in particular at exact cusps.

In order to solve for a cusp, we look at 3 of the 4 components of $\mathbf{a}'$ and $\mathbf{b}'$, and set $\mathbf{a}' = \mathbf{b}'$ for each component. Since they are unit vectors, solving this for 3 components means the 4th will automatically be satisfied. With the 3 components, we use the first two to find $\zeta_+$ and $\zeta_-$ in terms of the parameters of the solution, and the third component is used to find a constraint on the parameter space, which is the main focus of interest. We will now solve these for each of the solutions.

### 3.4.1 Cusps on (1,5)(1)

In order to look at an explicit solution, we choose $n = 5$ in the solution (3.3.71,3.3.76). We choose to look at the first, third and fourth components of $\mathbf{a}'$ and $\mathbf{b}'$, since these

are the simplest. So the conditions to solve are the following:

$$\cos p \cos\zeta_- = \cos\psi\cos\chi\cos\zeta_+ + (\cos\chi\sin\psi\sin\theta\cos\phi + \sin\chi\sin\theta\sin\phi)\sin\zeta_+ \tag{3.4.100}$$

$$\sin p \cos(5\zeta_-) = \sin\psi\cos\zeta_+ - \cos\psi\sin\theta\cos\phi\sin\zeta_+ \tag{3.4.101}$$

$$-\sin p \sin(5\zeta_-) = -\cos\theta\sin\zeta_+. \tag{3.4.102}$$

We find that

$$\sin\zeta_+ = \frac{\sin p}{\cos\theta}\sin(5\zeta_-) \tag{3.4.103}$$

$$\cos^2(5\zeta_-) = \frac{-b \pm \sqrt{b^2-4ac}}{2a} \tag{3.4.104}$$

where

$$a = \left(\sin^2 p\left(1-\cos^2\psi\cos^2\phi\tan^2\theta - \frac{\sin^2\psi}{\cos^2\theta}\right)\right)^2 + 4\sin^4 p\cos^2\psi\sin^2\phi\tan^2\theta \tag{3.4.105}$$

$$\begin{aligned} b &= 2\sin^2 p\left(1-\cos^2\psi\cos^2\phi\tan^2\theta - \frac{\sin^2\psi}{\cos^2\theta}\right)\left(\sin^2 p\cos^2\psi\cos^2\phi\tan^2\theta\right. \\ &\quad \left. -\sin^2\psi\left(1-\frac{\sin^2 p}{\cos^2\theta}\right)\right) - 4\sin^4 p\cos^2\psi\sin^2\phi\tan^2\theta \end{aligned} \tag{3.4.106}$$

$$c = \left(\sin^2 p\cos^2\psi\cos^2\phi\tan^2\theta - \sin^2\psi\left(1-\frac{\sin^2 p}{\cos^2\theta}\right)\right)^2. \tag{3.4.107}$$

Finally we constrain the paramter, $\chi$, to be a function of the other parameters, thus giving the region of parameter space for which exact cusps occur,

$$\cos\chi = \frac{\cos p\cos\zeta_-(\cos\psi\cos\zeta_+ + \sin\psi\sin\theta\cos\phi\sin\zeta_+) + \sqrt{X}}{(\cos\psi\cos\zeta_+ + \sin\psi\sin\theta\cos\phi\sin\zeta_+)^2 + \sin^2\theta\sin^2\phi\sin^2\zeta_+}. \tag{3.4.108}$$

$$\begin{aligned} X &= ((\cos\psi\cos\zeta_+ + \sin\psi\sin\theta\cos\phi\sin\zeta_+)^2 + \sin^2\theta\sin^2\phi\sin^2\zeta_+)\sin^2\theta\sin^2\phi\sin^2\zeta_+ \\ &\quad -\sin^2\theta\sin^2\phi\sin^2\zeta_+\cos^2 p\cos^2\zeta_-. \end{aligned} \tag{3.4.109}$$

Substituting the values of $\zeta_+$ and $\zeta_-$ from equations (3.4.103,3.4.104) gives an expression for $\chi$ entirely in terms of the other parameters, although it is a very cumbersome formula. The following plots, Figure 3.4, show exact cusps on some 2D cross-sections through the parameter space (parameter values are chosen that somewhat simplify the situation).

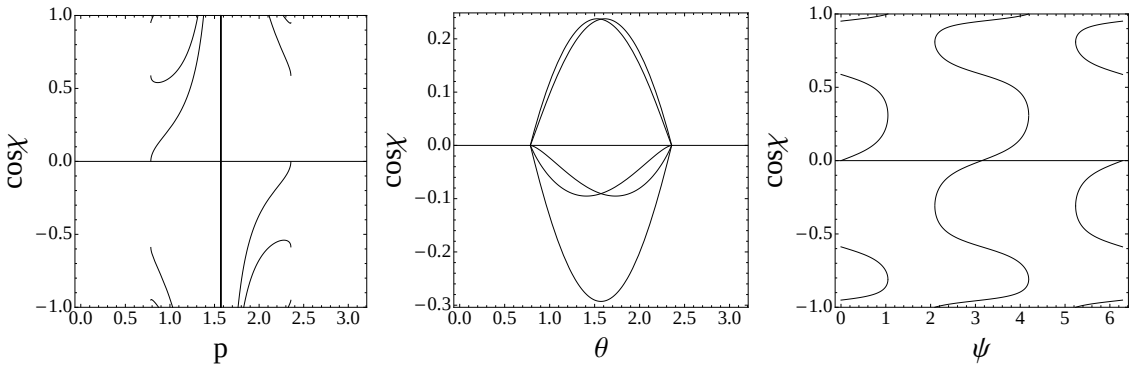


Figure 3.4: Exact cusps for the loop with harmonics 1 and 5. Parameter choices are, from left to right: 1) $\phi = 0$, $\psi = \pi/2$, $\theta = \pi/4$. 2) $\phi = 3\pi/4$, $\psi = \pi/2$, $p = \pi/4$. 3) $\phi = 0$, $p = \pi/3$, $\theta = 0$. The length of the internal dimension, $\omega$, is taken as 0.1.

### 3.4.2 Cusps on (1,3)(1)

As with the (1,n)(1) solution, for this we look at the first, third and fourth components of $\mathbf{a}'$ and $\mathbf{b}'$. We now have the following constraints to solve,

$$\cos\beta\cos\zeta_- = \cos\psi\cos\chi\cos\zeta_+ + (\cos\chi\sin\psi\sin\theta\cos\phi + \sin\chi\sin\theta\sin\phi)\sin\zeta_+ \tag{3.4.110}$$

$$\sin p\cos(5\zeta_-) = \sin\psi\cos\zeta_+ - \cos\psi\sin\theta\cos\phi\sin\zeta_+ \tag{3.4.111}$$

$$-\sin p\sin(5\zeta_-) = -\cos\theta\sin\zeta_+. \tag{3.4.112}$$

The situation this time is not so easy. Again, writing $\zeta_+$ in terms of $\zeta_-$ is simple enough,

$$\sin\zeta_+ = \frac{\cos\beta\sin\delta}{\cos\theta}\sin\zeta_-. \tag{3.4.113}$$

Also, again we can solve equation (3.4.110) for $\chi$ in terms of the other parameters, since it will simple be quadratic in $\chi$. However, solving for $\zeta_-$ in terms of the other parameters is more difficult, since it is given by a cubic equation. This will have a solution, but it will not be very enlightening to look at. Instead, we simply illustrate the cusps in various cross-sections of the parameter space, with a few simple choices of parameter slice, Figure 3.5. It is worth noting that the parameter spaces for all of these loop solutions are so large that the sections shown cannot give a good picture

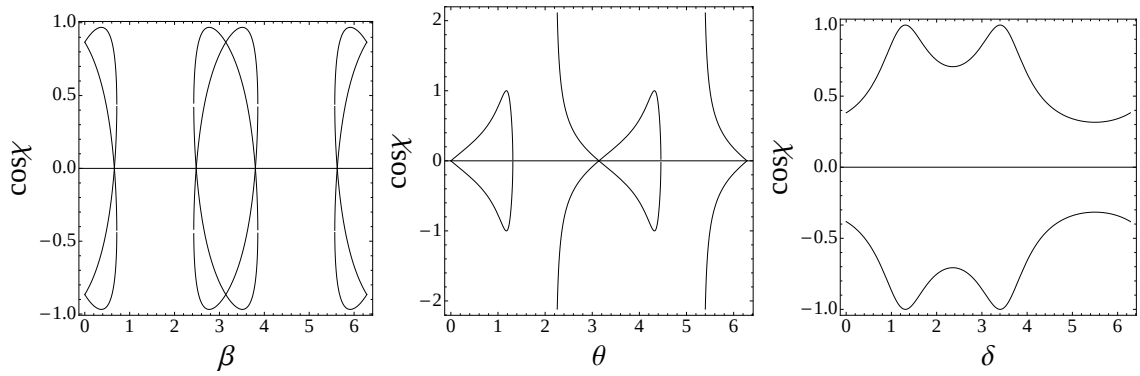


Figure 3.5: Exact cusps for the loop with harmonics 1 and 3. Parameter choices are, from left to right: 1) $\phi = 0$, $\psi = \pi/2$, $\theta = \pi/4$, $\delta = \pi/3$, $\alpha = 2\pi/3$. 2) $\phi = 3\pi/4$, $\psi = 0$, $\beta = 0$, $\delta = \pi/4$, $\alpha = \pi/2$. 3) $\phi = 0$, $\psi = 0$, $\theta = \pi/4$, $\beta = 0$, $\alpha = \pi/4$. The length of the internal dimension, $\omega$, is taken as 0.1.

of the whole parameter space. Instead it is hoped to give a general idea of the sort of patterns that appear.

### 3.4.3 Cusps on the loop with winding

The exact loop solution with winding, equations (3.3.94-3.3.96,3.3.99), is a little simpler to solve for exact cusps. We consider again the first, third and fourth components of $\mathbf{a}'$ and $\mathbf{b}'$. The following conditions must be solved,

$$a_2 \cos(2\zeta_-) - \alpha_2 \sin(2\zeta_-) - \frac{\omega}{2\pi} = \frac{\omega}{2\pi}, \tag{3.4.114}$$

$$-l \sin\phi \sin\zeta_+ = \frac{\omega}{\pi}\sqrt{2B}\left(\sin\frac{\theta}{2}\cos\zeta_- - \cos\frac{\theta}{2}\sin\zeta_-\right), \tag{3.4.115}$$

$$l\cos\psi\cos\zeta_+ + l\sin\psi\cos\phi\sin\zeta_+ =$$

$$-\left(\frac{\omega}{\pi}\right)^2 \frac{B^2}{2lk}(\cos(2\theta)\cos\zeta_- - \sin(2\theta)\sin\zeta_-) + \frac{lk}{2}\cos(5\zeta_-). \tag{3.4.116}$$

This gives $\zeta_+$ and $\zeta_-$ as

$$\zeta_- = \frac{1}{2}(\theta + \arccos(-1/B)) \tag{3.4.117}$$

$$\zeta_+ = \arcsin\left(\pm\frac{\omega}{\pi l}\frac{1}{\sin\phi}\sqrt{2(B - 1/B)}\right). \tag{3.4.118}$$

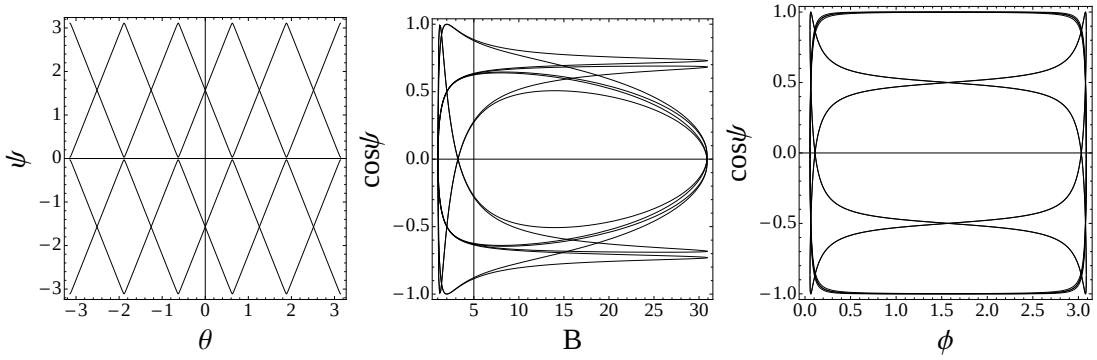


Figure 3.6: Exact cusps for the loop with winding. Parameter choices are, from left to right: 1) $B = 1$. 2) $\theta = 0$, $\sin\phi = 1$. 3) $\theta = 0$, $B = 2$. The length of the internal dimension, $\omega$, is taken as 0.1.

Then, from (3.4.116), we can write $\psi$ as a function of the other parameters in the solution, as follows

$$\cos\psi = \frac{\pm_1 l\sqrt{1-\left(\frac{\omega}{\pi l}\right)^2 \frac{2(B-1/B)}{\sin^2\phi}}Y \pm_2 \frac{\omega}{\pi\tan\phi}\sqrt{2(B-\frac{1}{B})(l^2-\left(\frac{\omega}{\pi}\right)^2 2(B-\frac{1}{B})-Y^2)}}{l^2-\left(\frac{\omega}{\pi}\right)^2 2(B-\frac{1}{B})} \tag{3.4.119}$$

$$Y = \frac{l}{2k}\left(\left(\frac{\omega}{\pi l}\right)^2 B^2\cos\left(\frac{5\theta}{2}+\frac{1}{2}\arccos\left(-\frac{1}{B}\right)\right)+k^2\cos\left(\frac{5\theta}{2}+\frac{5}{2}\arccos\left(-\frac{1}{B}\right)\right)\right) \tag{3.4.120}$$

The plots on Figure 3.6 show, again, a few slices through the parameter space. Notably, the second plot shows a set of loops for which a significant proportion may have NCE's, if the condition for an NCE is to be close to a solution for an exact cusp, as the cusp lines are densely packed in some parts of the parameter space.

# Chapter 4

# Gravitational wave signals

One of the most distinctive observational signals of cosmic strings is their emission of gravitational waves. These are particularly strongly emitted from oscillating loops of cosmic string, which is the main reason for the focus of this thesis on closed loops. In this Chapter we first review the calculation, made by Damour and Vilenkin [55], of the distinctive bursts of gravitational waves from cusps on cosmic strings. We then go on to modify this calculation to account for the presence of extra dimensions. This shows a significant modification to the observable amplitude. This work was published in [125, 126], and performed in collaboration.

## 4.1 Gravitational signals in 4D

This section reviews the calculation by Damour and Vilenkin [55] of the distinctive gravitational wave signal from cosmic string cusps (cusps are discussed in Section 3.1). A cusp is an instantaneous and singular event, which leads to its emitting a sharp burst of gravitational waves. The waveform will be calculated first, in Section 4.1.1. Secondly, the total signal from a cosmological network of loops, which could be detected on Earth, is calculated in Section 4.1.2.

### 4.1.1 Waveform in the local wave zone

In [55], the gravitational waves are treated as small perturbations about a background metric, and modelled using the linearised Einstein equations. Firstly, their

form is calculated in the local wave zone of the cosmic string. This is the region where one is far from the gravitational source (i.e. the loop of string), and yet at a small enough distance that cosmological expansion has no significant effect, i.e. a distance $r$ that is much less than the Hubble radius. In this region, the background is taken to be flat, and $g_{\mu\nu}^{local} = \eta_{\mu\nu} + h_{\mu\nu}$, where $\eta_{\mu\nu}$ is flat spacetime (equation 3.1.5) and $h_{\mu\nu}$ is the metric perturbation representing the gravitational waves.

After solving the linearised Einstein equations in this region, Damour and Vilenkin study the high frequency modes in the gravitational waveform. High frequency waves are only emitted by cusps and kinks, giving them distinct signals.

Firstly we will describe how the linearised Einstein equations are solved. Defining the trace-reversed metric perturbation, $\bar{h}_{\mu\nu} = h_{\mu\nu} - \frac{1}{2}h\eta_{\mu\nu}$, and taking the harmonic gauge, $\partial^\nu \bar{h}_{\mu\nu} = 0$, the equation to solve is

$$\Box \bar{h}_{\mu\nu} = -16\pi G T_{\mu\nu}, \tag{4.1.1}$$

where $T_{\mu\nu}$ is the energy-momentum tensor of the cosmic string. The generic solution to such an equation is given approximately by

$$\bar{h}_{\mu\nu}(\mathbf{x}, t) = \frac{4G}{r} \sum_{\omega} e^{-i\omega(t-r)} T_{\mu\nu}(\mathbf{k}, \omega) + \mathcal{O}\left(\frac{1}{r^2}\right), \tag{4.1.2}$$

where $\omega$ is the frequency of the gravitational wave, and $\mathbf{k} = \omega\mathbf{n}$, where $\mathbf{n}$ is the direction of emission, so $k^\mu = (\mathbf{k}, \omega)$ is the 4-frequency of the wave. Then in order to find a specific solution, the energy-momentum tensor for a cosmic string is required. This we will calculate from the Nambu action (2.3.16). A general energy-momentum tensor is given by

$$T_{\mu\nu} = \frac{2}{\sqrt{-g}} \frac{\delta \mathcal{L}}{\delta g^{\mu\nu}}, \tag{4.1.3}$$

where $\mathcal{L}$ is the Lagrangian density. In this case, the Lagrangian density from the Nambu action is

$$\mathcal{L} = -\mu \int d^2\zeta \sqrt{-\gamma} \delta^4[y^\lambda - x^\lambda(t, \zeta)]. \tag{4.1.4}$$

Here the delta-function ensures that when integrating this over the full spacetime coordinates ($y^\mu$), the action is confined to the worldsheet of the string (given by $x^\mu(t, \zeta)$). We work in flat space and with all of the gauge choices made in Section

3.1 (equations 3.1.3,3.1.8 and $\zeta^0 = t$), that is the transverse, temporal, conformal gauge, where

$$\frac{\delta\sqrt{-\gamma}}{\delta g^{\mu\nu}} = \frac{\delta\sqrt{-x'^2\dot{x}^2}}{\delta g^{\mu\nu}} = \frac{\delta\sqrt{-g^{\rho\sigma}\dot{x}_\rho\dot{x}_\sigma g^{\lambda\tau}x'_\lambda x'_\tau}}{\delta g^{\mu\nu}} = -\frac{1}{2}\left(\sqrt{\frac{-x'^2}{\dot{x}^2}}\dot{x}_\mu\dot{x}_\nu - \sqrt{\frac{\dot{x}^2}{-x'^2}}x'_\mu x'_\nu\right). \tag{4.1.5}$$

Then due to the conformal gauge (equation 3.1.8), the square roots are simply equal to 1. For flat space, $\sqrt{-g} = 1$, and so from (4.1.3) the energy-momentum tensor becomes

$$T_{\mu\nu} = \mu\int d^2\zeta\left(\dot{x}_\mu\dot{x}_\nu - x'_\mu x'_\nu\right)\delta^4[y^\lambda - x^\lambda(t,\zeta)]. \tag{4.1.6}$$

Then for the general solution (4.1.2), the Fourier transform of the energy-momentum tensor is required so that we have $T_{\mu\nu}(\mathbf{k},\omega)$. After taking the Fourier transform, Damour and Vilenkin put the general solution for a flat-space string loop (3.1.11) into the energy-momentum tensor. Re-writing in terms of the null worldsheet coordinates $\zeta_-$ and $\zeta_+$ (see Section 3.1), the Fourier transformed energy-momentum tensor separates into a product of two integrals, as follows:

$$T_{\mu\nu}(\mathbf{k}_m,\omega_m) = \frac{\mu}{l}I_+^{(\mu}I_-^{\nu)} \tag{4.1.7}$$

where

$$I_\pm^\mu = \int_0^l d\zeta_\pm\dot{x}_\pm^\mu e^{-(i/2)k_m.x_\pm} \tag{4.1.8}$$

and $x_-^\mu = (\mathbf{a},1)$, $x_+^\mu = (\mathbf{b},1)$. The frequency $\omega_m = 4\pi m/l$, where $4\pi/l$ is the fundamental frequency, since the period of the motion is $l/2$ (see Section 3.1).

The distinctive feature of both cusps and kinks is high-frequency radiation. Looking at the integral $I_\pm^\mu$ in the limit of large $m$, we see that the exponent will become very large, and the value of $I_\pm^\mu$ will approach zero due to this rapidly oscillating term. In fact, it generally approaches zero exponentially with an increase in $m$. There are a few specific situations in which this does not happen. The first is if there is a stationary point in the exponent, $k_{m\mu}x_\pm^\mu$. This occurs when $k_{m\mu}\dot{x}_\pm^\mu = 0$. Since $k^\mu$ and $\dot{x}_\pm^\mu$ are null vectors (the latter due to (3.1.15)), this occurs when $k^\mu$ and $\dot{x}_\pm^\mu$ align. Of course, if this occurs in only one of $I_\pm^\mu$, the other will decay exponentially with $m$, and therefore so will the energy-momentum tensor, which is the product of the two. Thus in order to have a slower decay at high frequencies, both $\dot{x}_+^\mu$ and $\dot{x}_-^\mu$

must simultaneously align with $k^\mu$. This corresponds to an alignment of $\mathbf{a}'$ and $\mathbf{b}'$, and therefore to a cusp. The direction of $k^\mu$ corresponds to the direction from which the gravitational radiation is observed − thus, the increased high-frequency radiation is observed only along a particular direction, corresponding to the direction of emission from the cusp.

The second way in which the integrals $I^\mu_\pm$ avoid going exponentially to zero at high frequencies is to have a discontinuity in $\dot{x}^\mu_\pm$ (which appears in the integrand, (4.1.8)). If this is the case for one of $\dot{x}^\mu_\pm$, this integral tends to zero more slowly with $m$, and the other integral tends to zero more slowly when $k^\mu$ is lined up with $\dot{x}^\mu_\mp$. Thus there is always a direction, $k^\mu$, in which an increase in higher frequency radiation is observed. This set of conditions corresponds to a kink, which is a permanent feature propagating along a loop, explaining why it is always observed in some direction.

We will focus now on cusps. The increased emission of higher-frequency radiation along the direction of a cusp does not require an *exact* alignment of $\dot{x}^\mu_+$ and $\dot{x}^\mu_-$. In fact it can be shown that a cusp beams high-frequency gravitational waves approximately in a cone around its direction of emission. In order to look at the cusp waveform, Damour and Vilenkin now use a Taylor expansion of the general solution (3.1.11) around a cusp, and calculate the metric perturbation $\bar{h}_{\mu\nu}$ as a function of frequency. They must then sum over frequencies to see it as a function of time.

They use the following truncated Taylor expansion around a cusp

$$x^\mu_\pm(\zeta_\pm) = l^\mu\zeta_\pm + \frac{1}{2}\ddot{x}^\mu_\pm\zeta^2_\pm + \frac{1}{6}x^{(3)\mu}_\pm\zeta^3_\pm \tag{4.1.9}$$

$$\dot{x}^\mu_\pm(\zeta_\pm) = l^\mu + \ddot{x}^\mu_\pm\zeta_\pm + \frac{1}{2}x^{(3)\mu}_\pm\zeta^2_\pm, \tag{4.1.10}$$

where $l^\mu$ is the direction of the cusp, and the derivatives on the RHS of the equations are evaluated at the cusp.

Then taking into account that $\dot{x}_\pm$ are null vectors, and that $k^\mu$ must be parallel to $\dot{x}^\mu_\pm$, as well removing some gauge freedom, their effective integrals $I^\mu_\pm$ become

$$I^\mu_\pm \simeq \ddot{x}^\mu_\pm \int_{\zeta_0}^{\zeta_0+l} d\zeta_\pm\zeta_\pm \exp\left(\frac{i}{12}\omega_m\ddot{x}^2_\pm\zeta^3_\pm\right). \tag{4.1.11}$$

Then the approximate value of this integral is calculated for a given value of $m$ and $\ddot{x}^{\mu}_{\pm}$. This gives

$$T^{\mu\nu}(\mathbf{k}_m, \omega_m) = -C\frac{\pi\mu}{l(2\pi|f|)^{4/3}}e^{2\pi i f t_c}A^{(\mu}_{+}A^{\nu)}_{-}, \tag{4.1.12}$$

with

$$C = \frac{4\pi(12)^{4/3}}{\left[3\Gamma\left(\frac{1}{3}\right)\right]^2}\ ; \quad A^{\mu}_{\pm} = \frac{\ddot{x}^{\mu}_{\pm}}{|\ddot{x}_{\pm}|^{4/3}}. \tag{4.1.13}$$

For consistency with Damour and Vilenkin's expressions, in (4.1.12) we have now written $f = \omega_m/(2\pi)$, and added in the term $e^{2\pi i f t_c}$ where previously the time of the cusp event, $t_c$, was set to zero.

The time-dependent waveform is given, by equation (4.1.2), as a sum over frequencies. Approximating the sum as an integral gives the waveform as an integral of $T_{\mu\nu}$ (equation (4.1.12)) over frequency. If we look simply at $t$ rather than $(t-r)$ in (4.1.2), the time-dependence is

$$h \sim |t - t_c|^{\frac{1}{3}}. \tag{4.1.14}$$

The absolute value indicates a sharp change at $t = t_c$. The tidal force associated with this gravitational disturbance, which is proportional to $|t-t_c|^{-5/3}$, clearly shows that the waveform has a spike at this point.

To find the amplitude of the gravitational wave we now define the *logarithmic Fourier transform*, such that a function $F(t)$ is written as a function of frequency, $f$, as follows

$$F(f) \equiv |f| \int dt e^{2\pi i f t} F(t). \tag{4.1.15}$$

We then consider the amplitude of the gravitational wave perturbation, $h = |h_{\mu\nu}|$. Using the logarithmic Fourier transform we can show that

$$h_{\mu\nu}(f) \simeq \frac{2Gl|f|}{r}T_{\mu\nu}(\mathbf{k}_m, \omega_m). \tag{4.1.16}$$

To find the amplitude more explicitly we approximate the numerical coefficients in $T_{\mu\nu}$ (equation (4.1.12)) to the nearest order of magnitude, and also replace $|\ddot{x}_{\pm}| \simeq 2\pi/l$. The latter may be deduced by assuming that the cosmic string loop contains only low harmonics, which means it will contain sine and cosine terms with the argument $(2\pi n\zeta_{\pm}/l)$ since the period in $\zeta_{\pm}$ is $l$, and for low harmonics $n \sim 1$. These

terms will be multiplied by vectors, and since we know that $\mathbf{a}'$ and $\mathbf{b}'$ have length 1, we deduce that their derivatives have length $2\pi/l$. This gives the amplitude $h(f)$ as

$$h(f) \sim \frac{G\mu l}{r(|f|l)^{1/3}}. \tag{4.1.17}$$

This form is used in the rest of the calculation.

Damour and Vilenkin then calculate the approximate angle around the direct line of emission for which this gravitational wave burst is observed. They do this by introducing a slight angular difference, $\theta$, between the line of sight, $k^\mu$ and the direction of the cusp, $l^\mu$ (see equation (4.1.10)). They write $l^\mu = \hat{k}^\mu + \delta^\mu$, where $\hat{k}^\mu$ is the unit wavevector $(\boldsymbol{n}, 1)$. Then, using the fact that $\hat{k}^\mu$ and $l^\mu$ are null vectors, it follows that

$$\delta^2 = 2(1 - \cos\theta) \simeq \theta^2, \tag{4.1.18}$$

where $\theta$ is the angle between the cusp direction and the line of sight. We then recalculate the Taylor expansion around the cusp, (4.1.10), in terms of $\hat{k}^\mu$, and therefore the approximate form of $I^\mu_\pm$ (see equations (4.1.8) and (4.1.11)), which gives that

$$I^\mu_\pm \simeq \int d\zeta_\pm (\delta^\mu + \ddot{x}^\mu_\pm) \exp\left(\frac{i}{2}\omega_m \left(\frac{1}{2}\delta^2\zeta_\pm + \frac{1}{2}\delta_\nu \ddot{x}^\nu_\pm \zeta^2_\pm + \frac{1}{6}(\ddot{x}_\pm)^2\zeta^3_\pm\right)\right). \tag{4.1.19}$$

In order to look for a stationary point in the exponent, which is characteristic of a cusp, it must be differentiated and set equal to zero,

$$\frac{1}{2}\delta^2 + \delta_\mu \ddot{x}^\mu_\pm \zeta_\pm + \frac{1}{2}(\ddot{x}_\pm)^2\zeta^2_\pm = 0. \tag{4.1.20}$$

This is a quadratic equation which only has real solutions when the discriminant,

$$(\delta_\mu \ddot{x}^\mu_\pm)^2 - \delta^2(\ddot{x}_\pm)^2, \tag{4.1.21}$$

is non-negative. Generically it will be negative unless $\delta$ is zero, so the stationary point disappears as we move away from the exact direction of a cusp, and the integral will once again tend exponentially to zero at large frequencies. However, we see that when $\delta$ is very small, the third term in the exponent dominates $I^\mu_\pm$ (4.1.19), and it will therefore be well-approximated by the exact cusp waveform. The approximate

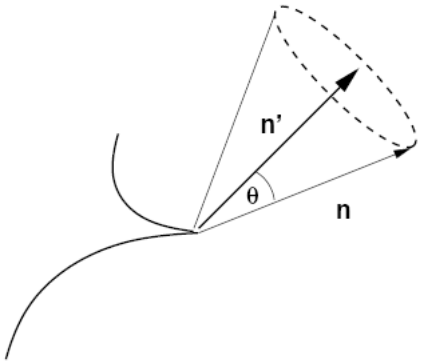


Figure 4.1: Sketch of high-frequency gravitational wave emission from a cusp (from [126]).

cut-off between the two regimes will be when the first term in (4.1.20) becomes comparable in size with the third, i.e.

$$\theta_{divide} \simeq |\ddot{x}_{\pm}|\zeta_{\pm} \tag{4.1.22}$$

(using $\delta^2 \simeq \theta^2$). The cut-off in $\zeta_{\pm}$ comes from the fact that most of the contribution to the integral (4.1.11) is from the region where the exponent is $\lesssim 1$, i.e.

$$\zeta_{\pm} \lesssim \left(\frac{12}{\omega_m |\ddot{x}_{\pm}|}\right)^{\frac{1}{3}}. \tag{4.1.23}$$

Using, once again, $|\ddot{x}_{\pm}| \simeq 2\pi/l$, along with the substitution $f = \omega_m/(2\pi)$, now gives

$$\theta_{divide} \simeq \left(\frac{2}{l|f|}\right)^{\frac{1}{3}}. \tag{4.1.24}$$

Therefore a cusp beams high-frequency radiation in a cone with angle $\theta_{divide}$, illustrated on Figure 4.1.

### 4.1.2 Cosmological signal

Having calculated the waveform, the propagation of the gravitational waves through a cosmological background is then considered, followed by a sum over the signal from all redshifts, to give the gravitational wave background that would be observed at a detector from a network of loops.

The assumption is made that its wavelength is much smaller than the scale of variation of the background metric. The following spatially flat expanding universe

is taken as a background

$$ds^2 = a^2(\eta)\left(d\eta^2 - d\hat{r}^2 - \hat{r}^2 d\Omega_{II}^2\right). \tag{4.1.25}$$

The $1/r$ fall-off of the gravitational wave amplitude in (4.1.17) is replaced by $1/(a(\eta)\hat{r})$. The waveform itself is parallelly propagated along the null geodesic that the gravitational wave follows. Considering the wavefunction in the Fourier domain, i.e. as a function of frequency, $f$, we have that

$$f_{emitted} = (1+z) f_{recieved} \tag{4.1.26}$$

where $z$ is the redshift, defined by $(1+z) = a_{recieved}/a_{emitted}$. Thus we simply replace $f$ with $(1+z)f$ in the gravitational waveform (4.1.17), as well as replacing $1/r$ with $1/(a\hat{r})$. $a_{recieved}\hat{r}$, the physical distance, can be written as a function of redshift in terms of the angular diameter distance, $D_A$,

$$a_{received}\hat{r} = a_{recieved}\int_{t_e}^{t_0}\frac{dt}{a} = \int_0^z \frac{dz}{H} = (1+z)D_A(z) \tag{4.1.27}$$

where $t_0$ is the current age of the universe, and $H = \dot{a}/a$ is the Hubble parameter. This gives the Fourier-transformed gravitational wave amplitude as a function of frequency and redshift

$$h(f) \sim \frac{G\mu l}{((1+z)fl)^{1/3}}\frac{1}{(1+z)D_A(z)}. \tag{4.1.28}$$

Since $\theta_{divide}$ depends on frequency, it also gains a dependence on redshift according to (4.1.26).

Using a simple model for a string network in which it scales with the cosmological horizon, the average length of loops produced at a given time also scales, $l \sim \alpha t$, where $\alpha$ is a constant. Re-writing $t$ as a function of redshift allows the loop length, $l$, in the gravitational wave amplitude (4.1.28) also to be replaced by a function of redshift. $t(z)$ depends on the scale factor, $a$, which changes as we move from the radiation era to the matter era. Damour and Vilenkin therefore use an interpolating function to define $t(z)$,

$$t \simeq t_0 \varphi_l(z) \tag{4.1.29}$$

$$\varphi_l(z) = (1+z)^{-3/2}(1+z/z_{eq})^{-1/2} \tag{4.1.30}$$

where $z_{eq}$ is the redshift at matter-radiation equality. Therefore $l$ is replaced by $\alpha t_0 \varphi_l(z)$ in both the amplitude (4.1.28) and in the angular cut-off, $\theta_{divide}$, where it also appears (equation (4.1.24)). This gives the amplitude as

$$h(f) \sim \frac{G\mu(t_0\alpha\varphi_l)^{2/3}}{(1+z)^{4/3} f^{1/3} D_A(z)}, \tag{4.1.31}$$

and the cut-off angle (neglecting the factor of $2^{1/3}$ for an order of magnitude estimate),

$$\theta_{divide} \simeq \left((1+z) f \alpha t_0 \varphi_l\right)^{-\frac{1}{3}}. \tag{4.1.32}$$

Now, in order to sum over the contribution from all loops, an estimate of the total number density of loops at a given redshift is required. In the simple scaling solution, the number density goes like

$$n_l \sim \frac{1}{\alpha t^3}. \tag{4.1.33}$$

After introducing a constant, $c$, representing the average number of cusps per loop oscillation period, an estimate may be made of the rate of gravitational wave bursts from cusps in the redshift interval $dz$. This is then integrated over redshift to provide the rate of gravitational wave busts of a given frequency that will be detected on earth. Then, putting in a reasonable detection rate, of, for example, one per year, one can calculate the dominant redshift interval for this frequency, and from this the amplitude of such bursts.

The rate of gravitational wave bursts in the redshift interval $dz$ will be approximately

$$d\dot{N} \sim \frac{1}{4}\theta_m^2 (1+z)^{-1} \nu(z) dV(z) \tag{4.1.34}$$

where we have redefined $\theta_m \equiv \theta_{divide}$, to reflect the fact that it depends on frequency. The first term, $\frac{1}{4}\theta_m^2$, represents the fraction of cusp events for which the beaming cone will lie in the direction of observation. The factor of $(1+z)$ comes from the link between the observation time (entering the rate, $\dot{N}$, on the LHS) and the time of emission. $\nu(z)$ is the number of cusp events per unit spacetime volume, and $dV$ is the proper spatial volume between redshifts $z$ and $z+dz$. The number of cusps per unit volume is given by,

$$\nu(z) \sim \frac{c}{T_l} n_l(t), \tag{4.1.35}$$

where $n_l \sim \alpha^{-1}t^{-3}$ is the number density of loops, $c$ is the number of cusps per loop period and $T_l = l/2 \sim \alpha t/2$ is the time-period of a loop. As a result,

$$\nu(z) \sim 2c\alpha^{-2}t^{-4} \sim 2c\alpha^{-2}(t_0\varphi_l(z))^{-4}. \tag{4.1.36}$$

Finally, the proper spatial volume, $dV$, is equal to the incremental volume $4\pi\hat{r}^2 d\hat{r}$ multiplied by the volume factor $a^3$, at the relevant redshift. Thus $dV$ takes the following form (see equation (4.1.27)),

$$dV = 4\pi D_A(z)^2 \frac{dz}{(1+z)H(z)}. \tag{4.1.37}$$

We then put all of this together into (4.1.34) to find $d\dot{N}$. Integrating over redshift from 0 to $z_m$ then gives $\dot{N}$ as a function of frequency, $f$, and redshift, $z_m$. It is apparent that higher rates come from large redshifts where the density of loops was much larger. Inverting this relation gives the dominant redshift interval for a given frequency and rate. The amplitude will be higher from smaller redshifts (as this means we are closer to the source of emission), which corresponds to smaller rates, and thus we choose $\dot{N}$ as small as is reasonable for detection, to find the maximum amplitude of gravitational wave bursts. The amplitude is then given by (4.1.31).

It will be most informative to illustrate the result with plots, rather than giving it explicitly. Damour and Vilenkin take the number of cusps per loop, $c$, at two different values, and plot the amplitude as a function of the parameter $\alpha$, which is proportional to the cosmic string tension, $\mu$. They take a detection rate of 1 per year and look at the frequencies corresponding to the LIGO detector [4], and the planned space-based gravitational wave detector, LISA [5]. The plots, Figures 4.2 and 4.3 show that these signals may be detectable by both detectors. They also show the kink signal, which is a few orders of magnitude smaller than that from cusps. It is clear from the plots that the signals should be easily distinguishable above the gravitational wave background.

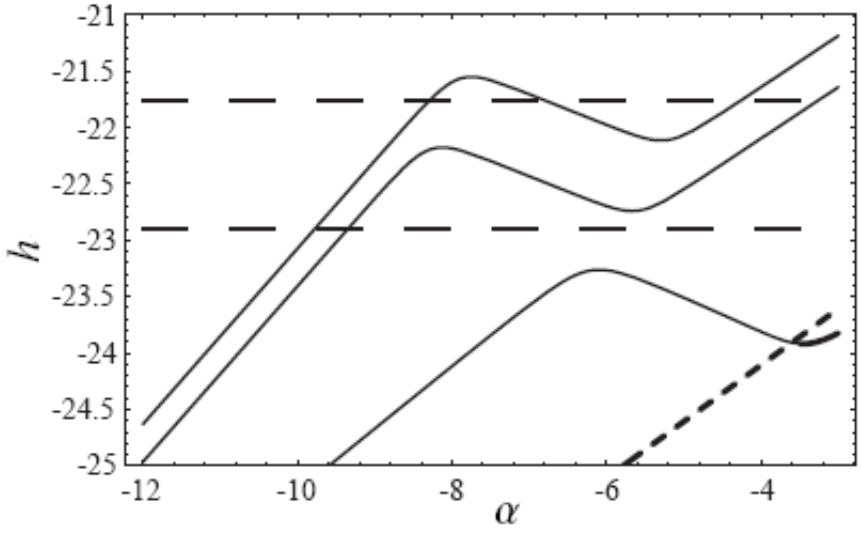


Figure 4.2: The amplitude from gravitational wave bursts at the LIGO frequency, plotted as a function of $\alpha$, which is proportional to the cosmic string tension, and unknown. The top solid line is from cusps with cusp probability $c = 1$, the second line is from cusps with $c = 0.1$, and the bottom line is from kinks. The dotted horizontal line is the detectable level and the diagonal dotted line is the gravitational wave background level. The numbers on the axes are powers of 10. From [55].

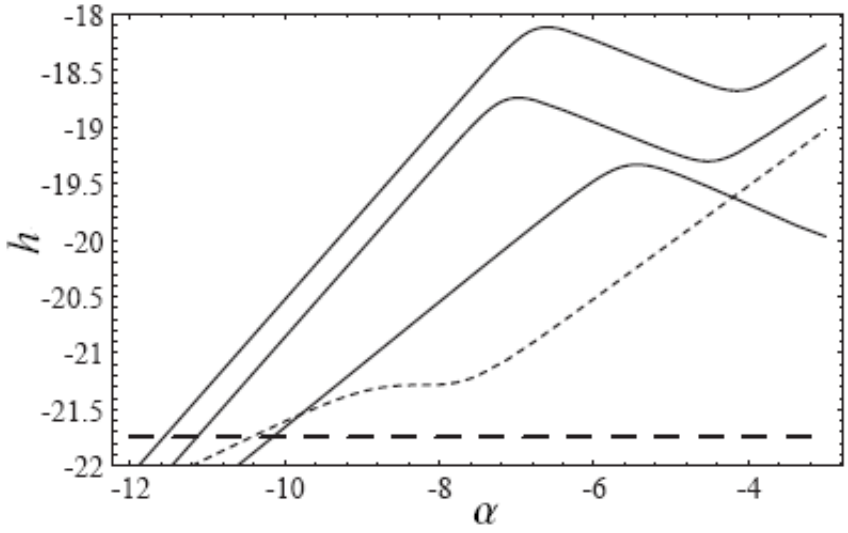


Figure 4.3: The amplitude from gravitational wave bursts at the LISA frequency, plotted as a function of $\alpha$. All lines are identified as above (Figure 4.2). From [55].

## 4.2 Gravitational waves from cusps in higher dimensions

In this Section we extend the calculation from Section 4.1 to higher dimensions. This work is published in [125, 126].

### 4.2.1 Including all loop solutions

There are two main differences to the signal that arise in higher dimensions. As discussed in Section 3.2.1, the probability of an exact cusp occurring on a loop is strictly zero, and so only "near cusp events" (NCE's) occur, and with a much reduced probability. Thus, firstly, when calculating the gravitational waveform we must take into account that the cusp will not be exact. Secondly, the reduced probability of NCE's leads to a large reduction in the overall cosmological signal.

We will look firstly at the comparison of an NCE with an exact cusp. We re-define the $(D-1)$-dimensional spatial vectors representing the cosmic string as $\mathbf{A}(\zeta_-)$ and $\mathbf{B}(\zeta_+)$, and the 3D-parts remain as $\mathbf{a}$ and $\mathbf{b}$. In order to compare with an exact cusp, we assume that the string velocities in the internal dimensions are small, and thus

$$\mathbf{a}'^2 = 1 - a^2 \tag{4.2.38}$$

$$\mathbf{b}'^2 = 1 - b^2, \tag{4.2.39}$$

where $a$ and $b$ are small. We define the separation vector,

$$\boldsymbol{d} = \frac{1}{2}(\mathbf{a}' - \mathbf{b}'), \tag{4.2.40}$$

and the NCE may be defined to lie in the direction

$$\frac{\mathbf{a}' + \mathbf{b}'}{|\mathbf{a}' + \mathbf{b}'|}. \tag{4.2.41}$$

This direction lies between $\mathbf{a}'$ and $\mathbf{b}'$, so it is the closest that $\hat{k}^\mu$ can get to aligning with both. Then, looking along the line of the NCE is equivalent to looking in a direction $\hat{k}^\mu$ that has an angle $\theta \simeq |\boldsymbol{d}|$ away from an exact cusp. We look at the condition for an NCE,

$$|\mathbf{A}' - \mathbf{B}'| = 2\Delta, \tag{4.2.42}$$

and assuming $a$ and $b$ are small gives that $|\boldsymbol{d}| \simeq \Delta$. This therefore results in a reduction in the opening angle of the cone of emission of gravitational waves, of the form

$$\theta_\Delta \simeq \theta_m - \Delta \simeq \left(\frac{2}{lf}\right)^{\frac{1}{3}} - \Delta. \tag{4.2.43}$$

Note that this provides a cut-off at very high frequencies, where the opening angle goes to zero and thus no radiation above a given frequency is emitted.

In this calculation the fact that the 4D vectors are not exactly null is not actually taken into account. The velocities in the internal dimensions are assumed to be small and thus effectively ignored. Looking at the full signal in D-dimensions, the D-dimensional vectors are in fact null, so this is equivalent to ignoring the part of the radiation that goes into the internal dimensions and assuming it is all emitted into 4D.

The second effect is the introduction of the NCE probability, which is shown in Section 3.2.1 to be

$$P_{NCE} \simeq \Delta^{D-4} = \Delta^n, \tag{4.2.44}$$

where we define $n$ as the number of "extra" dimensions. In order to find the event rate, $\dot{N}$, we must integrate over all possible NCE's, i.e. all possible values of $\Delta$. Therefore, instead of simply multiplying $\dot{N}$ by a cusp probability, $c$, as in Damour and Vilenkin's calculation, we multiply it by a probability density function and integrate over $\Delta$. The probability density is the derivative,

$$\mathcal{C}(\Delta) \simeq n\Delta^{n-1}. \tag{4.2.45}$$

We therefore have

$$\frac{\partial^2 \dot{N}_{NCE}}{\partial z \partial \Delta} = n\Delta^{n-1}\theta_\Delta^2 \frac{n_l(z)}{PT_l(z)} \frac{D_A(z)^2}{(1+z)^2 H(z)}. \tag{4.2.46}$$

Here the number density, $n_l$, has been enhanced by a factor of $1/P$, where $P$ is the reconnection probability (see Section 3.2.1). This is done because the network density is said to be enhanced via a reduction in correlation volume, $L \propto P$ (see Section 2.7 and references [61, 93], but see also [144]). This means the parameter $\alpha$ in equation (4.1.33) also gains a factor of $P$. Focussing on the $\Delta$-dependent parts

from (4.2.46), the integral over $\Delta$ gives

$$\int_0^{\theta_m} n\Delta^{n-1}(\theta_m - \Delta)^2 d\Delta = \frac{2\theta_m^{n+2}}{(n+1)(n+2)}. \tag{4.2.47}$$

We integrate up to $\theta_m$ because this is the cut-off where the opening angle, $\theta_\Delta$, goes to zero, meaning that no gravitational radiation of that frequency is emitted (see equation (4.2.43)).

Finally, the event rate, differentiated by redshift, becomes

$$\frac{\partial \dot{N}}{\partial z} = \frac{2\pi\theta_m(z)^{n+2}}{(n+1)(n+2)} \frac{n_l(z)}{PT_l(z)} \frac{D_A(z)^2}{(1+z)^2 H(z)}. \tag{4.2.48}$$

This can then be integrated over redshift and used to compare the amplitude of gravitational wave bursts from a higher-dimensional network of loops with the 4D case studied by Damour and Vilenkin in [55]. The plots in Figures 4.4 and 4.5 show Damour and Vilenkin's result compared directly with the results for 1, 3 and 6 internal dimensions. It is clear that there is approximately an order of magnitude reduction in the signal with the addition of each extra dimension. This is mainly due to the reduced probability of NCE's, which is a large effect that dominates over a possible enhancement to the signal from the increased number of loops. The increased density of loops is due to a reduced reconnection probability, which is taken as $P = 10^{-3}$.

The reduction in amplitude of the signal due to internal motion takes the signals out of the observable range for most cases. For the LISA detector, with one internal dimension, $n = 1$, the signal is likely be observable (compare Figures 4.5 and 4.3), but for large numbers of internal dimensions it appears unlikely that cosmic strings could be observed.

We have also plotted the rate of gravitational wave bursts, $\dot{N}$, at the minimum observable amplitude for the LIGO detector, on Figure 4.6. The horizontal line on the plot represents a detection rate of 1 per year, below which it is unlikely that a detection will be made. This plot makes it clear that with the addition of even one extra dimension, the cusp signal will no longer be detectable by LIGO. This calculation was made using the method in [155].

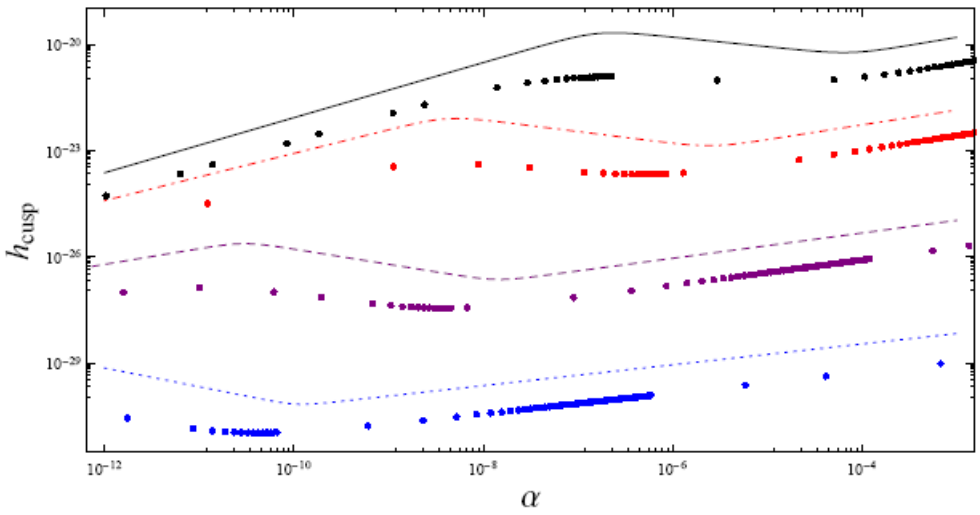


Figure 4.4: The amplitude from gravitational wave bursts at the LIGO frequency, $f$ =150Hz. The individual dots are exact numerical redshift integrations, using $t(z)$, $D_A(z)$ from the concordance cosmology. The solid, dotted or dashed lines use the interpolating functions in [55]. Black lines, Damour and Vilenkin's result (4D); red, $n = 1$ (1 extra dimension); purple, $n = 3$; blue, $n = 6$. Reconnection probability $P = 10^{-3}$. Figure from [125].

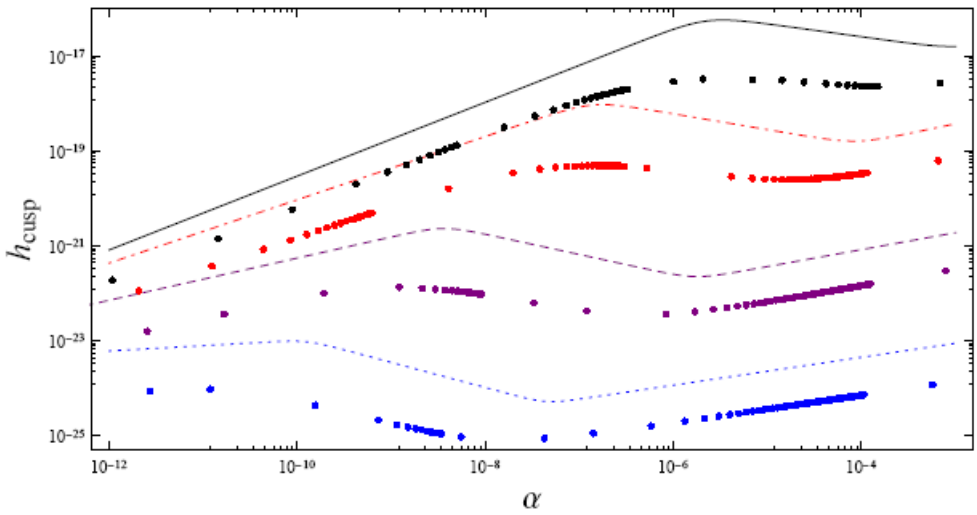


Figure 4.5: The amplitude from gravitational wave bursts at the LISA frequency, $f$ = 3.9mHz. All lines identified as above (Figure 4.4), and $P = 10^{-3}$. Figure from [125].

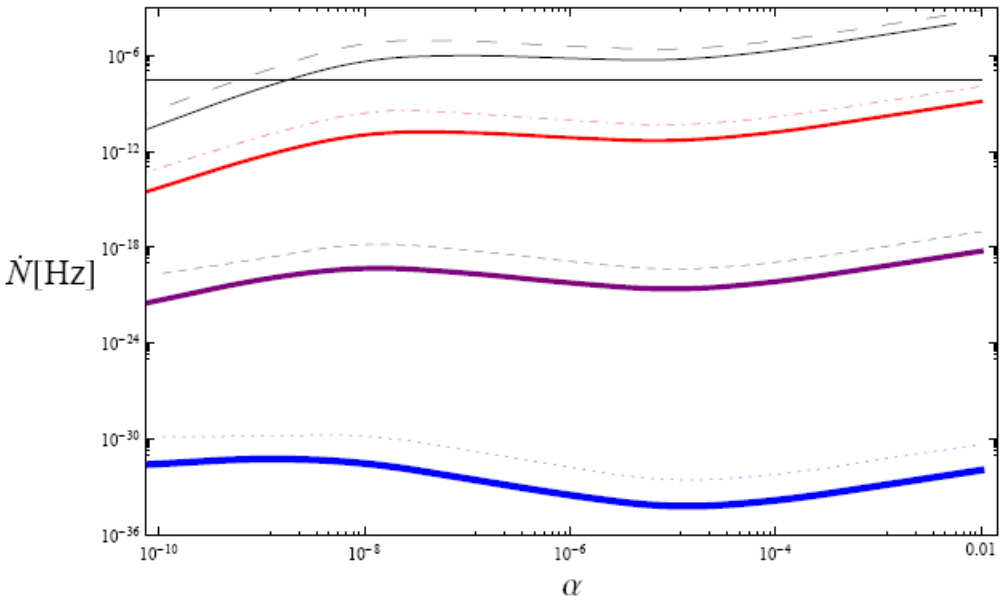


Figure 4.6: The rate of gravitational wave bursts at the LIGO frequency, $f = 150$Hz, at the amplitude $10^{-21}s^{-1/3}$. The lines are colour-coded as above (Figure 4.4), except that now the thick solid lines are the numerical results. Reconnection probability $P = 10^{-3}$. Horizontal line shows a detection rate of 1 per year. Figure from [126].

### 4.2.2 Eliminating unrealistic loops

In Section 4.2.1 we assumed that a string may be in any part of the full parameter space of higher-dimensional solutions. However, this may not in fact be realistic, and in this section we look at perhaps a more realistic set of loops, and show that the reduction in signal due to extra dimensions may not be as dramatic as first proposed.

It is realistic to assume that there is little motion in the internal dimensions. As well as arguments that strings would be confined at the bottom of a warped throat (see next chapter), it is physically realistic that movement will be limited due to the small size of these dimensions. How much movement can occur depends essentially on the ratio between the size of the internal dimension and the width of a cosmic string. While it is possible for them to move a long way into the internal dimensions by wrapping them many times, once they have wrapped several times, they become much more likely to self-intersect, and thus to break off (See Section 3.2). Therefore, we now assume that the realistic loop solutions are those that lie close to the 4D

trajectories, and therefore close to loop solutions with exact cusps.

We model this by restricting $\Delta$ to be smaller than a certain limit, $\Delta_0$, i.e. restricting the possible NCE's to be in some way close to exact cusps. When integrating over $\Delta$ (for example equation (4.2.47)), the maximum limit of integration will be $\Delta_0$. The probability density must be renormalised accordingly, so that

$$\int_0^{\Delta_0} \mathcal{C}(\Delta) d\Delta = 1 \tag{4.2.49}$$

which gives the probability density,

$$\mathcal{C}(\Delta) = \frac{n}{\Delta_0^n} \Delta^{n-1}. \tag{4.2.50}$$

Therefore, the integral that appears in $\dot{N}$ becomes

$$\int_0^{min\{\Delta_0, \theta_m\}} \mathcal{C}(\Delta) \left(\theta_m(z) - \Delta\right)^2 = \theta_m(z)^2 \mathcal{F}_n \left[\frac{\theta_m}{\Delta_0}\right] \tag{4.2.51}$$

$$\mathcal{F}_n[x] = \frac{2x^n}{(n+1)(n+2)} \Theta(1-x) + \left(1 - \frac{2n}{(n+1)x} + \frac{n}{(n+2)x^2}\right) \Theta(x-1) \tag{4.2.52}$$

where $\Theta$ is the Heaviside step function. This changes the previous result only when $\Delta_0 < \theta_m$. In that case, as the ratio $\theta_m/\Delta_0$ becomes larger, the function $\mathcal{F}_n$ approaches 1, and so the integral approaches its 4D form, $\theta_m^2$. This shows that restricting the strings to be closer and closer to 4D solutions removes the effect of the internal dimensions.

As discussed above, the amount of movement in the internal dimensions is related to the ratio of string width to the internal dimension size. It is therefore reasonable to have $\Delta_0$ depend on this ratio. We could perhaps use a heuristic expression such as $\Delta_0 \simeq 1 - \frac{\delta}{\omega}$, where $\delta$ is the string width and $\omega$ the size of the internal dimension, but further study of string motion is required to model this dependence accurately.

We have plotted the rate of gravitational wave bursts at the minimum detectable amplitude, with various values of $\Delta_0$. It is shown that the rate significantly increases, back towards the 4D value, as we restrict $\Delta_0$. Depending on the amount of internal motion, then, it is possible that cosmic strings may still be detectable if extra dimensions exist. However, the effect is still dramatic. Figure 4.8 fixes $\Delta_0 = 10^{-3}$ and shows the rate with different numbers of internal dimensions. We see that with one internal dimension the signal may be detectable by LIGO, but that there is still an

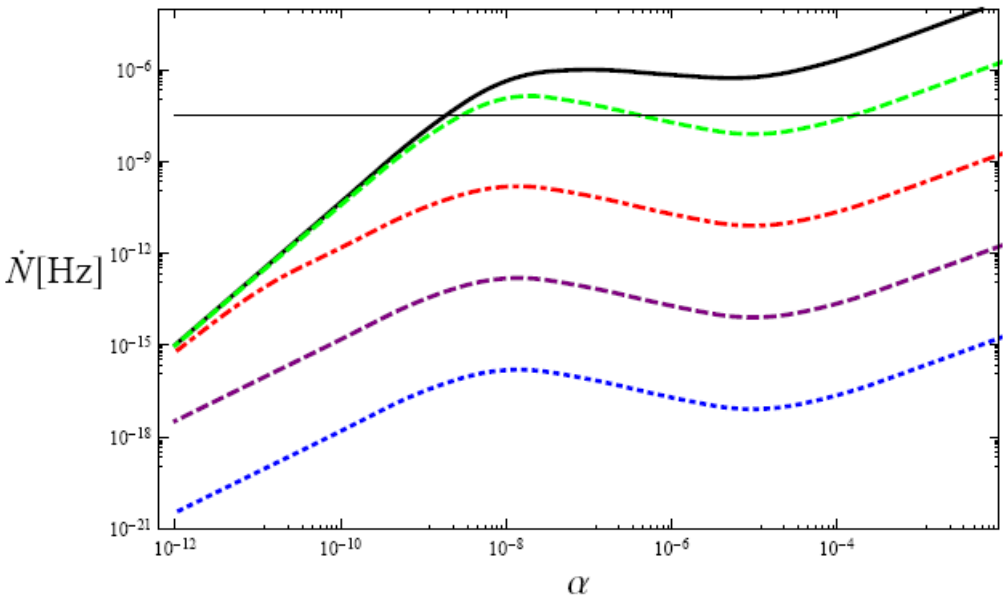


Figure 4.7: The rate of gravitational wave bursts at the LIGO frequency, $f = 150$Hz, at the amplitude $10^{-21}s^{-1/3}$. Here each line is at a different value of $\Delta_0$, and the number of extra dimensions is fixed at $n = 3$. From the top: Black, 4D result. Green, $\Delta_0 = 10^{-4}$. Red, $\Delta_0 = 10^{-3}$. Purple, $\Delta_0 = 10^{-2}$. Blue, $\Delta_0 = 10^{-1}$. As above, $P = 10^{-3}$, and the horizontal line is a rate of 1 per year. Figure from [126].

order-of-magnitude reduction in rate. Note that the difference is more pronounced for higher-tension strings (higher values of $\alpha$). This is due to the dependence of $\theta_m$, equation (4.1.24), on $\alpha$, or equivalently the cosmic string tension, $\mu$. $\theta_m \propto l^{-1/3}$, and $l \propto \alpha \propto \mu$. This means that for higher tension strings, the beaming angle $\theta_m$ is smaller, and thus reducing it by a given value, $\Delta$, has a proportionally greater effect.

### 4.2.3 Signal from kinks

Gregory and O'Callaghan have later extended the calculation of the gravitational wave signal from cosmic string loops in higher dimensions to include the signal from kinks [127]. As mentioned in Section 3.2, the existence of kinks is not affected by the higher-dimensional nature of the solutions. In fact, the enhancement of the network density and the potential existence of 3-string junctions, which may increase the number of kinks on a loop (see Section 2.6), may act to enhance the kink signal.

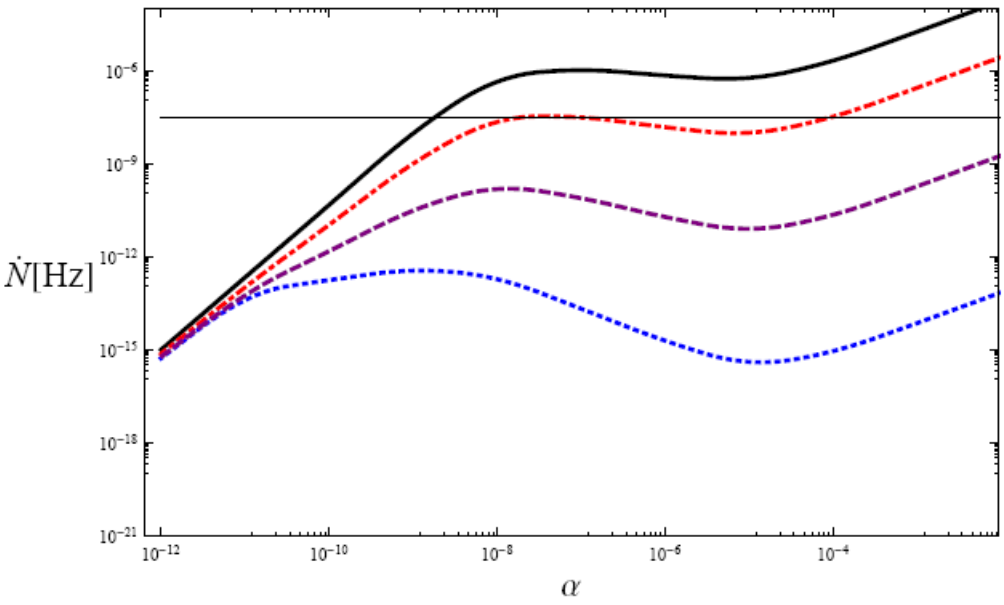


Figure 4.8: The rate of gravitational wave bursts at the LIGO frequency, $f = 150$Hz, at the amplitude $10^{-21}s^{-1/3}$. $\Delta_0$ is fixed at $10^{-3}$. From the top line, moving downwards, we have $n = 0, 1, 3$ and 6. As above, $P = 10^{-3}$, and the horizontal line is a rate of 1 per year. Figure from [126].

However, there will be an effect from the internal velocities, which are assumed to be small but prevent the 4D wavevector being exactly null. Similarly to the reduction in the beaming cone angle of a cusp, there is then a reduction to the beaming angle from a kink (kinks, like cusps, emit high-frequency radiation in a cone around their exact direction). It is found that the reduction to the beaming angle is simply depends on the magnitude of the internal velocity, and is therefore essentially independent of the number of extra dimensions.

The integrals that make up the energy-momentum tensor are given by equation (4.1.8). A kink occurs when the wavevector, $k^\mu$, is lined up with one of $\dot{x}^\mu_\pm$, say $\dot{x}^\mu_+$, so $I^\mu_+$ goes to zero with frequency like a power law rather than an exponential, and there is a discontinuity in the exponent in the other intergral, $I^\mu_-$. At any time, the kink beams high-frequency radiation at the point of the discontinuity, in the direction of $\dot{x}^\mu_+$. The effect of the internal motion affects $I_+$ in the same way that it does for a cusp, since the 4D part of the vector $\dot{x}^\mu_+$ will not be exactly null and therefore cannot line up exactly with the null 4-vector $k^\mu$.

If we write the 3D part of $\dot{x}^{\mu}_{+}$ as $\mathbf{b}'$, as before, then

$$\mathbf{b}'^2 = 1 - b^2 \tag{4.2.53}$$

where $b^2$ is small and equal to the square internal velocity, and so the beaming angle is reduced by $b$, becoming

$$\theta_b = \theta_m - b, \tag{4.2.54}$$

where the opening angle with no extra dimensions, $\theta_m$, is the same as that for cusps. It is found in [127] that this effect leads to an overall reduction in the gravitational wave signal.

Gregory and O'Callaghan plot the amplitude of gravitational wave bursts received on earth with an event rate of 1 per year, at the frequencies of LIGO and LISA detectors, Figure 4.9. These are compared with the signal from cusps. It is seen that although the kink signal is reduced, the reduction is of a similar order of magnitude to the reduction in cusp signal from only one extra dimension. Therefore with several extra dimensions the kink signal may be enhanced relative to that of cusps.

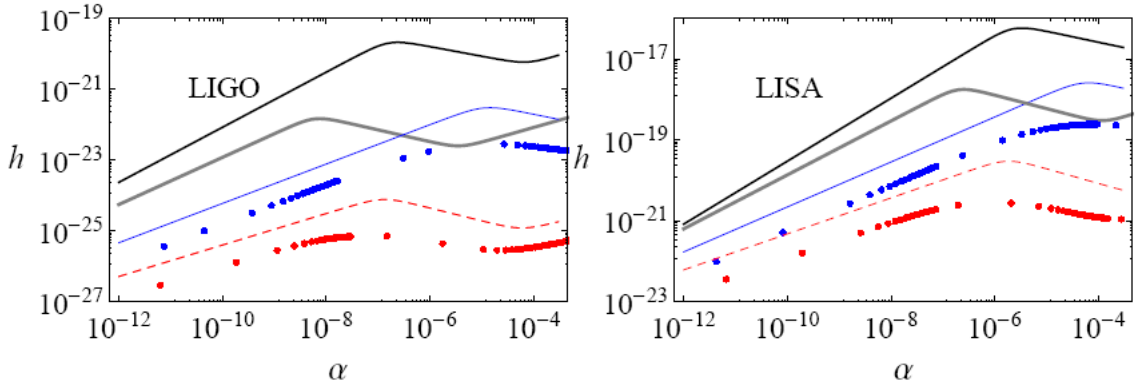


Figure 4.9: Amplitude of kink signal, in 4D case (blue) and in higher-dimensional case (red), plotted against $\alpha$ for LIGO and LISA frequencies ($f = 150$Hz and $f = 3.9$mHz, respectively). The individual dots are numerical integration values and the dashed/solid lines use interpolating functions from [55]. The black line is the 4D cusp signal, and the grey line is the signal from cusps with one extra dimension. Reconnection probability is again $P = 10^{-3}$. Plot from [127].

# Chapter 5

# Cosmic string trajectories in warped compactifications

In this Chapter, we consider the impact of warped internal dimensions on the motion of cosmic superstrings. This work was done in collaboration with Ruth Gregory and Tasos Avgoustidis and published in [13].

Strings are believed to be formed during brane-antibrane annihilation, and typically brane inflation involves a mobile D3-brane falling to the tip of a throat. Moreover, computations of the D3-brane potential including UV corrections and interactions with other wrapped branes show an attractive force to the tip of the throat (see for example [118]). There is thus good reason to suppose that cosmic strings will be located near to the tip region of any warped throat. However, to absolutely fix the string at the throat tip, a quantum mechanical argument is then used: worldsheet intuition regards the string positions in the internal dimensions as worldsheet scalar fields [124], which at low energies acquire masses and stabilise.

However, at late times, and the *very* low energies we are considering in current day cosmology, it is not clear that such a quantum mechanical interpretation is appropriate. The cosmic string, if it survives, is a topological defect, and as such is a classical object from the macroscopic perspective. Whether or not it remains fixed in the internal dimensions depends on whether a classical perspective in the internal dimensions is reasonable. The internal dimensions are already being modelled classically − as a spacetime manifold, and the string is a finite width defect. Hence

provided the string width is small compared with the local scale of the tip, there is no reason to suppose that the string will not behave as the classical soliton it is with regards to its dynamics.

If the strings were indeed fixed at the tip of the throat, there would be no internal motion, and this would significantly alter the conclusions of Chapter 4. But even if they are not fixed, the effect of a warped spacetime on their dynamics may be signficant. To investigate this, we study the classical motion of loops in warped spacetime, treating the string like a topological defect, but assuming that it will remain close to the tip where it is formed.

Since the classical approximation is only reasonable if the string width is small compared with the size and curvature scale of the internal space, we first check that this is the case. While the precise value of the internal string width is model-dependent, we can get a ballpark estimate by using general statements about the warped throat. There are typically two length scales associated with the throat: $L$, the radius of curvature of the spacetime, which must be large in string units in order for the spacetime manifold to be a good approximation, and $r_0$ (or $\epsilon^{2/3}$), a deformation parameter, which sets the scale at which the throat is rounded off. Requiring that the spacetime curvature in the throat remains of similar size along the throat gives $h_0 \sim L^4/r_0^4$, where $h_0$ is the warp factor near the tip (see (5.1.3)). In addition, the throat is typically used to generate a hierarchy between the string and 4D Planck scale, which is bounded by a weighted volume integral in the throat,

$$M_p^2 > \frac{1}{\kappa_{10}^2} \int h d\tilde{V}_6 \simeq L^4 r_{UV}^2/\alpha'^4. \tag{5.0.1}$$

Thus we can estimate the order of magnitude of the internal width $\tilde{w}_6 \sim w_4 h^{-1/2}$ relative to the local tip scale $r_0$ via

$$\frac{\tilde{w}_6^2}{r_0^2} < w_4^2 M_p^2 \left(\frac{\alpha'}{L^2}\right)^4 \left(\frac{r_0}{r_{UV}}\right)^2. \tag{5.0.2}$$

Now, on the one hand, $w_4^2 M_p^2 \simeq 1/(G\mu) \sim 10^7 - 10^{12}$, is very large, but the spacetime curvature radius must also be large, $L^2/\alpha' > 10^2$, and for typical compactification data considered in brane inflation models, $r_0/r_{UV} \lesssim 10^{-3}$ is very small and thus $\tilde{w}_6^2/r_0^2 < 10^{-14} w_4^2 M_p^2$, and so the local size of the string is indeed small in the tip region.

Thus, at late times, when the strings are part of a cosmological network and are effectively topological defects existing at low energies, it seems reasonable to assume that if they are semi-classical objects as far as our 4D universe is concerned, then they also have a semi-classical nature in the extra dimensions. We therefore allow the string to be free to move in the internal dimensions, and study the dynamics of string loops in a warped throat modelled by the Klebanov-Strassler (KS) solution [106]. We find that, although there is an attractive force towards the bottom of the throat, there is no friction to ensure stabilisation. On the contrary, there is continuous exchange of energy between the external and internal sectors, reinforcing motion in the internal manifold. This provides strong evidence that string loops can have significant motion in the internal dimensions, even in a strongly warped spacetime.

## 5.1 Strings on a warped internal manifold

The main feature of a warped compactification is that the spacetime manifold, in particular distances on our noncompact 4D universe, are strongly dependent on the internal dimensions. A generic ten-dimensional warped metric can be written as

$$ds_{10}^2 \equiv G_{MN}dx^M dx^N = h^{-1/2}g_{\mu\nu}dx^\mu dx^\nu - h^{1/2}\tilde{g}_{mn}dy^m dy^n, \tag{5.1.3}$$

where $g_{\mu\nu}(x)$ is our 4D spacetime metric and $\tilde{g}_{mn}(y)$ is the internal 6D metric. We use capital indices $M, N, ..$ for the 10D metric. The warp factor is $h$, a monotonic function, which becomes large in the infrared. Conventionally, this is taken to be at $r \to 0$, where $r$ is a radial coordinate on the internal manifold. For example, in the canonical adS/CFT $adS_5 \times S^5$ manifold, the internal 6D space is flat, and $h(r) \propto r^{-4}$.

Although there is no known *exact* metric for a warped compactification, it is expected that the manifold is well approximated by an exact throat metric (5.1.3) which in the UV (large $r$) is closed off by some Calabi-Yau manifold. The details of this matching will induce perturbations to the (usually highly symmetric) metric (5.1.3). However, these will be subdominant, and it is a good approximation to take (5.1.3) as the background for string motion. We will also assume that the throat has a smooth tip at $r = 0$, with warp factor $h_0 = h(0) \gg 1$.

The general equations of motion for a cosmic string from the classical Nambu effective action (2.3.16), are given by equation (2.3.23). Because our metric (5.1.3) is nontrivial, we cannot take the usual temporal conformal gauge used in Chapter 3, in which the induced metric on the string worldsheet is conformally flat with worldsheet and bulk time identified, and in which the motion of the string reduces to left and right moving uncoupled waves. Instead, we choose the transverse temporal gauge: $\zeta^0 = x^0 \equiv t$, $\dot{x}^M x'_M = 0$. This identifies worldsheet time with background time and imposes diagonality on the worldsheet metric $\gamma_{ab} = x^M_{,a} x^N_{,b} G_{MN}$. The diagonality of the worldsheet metric reduces the equation of motion to equation (3.1.4), and further imposing $\zeta^0 \equiv t$ with a general background metric, the Nambu equations of motion become:

$$\begin{aligned} &\Box x^M + \Gamma^M_{NP} x^N_{,a} x^P_{,b} \gamma^{ab} = 0 \quad \Rightarrow \\ &\frac{\partial}{\partial t}\left(\frac{\dot{x}^M x'^2}{\sqrt{-\gamma}}\right) + \frac{\partial}{\partial \zeta}\left(\frac{x'^M \dot{x}^2}{\sqrt{-\gamma}}\right) \quad + \frac{1}{\sqrt{-\gamma}} \Gamma^M_{NP}\left(x'^2 \dot{x}^N \dot{x}^P + \dot{x}^2 x'^N x'^P\right) = 0\,, \end{aligned} \tag{5.1.4}$$

where dot denotes differentiation with respect to time and prime the spacelike worldsheet coordinate $\zeta^1 \equiv \zeta$.

It is now straightforward to see why the conformal gauge (equation (3.1.8)) cannot be simultaneously chosen with the synchronous gauge, even if our four-dimensional universe is flat, by examining the $M = 0$ equation, which reduces to

$$\frac{\partial}{\partial t}\left(\sqrt{\frac{-x'^2}{h\dot{x}^2}}\right) = 0 \tag{5.1.5}$$

for the case $g_{\mu\nu} = \eta_{\mu\nu}$. Clearly, if $h$ varies significantly over the timescales of interest, then the synchronous gauge will not be a good approximation.

In flat spacetime, it is easy to obtain analytic solutions to the equations of motion (see Chapter 3). In warped spacetime, however, the equations of motion are coupled non-linear PDE's and it is very difficult to find an analytic solution[1].

[1]One exception to this is the rather special case in which the string sits precisely at the tip of the Klebanov-Strassler throat, [29,112]. However note that the trajectory considered in [29] is not a wave, but occurs at a polar singularity and actually corresponds to a circular loop boosted along its length to the speed of light.

In order to sample realistic yet tractable internal trajectories, we restrict motion to a consistent 2D submanifold of the throat, which we can write as

$$d\tilde{s}^2 = dr^2 + B^2(r)d\phi^2 \,. \tag{5.1.6}$$

where $B^2$ is model dependent. Note that $B^2$ does not necessarily vanish as $r \to 0$, and indeed for the explicit metric we use in our numerics (the Klebanov-Strassler throat, [106]) it does not. Modelling the motion of string loops in this way should capture the main features of their dynamics in the full 10D spacetime.

The string worldsheet is therefore represented by:

$$x^M(t,\zeta) = (t, \mathbf{x}(t,\zeta), r(t,\zeta), \phi(t,\zeta)) \,, \tag{5.1.7}$$

and substituting into the equation of motion, (5.1.4), gives the explicit set of equations for the spacetime coordinates of the string worldsheet:

$$\ddot{\mathbf{x}} = \frac{1}{E}\left(\frac{\mathbf{x}'}{Eh}\right)' \tag{5.1.8}$$

$$\ddot{r} = \frac{1}{Eh}\left(\frac{r'}{E}\right)' + \frac{h_{,r}\mathbf{x}'^2}{2E^2h^3} - \frac{h_{,r}}{h}\frac{\dot{r}^2}{2} + \frac{(B^2h)_{,r}}{h}\frac{\dot{\phi}^2}{2} - BB_{,r}\frac{\phi'^2}{E^2h} \tag{5.1.9}$$

$$\ddot{\phi} = \frac{1}{E}\left(\frac{\phi'}{Eh}\right)' + \left(\frac{h_{,r}}{h} + \frac{2B_{,r}}{B}\right)\left(\frac{\phi' r'}{E^2h} - \dot{\phi}\dot{r}\right) \,, \tag{5.1.10}$$

where

$$E = \sqrt{\frac{-x'^2}{h\dot{x}^2}} = \sqrt{\frac{\mathbf{x}'^2 + h\left(r'^2 + B^2\phi'^2\right)}{h\left(1 - \dot{\mathbf{x}}^2 - h\left(\dot{r}^2 + B^2\dot{\phi}^2\right)\right)}} \,. \tag{5.1.11}$$

From the equation of motion for $t$, (5.1.5), we have $\dot{E} = 0$, i.e. $E$ is a conserved quantity. It is related to the conserved energy of the system, $\mathcal{E}$, by:

$$\mathcal{E} = \mu \int E(\zeta) d\zeta \,. \tag{5.1.12}$$

Given that $E$ is conserved, and presuming the string is not highly relativistic all along its length, then as the string falls down the throat, the $x'^2$ term must increase to compensate for the increase in $h$. Thus a string falling down the throat will grow in the noncompact directions as well as stretching out in the internal directions. However, if the throat has a smooth tip (which we take to be the case) then without a friction term the string is free to 'bounce' back up the throat again.

This behaviour is generic and follows from the monotonicity of $h$. We confirm this first by deriving some general results for a flat 4D universe to isolate the impact of warping, then focussing on an explicit throat geometry, before turning to cosmological solutions in the next section.

Note, it is the dependence of $\mathcal{E}$ on $1/\sqrt{h}$ that is often interpreted as a reduction in the effective tension, $\mu_{eff} \sim \mu/\sqrt{h}$, of the string (see for example [60, 90]). We interpret this instead as an increase in string length. These apparently contradictory interpretations can be reconciled by noting that we are considering loops of a fixed *energy*, whereas considering a loop of a particular *length*, the factor of $1/\sqrt{h}$ indeed reduces the energy of such a loop, and therefore $\mu_{eff}$. This is a relevant interpretation since loops are expected to be formed with a given length, $l$, depending on the correlation length of the network. However, our interpretation is relevant when considering the dynamics of individual loops, since for a given loop the energy is fixed and the length of the loop appears to change over time due to internal motion.

### 5.1.1 General warped throat

In order to extract some generic qualitative results, consider a set-up in which a cosmic string loop is pointlike in the internal dimensions and circular in the external dimensions:

$$x^M = (t, \rho(t)\cos\zeta, \rho(t)\sin\zeta, 0, r(t), \phi(t)) \ . \tag{5.1.13}$$

The time-independent quantity $E$, given by equation (5.1.11), is now also independent of the spacelike worldsheet coordinate, $\zeta$, so it is an absolute constant, $E_0$, and there is now a conserved angular momentum in the throat:

$$J = \dot{\phi} h B^2 = const. \tag{5.1.14}$$

The equations of motion for $\rho$ and $r$ are also greatly simplified, and in fact we have a Hamiltonian system with the conserved quantity $E_0$ being the Hamiltonian. Rearranging (5.1.11) using (5.1.14) expresses the system as motion in an effective potential:

$$\dot{\rho}^2 + \dot{R}^2 = 1 - \frac{\rho^2}{E_0^2 h} - \frac{J^2}{hB^2} = 1 - V_{\text{eff}}(\rho, R)\,, \tag{5.1.15}$$

where

$$dR = \sqrt{h}dr \tag{5.1.16}$$

is an alternative conformal radial coordinate. In this system, since $E$ is conserved, we have free motion with no energy being lost[2].

We can now see the effect of motion in the throat from the form of this potential. First note that $E_0^2 h$ sets the scale of oscillations in $\rho$, thus as the string moves down the throat, the overall size of the string in the noncompact directions will increase as already noted. It is also clear that the string will continue to oscillate back up and down the throat. The timescales of these relative oscillations depend on the initial scale of $\rho$, and the compactification parameters.

To get an estimate of these scales, consider the case where the loop has only radial motion in the throat and is very close to the tip. Expanding the warp factor near the tip as $h \simeq h_0 (1 - h_2 r^2)$, where $h_2 \gg 1$, we obtain

$$V_{\text{eff}}(\rho, R) = \frac{\rho^2}{E_0^2 h_0} \left(1 + \frac{h_2}{h_0} R^2\right). \tag{5.1.17}$$

We can now see the hierarchy of scales: provided $R^2 \ll h_0/h_2$, $\rho$ will have harmonic motion at a frequency $\omega_\rho \sim 1/(E_0\sqrt{h_0})$. Since the scale of $\rho$ is set by the string length, $l$, which is of order the Hubble scale for current day cosmic strings, this frequency is of order $l^{-1}$, as might be expected for a cosmic string. However, superimposed on this general behaviour are oscillations in $R$, which have a frequency set by the compactification parameters: $\omega_R \sim \sqrt{h_2/h_0} \gg \omega_\rho$.

This is of course a "broad brush" behaviour. Once $\rho$ becomes very small, the timescale of motion in $R$ lengthens, and $R$ can potentially move further up the throat. In fact, there is no reason in principle for the motion not to explore all regions of the effective potential. As this is a Hamiltonian system, it does not have attractors, and therefore there is no mechanism by which a string could be completely confined at the tip of the throat. Indeed, for small $J$, the potential is strongly 'creased' at $\rho = 0$, with a sharp valley along the $R$-direction. This makes

[2]In reality, of course, the string will be losing some energy, for example through gravitational radiation, which we model in section 5.2.2.

the motion very sensitive to initial conditions should the loop happen to hit this direction in phase space. We see this in some of our numerical integrations.

The picture with angular momentum is broadly similar, as unless $J$ is improbably large, the term in (5.1.15) is generally small. The main qualitative difference with angular momentum is that it gives a hard bound on how far up the throat the string can move, since $hB^2$ decreases in the UV and

$$\frac{J^2}{hB^2} \leq 1\,. \tag{5.1.18}$$

In general, loops can have an arbitrary shape in both internal and external dimensions, and $E$ is not an absolute constant, but depends on the spacelike worldsheet coordinate, $\zeta$. There is also no longer a conserved angular momentum. However, qualitative information can still be drawn from the equations of motion. In (5.1.9), there is a non-kinetic term dependent on the derivative of the warp factor: $h_{,r}\mathbf{x}'^2/2E^2h^3$. This is attractive and encourages oscillations of the string up and down the throat, just as in the pointlike case already discussed. However, since our more generic loop is not pointlike in the internal space, we expect its own tension to pull parts of it in different directions, resulting in much more complex dynamics.

Consider again a loop close to the tip of the throat, then we can do a similar expansion to that in (5.1.17). First make the transformation $\zeta \to \tilde{\zeta}$ such that $d\tilde{\zeta} = E(\zeta)d\zeta$. Then $\tilde{\zeta}$ runs from 0 to $l$, the (10D) length of the loop, and the equation of motion for the external part of the loop, (5.1.8), becomes:

$$\ddot{\mathbf{x}} = \frac{1}{h}\left(\mathbf{x}'' - \frac{\mathbf{x}'h_{,r}r'}{h}\right) \tag{5.1.19}$$

where prime is now differentiation with respect to $\tilde{\zeta}$.

For cosmological loops, most of the length of the string will be in the external dimensions, giving $|\mathbf{x}| \sim \mathcal{O}(h^{\frac{1}{2}}l)$. Then, assuming the loop can be approximated by low harmonics, we also have

$$|\mathbf{x}'| \sim \mathcal{O}(h^{\frac{1}{2}}) \quad ; \quad |\mathbf{x}''| \sim \mathcal{O}\left(\frac{h^{\frac{1}{2}}}{l}\right) \quad ; \quad r' \sim \mathcal{O}\left(\frac{r}{l}\right). \tag{5.1.20}$$

As before, replacing $h \simeq h_0\,(1 - h_2 r^2)$ gives $\frac{h_{,r}}{h} \simeq -2h_2 r$ close to the tip. This implies that

$$\frac{h_{,r}r'}{h} \sim \mathcal{O}\left(\frac{h_2 r^2}{l}\right), \tag{5.1.21}$$

and hence the second term on the RHS of (5.1.19) is $\mathcal{O}(h_2 r^2)$ suppressed relative to the first. Thus the motion of the loop will be close to a 4D flat-space solution, with corrections (roughly) of order $\mathcal{O}(h_2 r^2)$. We see this order of magnitude behaviour in explicit numerical solutions (given below). Note, however, that even a small correction can have a significant impact on observational signatures – see Section 4.2.

### 5.1.2 Numerical results

For a circular loop of the form (5.1.13), given a particular throat, it is straightforward to solve the equations of motion numerically. For practical reasons, we cannot access the most physically realistic huge hierarchies between the scale of the throat and the current cosmological cosmic string network scale. However, we can test the general understanding that was built up by analysing the system qualitatively, above.

For our modelling, we use the concrete example of the warped deformed conifold, or Klebanov-Strassler, solution [106]. This is an exact supergravity solution with D3 and wrapped D5 branes, interpolating from a regular $\mathbb{R}^3 \times S^3$ tip, to an $\mathbb{R} \times T^{1,1}$ cone in the UV. The warp factor, $h$, is given by:

$$h = 2(g_s M \alpha')^2 \, \epsilon^{-8/3} \, I(\eta), \tag{5.1.22}$$

where

$$I(\eta) \equiv \int_\eta^\infty dx \frac{x \coth x - 1}{\sinh^2 x} (\sinh x \cosh x - x)^{1/3}, \tag{5.1.23}$$

and $\eta$ is given implicitly by

$$dr = \frac{\epsilon^{2/3}}{\sqrt{6}} \frac{\sinh \eta d\eta}{(\sinh \eta \cosh \eta - \eta)^{1/3}}. \tag{5.1.24}$$

$M$ is a compactification parameter representing the number of dissolved D5 branes in the background, and $\epsilon$ is a dimensionful parameter measuring the deformation of the conifold. The string coupling and string scale are given as usual by $g_s$ and $\alpha'$. (For details on the warped deformed conifold, and coordinate systems, see e.g. [36, 84, 106, 120].) For a consistent angular trajectory, the string must move around the non-contractible $S^3$, and for our examples $B^2 = \epsilon^{4/3} \frac{1}{2} (\sinh \eta \cosh \eta - \eta)^{1/3} \tanh \eta/2$.

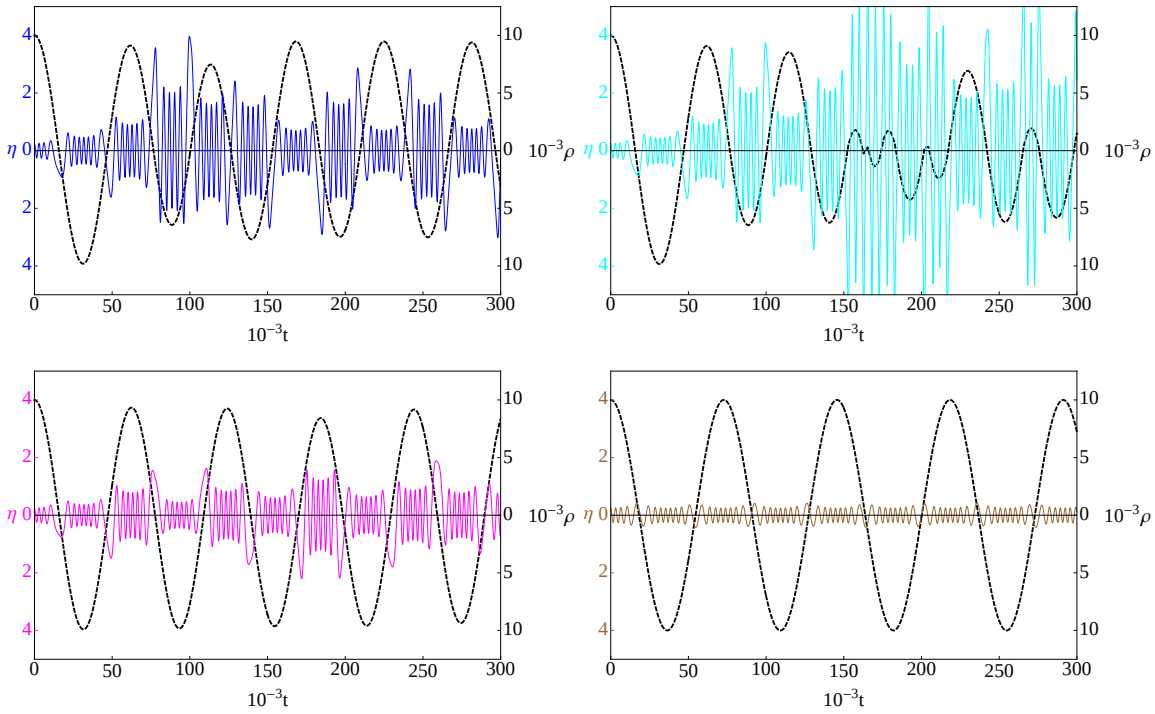


Figure 5.1: Numerical solutions for the circular loop Ansatz (5.1.13) showing the internal location $\eta(t)$ (in colours) and the external radius $\rho(t)$ (in dashed black) of the loop, demonstrating the interplay between external and internal motion and the effect of angular momentum in the internal dimensions. The plots show a loop of size $\rho_0 = 10^4\sqrt{\alpha'}$ initially starting at rest at $\eta_0 = 0.25$, with $J = 0, 5, 10$, and 50% of the relativistic maximum $\sqrt{h(\eta_0)}B(\eta_0)$, with $\eta(t)$ shown in blue, cyan, magenta, and brown respectively. In all plots, the external loop radius, $\rho$, is shown in dashed black.

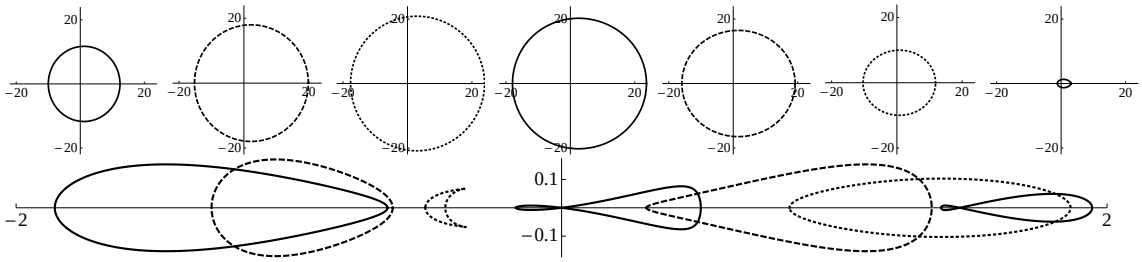


Figure 5.2: Snapshots of a string loop evolving both externally (upper) and internally (lower), where the initial internal loop is displaced up the throat. In the lower plot, the axes are $\eta\cos\phi$ and $\eta\sin\phi$, and the snapshots are selected some time after the start of the integration.

Figure 5.1 shows a demonstration of the qualitative motion described in the previous subsection by integrating (5.1.8-5.1.10) with varying angular momenta for the parameter values $\epsilon = 0.1$, $g_sM = 100$, $\rho(0) = 10^4$, and $\eta(0) = 0.25$ (implying $R(0) = 57.86$). Note that we have set $\alpha' = 1$ for simplicity, and we show the internal motion in the conventional $\eta$ coordinate. Using (5.1.17) for vanishing angular momentum these give the values $E_0 = 4.4$, $\omega_\rho = 1.1 \times 10^{-4}$, and $\omega_R = 2.2 \times 10^{-3}$. In the external dimension the loop oscillates with approximately the frequency $\omega_\rho \sim 1/E_0\sqrt{h_0}$, while in the throat the loop oscillates faster, and when $\rho$ becomes small, it 'coasts', since the potential (5.1.17) is effectively flat. Note how this behaviour leads to the loop moving occasionally further up the throat, where the analytic approximation to the potential will break down – even so, the broad brush behaviour continues, although the internal oscillations seem to prefer being stronger than the initial conditions would suggest.

For a more general loop solution, a numerical integration of the PDE's (5.1.8-5.1.10) is necessary. Figures 5.2 and 5.3 show snapshots of two loop trajectories chosen to illustrate different aspects of the interplay between the internal and external loop motion. For numerical expedience the compactification parameters, $g_sM = 10$ and $\epsilon = 0.5$ were used, and the radii of the internal and external extent are more similar.

Figure 5.2 shows an example with the loop starting up the throat. Although the loop is clearly no longer pointlike in the internal dimensions, it is fairly localised,

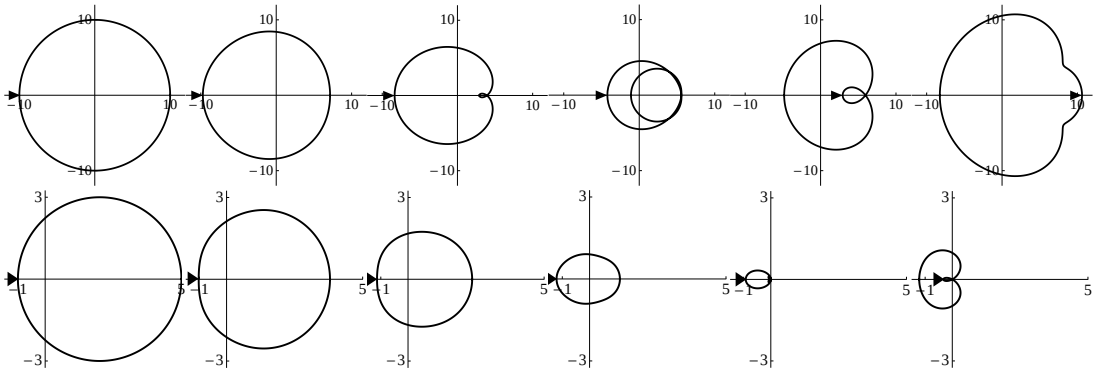

Figure 5.3: From left to right, snapshots of a string loop at evenly spaced time intervals, the upper sequence showing the loop in the external dimensions, and the lower sequence in the internal dimensions. This solution demonstrates how the circular shape is distorted by internal motion, and develops apparent kinks and crossings (although the loop does not self intersect as it misses in the internal dimensions). The arrow denotes the position on the loop where $\zeta = 0$ for comparison of the location of the features.

making the situation somewhat similar to that of the previous trajectories. A fairly coherent oscillation of the internal loop up and down the throat is observed, with the external string loop remaining roughly circular and oscillating, with the maximum radius increasing when the internal loop is close to the tip. This consistency of the full system with the simpler case reinforces the conclusions made.

Figure 5.3 focuses instead on a loop whose initial internal configuration encircles the origin with significant variation in $\eta$. Here, the part of the loop at larger $\eta$ starts to fall down the throat, whereas the part at lower $\eta$ begins to move up. As the loop then has varying motion internally, this feeds into the external motion, causing the loop there to start curling. This particular example shows a dramatic change of shape in the external dimensions, which we expect will be muted as the radius of the loop in the external dimensions is increased to more realistic cosmological scales.

It is interesting to note that even for a finite energy, $\mathcal{E}$, there is no hard bound on how far from the tip of the throat a string can move. While we can bound the variation in $\eta$ at a particular time ($\mathcal{E} \geq \mu \int d\zeta |r'| = \mathcal{O}(\mu \Delta r(t))$), we can nonetheless have the loop high up the throat if it is strongly localised and we 'freeze' it in the

external dimensions (i.e. temporarily have the loop very small and nonrelativistic). Such a situation, however, would require a conspiracy of internal and external motion that makes it unlikely, or a rare event. More generically, we expect a loop to approximately remain within an order of magnitude or so of its inital data (in the absence of cosmological evolution) as it is unlikely for a loop with general internal shape to move significantly up the throat. Even this, however, is enough to maintain sufficient internal motion, and does not preclude significant local alterations, such as the quirks exhibited in Figure 5.3.

### 5.1.3 Observational consequences

So far in this section we have discussed purely the motion of the string in a flat 4D background with a warped internal throat, however it is the consequences of this motion that are key. In Chapter 4 it was shown that the presence of even an apparently small internal velocity could make a remarkable difference to the gravitational wave signal given off by string loops. This is because the dominant signal, being from cusps, is highly dependent on the strongly relativistic nature of the events. The internal velocity causes the cusps on the string motion to be rounded off, and also to be less likely to form. This effect was measured by a "near cusp event" parameter $\Delta \simeq \sqrt{1-\dot{\mathbf{x}}^2}/2$, which we can compute by finding local maxima of the external velocity, $|\dot{\mathbf{x}}|$, for these simple trajectories.

For the loops plotted in Figure 5.1, we computed $\langle\Delta\rangle = 0.071, 0.059, 0.099$, and $0.252$ for $J = 0, 5\%, 10\%$, and $50\%$ of $J_{\max}$ respectively. The large value of $\langle\Delta\rangle$ for large $J$ is not surprising: in this case the loop has, by construction, a (conserved) relativistic internal motion. The values of $\langle\Delta\rangle$ for small, or zero, $J$ are more relevant, as these represent initial conditions where there is little relativistic motion internally. Exploring further the parameter space for $J = 0$ yields $\langle\Delta\rangle = 0.012, 0.048$, and $0.035$ for initial loop radii of $20\mathrm{K}\sqrt{\alpha'}$, $30\mathrm{K}\sqrt{\alpha'}$ and $40\mathrm{K}\sqrt{\alpha'}$ respectively, indicating that this is not a parameter that drops as the loop size is increased, but rather seems to respond more to the interplay between the internal and external dimensions. We conclude therefore that for this particular loop trajectory the near cusp parameter is $\mathcal{O}(10^{-2})$, and hence the gravitational wave signal from cusps will be significantly

damped (see Section 4.2.2).

For a more general loop, we estimated that for a string close to the tip of the throat the external part of the string would be close to that of a loop in 4D flat space, with the order of magnitude of corrections being $\sim h_2 r^2$. In the Klebanov-Strassler coordinates this translates to a correction of order $\mathcal{O}(\eta^2)$. Given the initial data $\eta_0 = 0.25$ in Figure 5.1, this would suggest a discrepancy of order 0.06 from the exact 4D Nambu string, which is indeed the ballpark of the estimates for $\Delta$, and suggests that the result is quite robust.

In Section 4.2.2, the overall effect on the gravitational wave signal for cusps was obtained by marginalising over the $\Delta$ parameter up to a maximum value $\Delta_0$. The results here indicate that $\Delta_0 \sim 10^{-3}$ might be a conservative but sensible value to take, in which case (referring to Figure 4.7), we see that the expected detection rate of a cusp event at the LIGO detector is likely to be in the region of one every 100 years.

## 5.2 Cosmological loops

We have shown that loop motion in a flat 4D spacetime with warped extra dimensions will include all dimensions, and will not be localised at the tip of the throat. In order for the internal motion to be confined, the string would have to lose energy in the internal dimensions, which would require some kind of friction. Cosmological expansion is one possible cause, and energy loss via emission of gravitational radiation another. We now consider both of these effects and find that our conclusions remain unchanged.

### 5.2.1 Cosmological expansion

In an expanding universe, the velocities of long strings are damped [100, 116]. Thus cosmological expansion might prove to be a source of damping in the internal dimensions. The important quantity to consider is the relative magnitude of internal and external damping, since a stronger damping in the internal dimensions would result in internal motion being effectively brought to a standstill, whilst the external

part of the loop would continue to evolve, giving an effectively 4D motion. In [10], this was explored for long strings, and it was found that internal damping is in fact very weak, and does not localise the strings at the tip of the throat.

The effect of expansion on closed loops is more interesting. While outside the horizon scale, they behave similarly to long strings: expansion effectively has a "stretching" effect, and reduces the velocity of the string. For the closed loop, stretching increases its total energy, and does slow down the motion of the loop for a while, but eventually the tension of the loop causes it to contract and fall inside the horizon. Once the loop is well inside the horizon, expansion ceases to affect its motion. The transition between these two stages, when the loop is comparable to the horizon size, can have interesting dynamics.

For an FRW universe, the metric now takes the form:

$$ds^2 = h^{-\frac{1}{2}}(dt^2 - a^2 d\mathbf{x}^2) - h^{\frac{1}{2}}\tilde{g}_{mn}dy^m dy^n\,, \tag{5.2.25}$$

so that the physical distance in the external dimensions is now $a\mathbf{x}$. The scale factor, $a$, can be taken to be proportional to $t^\beta$, where $\beta = \frac{1}{2}, \frac{2}{3}$ respectively in the radiation and matter eras. The scalar $E \equiv \sqrt{\frac{-x'^2}{h\dot{x}^2}}$, which in flat spacetime was conserved, now depends explicitly on the scale factor $a = a(t)$:

$$E = \sqrt{\frac{a^2\mathbf{x}'^2 + h\left(r'^2 + B^2\phi'^2\right)}{h\left(1 - a^2\dot{\mathbf{x}}^2 - h\left(\dot{r}^2 + B^2\dot{\phi}^2\right)\right)}}\,. \tag{5.2.26}$$

The equations of motion become:

$$\dot{E} = -E\frac{\dot{a}}{a}\left(a^2\dot{\mathbf{x}}^2 - \frac{a^2\mathbf{x}'^2}{E^2h}\right) \tag{5.2.27}$$

$$\ddot{\mathbf{x}} = \frac{1}{E}\left(\frac{\mathbf{x}'}{Eh}\right)' - \frac{\dot{a}}{a}\dot{\mathbf{x}}\left(2 - a^2\dot{\mathbf{x}}^2 + \frac{a^2\mathbf{x}'^2}{E^2h}\right) \tag{5.2.28}$$

$$\begin{aligned}\ddot{r} = {} & \frac{1}{Eh}\left(\frac{r'}{E}\right)' + \frac{h_{,r}\mathbf{x}'^2}{2E^2h^3} - \frac{h_{,r}}{h}\frac{\dot{r}^2}{2} - BB_{,r}\frac{\phi'^2}{E^2h} \\ & + \frac{(B^2h)_{,r}}{h}\frac{\dot{\phi}^2}{2} + \frac{\dot{a}}{a}\dot{r}\left(a^2\dot{\mathbf{x}}^2 - \frac{a^2\mathbf{x}'^2}{E^2h}\right)\end{aligned} \tag{5.2.29}$$

$$\ddot{\phi} = \frac{1}{E}\left(\frac{\phi'}{Eh}\right)' + \left(\frac{h_{,r}}{h} + \frac{2B_{,r}}{B}\right)\left(\frac{\phi' r'}{E^2h} - \dot{\phi}\dot{r}\right) + \frac{\dot{a}}{a}\dot{\phi}\left(a^2\dot{\mathbf{x}}^2 - \frac{a^2\mathbf{x}'^2}{E^2h}\right) \tag{5.2.30}$$

We see directly from (5.2.27) that the quantity $E$ in (5.2.26), and therefore the total energy, $\mathcal{E} = \int d\zeta E$, is no longer conserved, as anticipated from its scale factor depen-

Table 5.1: Approximate behaviour of $E$ when different length- and velocity-squared terms are dominant.

| $\frac{a^2\mathbf{x}'^2}{E^2h}$ | $a^2\dot{\mathbf{x}}^2$ | Internal velocity and length terms | $E$ |
|---|---|---|---|
| large | small | small | $\propto a$ |
| small | large | small | $\propto 1/a$ |
| small | small | large | $\sim$constant |

dence. A straightforward consequence of (5.2.26) is that $-1 \leq \left(a^2\dot{\mathbf{x}}^2 - \frac{a^2\mathbf{x}'^2}{E^2h}\right) \leq 1$, and hence

$$|\dot{E}| \leq E\frac{\dot{a}}{a}\,. \tag{5.2.31}$$

From this it follows that in order for $\dot{E}$ to be significant, $E$ must be a sizeable fraction of the horizon scale, i.e. $E \sim (\dot{a}/a)^{-1} = H^{-1}$. Physically, $\dot{E} \sim HE$ corresponds to a large, non-relativistic loop, where the energy is given by its rest-mass (length) and the dominant mechanism in (5.2.27) is conformal stretching, increasing the total energy. On the other hand, $\dot{E} \sim -HE$ corresponds to an ultra-relativistic loop, for which the relevant mechanism is velocity redshifting in the directions transverse to the string, decreasing the energy.

Useful insights into the behaviour of string loops in the spacetime (5.2.25) can be gained by focussing on the quantity $E$. Table 5.1 details extreme cases of string motion (i.e. cases in which the dynamics are dominated by certain types of terms), and the corresponding behaviour of $E$. We expect, and indeed find numerically, that energy is generally transferred back and forth between length, velocity (columns 1 and 2) and the extra dimensional motion (column 3). This implies that $E$ can attain its limiting behaviour – increasing proportionally to the scale factor – only part of the time. In general, its growth will be slower, and, at certain intervals during the loop's evolution, $E$ can even decrease. On the other hand, the scale factor, $a$, will always be increasing as $t^\beta$ in a given era, and the horizon scale will grow even faster ($\propto t$). Thus, in finite time, $E$ will no longer be a significant fraction of the horizon scale, $\dot{E}$ will decrease, and $E$ will return to being constant as in the case of non-expanding space. In other words, a large, horizon-scale loop is affected by expansion until it falls inside the horizon.

We see this behaviour in the Ansatz (5.1.13). Evolving numerically from such a circular configuration, with superhorizon physical radius and zero velocities in all dimensions, we see that that $E$ begins by increasing proportionally to the scale factor, then oscillates up and down as the circular loop oscillates in and out, and approaches a constant value over time (Fig.5.4). An interesting difference with respect to the pure 4D case becomes apparent. In 4D, a static, superhorizon loop starts with $\dot{E} \simeq (\dot{a}/a)E$ and this rate gets gradually reduced over cosmological timescales as the loop velocity slowly builds up from 0. Here, there is a second scale – that of the warping – which is hierarchically smaller than the expansion rate, and causes the build-up of velocities in the compact dimensions over a much shorter timescale, through the gradient terms in equation (5.2.29). As a result, the loop energy very quickly turns to a significantly slower expansion with $\dot{E} \sim (1/2)(\dot{a}/a)E$ (see Fig.5.5), which can be understood from equation (5.2.27) with[3] $a^2\dot{\mathbf{x}}^2 \to 0$ and $h\dot{r}^2 \lesssim 1$. Thus, the horizon, growing linearly in time, catches up with the physical loop size earlier than in 4D. Note, however, that a similar behaviour also occurs in 4D if the initial loop has small-scale structure. In that case, the small-scale curvature generates velocity over short timescales and the situation is similar to the one we just discussed.

Having looked at the overall behaviour of $E$, we turn our attention to the Hubble terms proportional to $\frac{\dot{a}}{a}$ that appear in equations (5.2.28)-(5.2.30). Since these terms scale as $\frac{\dot{a}}{a} \propto \frac{1}{t}$, their relative effect generally becomes less important at later times, but they can still dominate during short intervals when the string radius crosses zero and $E$ is kinetic-energy dominated. The term in the equation for external motion, (5.2.28), is a damping term, while the terms in the internal equations, (5.2.29) and (5.2.30), can in general have positive or negative sign with respect to the corresponding internal velocity.

It is important to note, however, that although there is a damping term in the equation for $\mathbf{x}$, which reduces the size of its oscillations over time, the physical

[3]In fact, the internal velocity $v_I = \sqrt{h}\dot{r}$ oscillates in the interval $(-1, 1)$ and the rate $\dot{E}$ changes accordingly on short timescales. Over larger timescales, the evolution can be approximated by taking the root-mean-squared velocity, which is close to $1/2$.

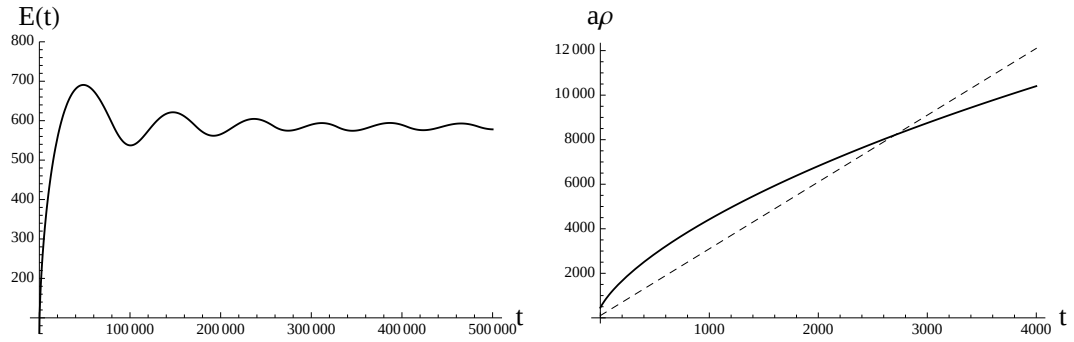


Figure 5.4: Left: Evolution of $E(t)$ for an initially static superhorizon loop. $E$ is initially increasing but starts oscillating after the loop falls inside the horizon, and eventually approaches a constant as in flat space. Right: Early evolution of the loop's physical radius $a\rho$ (solid line) until it falls inside the horizon scale (dashed line). Over larger timescales (not shown), $a\rho$ undergoes oscillations with an amplitude that gets smaller with respect to the horizon, in accordance with the energy plot on the right. Plot from [13].

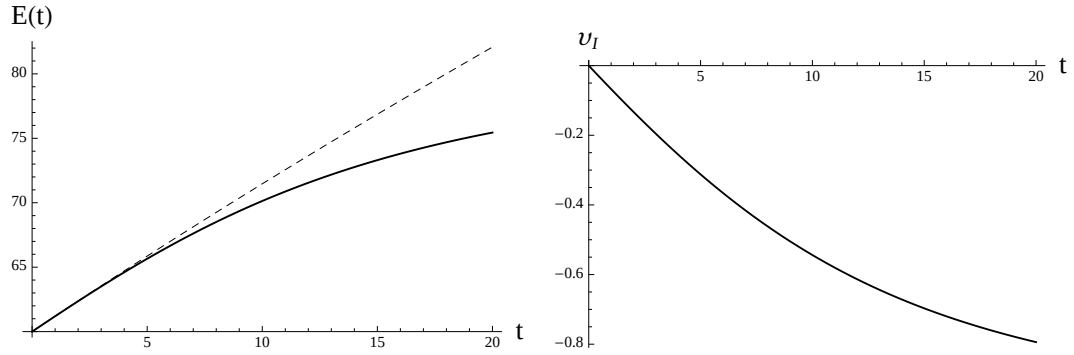


Figure 5.5: Left: Early time evolution starts as $E(t) \propto a(t)$ initially, but quickly drops to a slower rate as internal velocities (shown in the right plot) build up. The dashed line shows the $E(t) \propto a(t)$ growth, which would have been expected if there were no internal velocities. Right: Build up of internal velocity $v_I \equiv \sqrt{h}\dot{r}$ over the same timescale, which, in view of equation (5.2.27), is responsible for the reduction of the rate $\dot{E}$ in the left plot. Over larger timescales (not shown), $v_I$ oscillates with $-1 \leq v_I \leq 1$ and the rate $\dot{E}$ changes accordingly, so on much larger timescales the evolution can be approximated by taking the root-mean-squared $\langle v_I^2 \rangle \simeq 1/2$. Plot from [13].

variable, $a\mathbf{x}$, does not get smaller. The damping term in equation (5.2.28) is stronger when the term $\frac{a^2\mathbf{x}'^2}{E^2 h}$ is larger, corresponding to the loop radius being close to a local maximum. This implies that the comoving velocity, $\dot{\mathbf{x}}$, which is on average lowest in such configurations, will be slowed down even more in this region, so the string will tend to spend longer in such configurations. Then, looking back at the other equations, we see that this corresponds to the region where $E$ is increasing and where the internal coordinates, $\eta$ and $\phi$, are being damped. This suggests that, overall, the energy of a loop will slightly increase, and the extra dimensional motion will be slightly damped. The overall increase of energy is seen in the simple Ansatz, Figure 5.4, and makes intuitive sense as the string is initially "stretched" by the expansion of space. The slight damping agrees with [10], but again it is not enough to localise the string. Then, after the loop falls inside the horizon, $E$ becomes constant, and the string behaves exactly as it did in non-expanding space, as discussed above. Thus, we confirm that Hubble damping alone cannot localise the strings in the internal dimensions. In fact, if $E$ has increased from its starting value, motion in both sectors will be larger overall.

Figure 5.6 shows the evolution of the comoving radius, $\rho$, and the radial position, $\eta$, in the throat (left plot), together with the corresponding velocity evolutions (right plot), for the same loop considered above. Note that the apparent damping in the motion of the comoving radius is compensated by the scale factor growth $a(t) \propto t^{\beta}$, so overall the physical loop radius does not shrink at late times. (Here, we neglect gravitational radiation, to be studied in the next subsection 5.2.2.) As we have discussed, there is a small damping in the $\eta$ motion, but the amplitude increases back again as energy is exchanged between the two sectors.

### 5.2.2 Gravitational radiation

Cosmic strings or superstrings lose energy via gravitational radiation, and while this is by no means the only form of radiation they produce, it is the most generic, as it depends on the tension, $\mu$, and is otherwise model-independent. A discussion of other forms of radiation may be found in Section 2.8, but these other emissions are strongly model-dependent. Gravitational radiation is also likely be the dominant

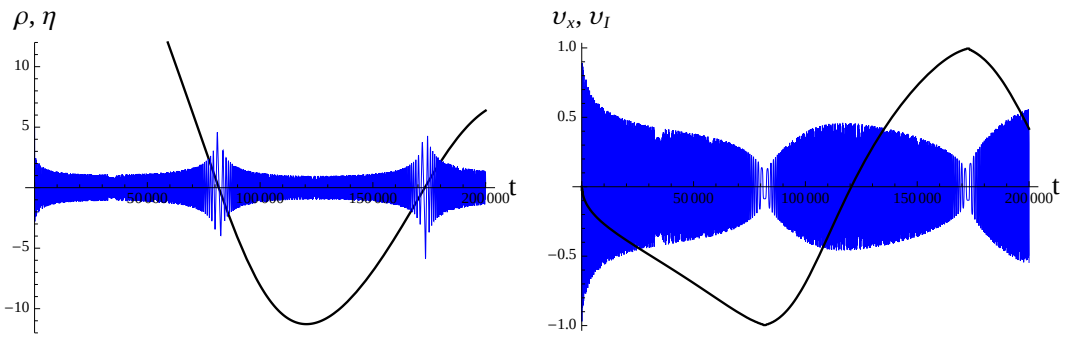


Figure 5.6: Left: Evolution of the comoving loop radius $\rho$ (thick black line) and the internal radial coordinate $\eta$ (thin blue line) for the initially superhorizon-sized loop discussed above. The motion of $\eta$ exhibits high-frequency oscillations up and down the throat, with an amplitude profile that is correlated with the 3D motion of $\rho$. The amplitude of $\eta$ reaches a local maximum when $\rho$ passes from 0, at which point **almost** all kinetic energy is in the 3D motion (cf. right plot). Right: Evolution of the physical velocities $v_x$ (thick black line) and $v_I$ (thin blue line) corresponding to $\rho$ and $\eta$ respectively. The internal velocity $v_I$ oscillates at a much higher frequency, determined by the warping, becoming very small when the 3D velocity becomes relativistic, as the radius, $\rho$, passes through 0 (cf. left plot). Plot from [13].

energy-loss mechanism for large cosmic string loops at late times, so we choose to model this effect. Note, however, that other forms of radiation could be modelled in a similar way.

The emission of gravitational radiation by cosmic string loops can be approximated by a constant rate of decrease of the overall energy of the loop, until the energy reaches zero and the string has disappeared. In flat 4D spacetime, the following formula was derived by Vachaspati and Vilenkin [168] for the rate of energy loss from a loop,

$$\frac{d\mathcal{E}}{dt} \sim \Gamma G\mu^2 \,, \tag{5.2.32}$$

where $\mathcal{E}$ is the invariant energy of the loop (defined in (5.1.12)), $\mu$ is the string tension and $G$ is Newton's constant. Equation (5.2.32) is similar to the quadrupole formula that applies to slow-moving sources, with the addition of a numerical factor, $\Gamma$, which is usually evaluated to be approximately 50, [149]. This factor results from the fact that cosmic string loops are fast-moving, and, in particular, part of the contribution to $\Gamma$ comes from cusps. As discussed in Chapter 3, allowing the string to move in extra dimensions greatly reduces the occurrence of cusps and may therefore affect the value of $\Gamma$. This would be likely to reduce the effective $\Gamma$, so taking $\Gamma \simeq 50$ could well be an over-estimate of the damping due to gravitational radiation.

The general behaviour, however, is independent of the numerical factor. The magnitude of the energy affects both how far away from the tip of the throat the string tends to move, and the maximum length of the loop. From (5.1.12) and (5.1.11), the energy is:

$$\begin{aligned} \mathcal{E} &= \mu \int d\zeta \sqrt{\frac{\mathbf{x}'^2 + h\left(r'^2 + B^2\phi'^2\right)}{h\left(1 - \dot{\mathbf{x}}^2 - h\left(\dot{r}^2 + B^2\dot{\phi}^2\right)\right)}} \\ &\geq \mu \int d\zeta \sqrt{\frac{\mathbf{x}'^2 + h\left(r'^2 + B^2\phi'^2\right)}{h(0)}} \,. \end{aligned} \tag{5.2.33}$$

The far right hand side of this equation is proportional to the total length of the string loop, from which one can see that as $\mathcal{E}$ decreases, the constraint on the maximum length of the loop becomes tighter.

There is no explicit constraint on $r$ (distance from the tip of the throat), since if the length of the string is zero at any point, $r$ can be arbitrarily large. However,

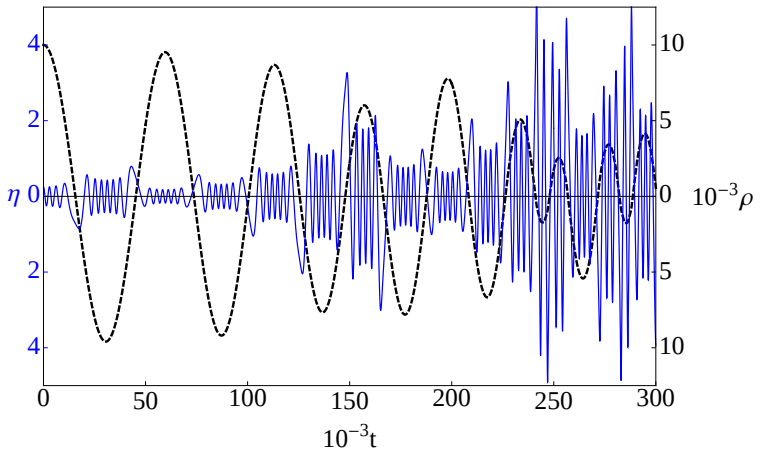


Figure 5.7: Including the gravitational radiation damping into the circular loops of section 5.1.2. The loop shown has no angular momentum, and corresponds to the damped version of the first plot in Figure 5.1. A rather large value of damping was chosen, corresponding to a halving of $E_0$ by the end of the integration.

the length of a loop will generally be non-zero, which gives a constraint on $r$ and confines the loop within a certain distance of the tip of the throat. From (5.2.33) we have:

$$\mathcal{E} \geq \mu \int d\zeta \sqrt{\frac{\mathbf{x}'^2 + h\left(r'^2 + B^2\phi'^2\right)}{h}}. \tag{5.2.34}$$

Again, the terms in the numerator give the length of the loop. Since $h$ is a decreasing function of $r$, this equation implies that the restriction on $r$ becomes tighter as $\mathcal{E}$ gets smaller. Using an analytic approximation for $h$ we can calculate the rate at which the restriction tightens. As $\mathcal{E}$ tends towards zero (as the loop loses energy), we find that the restriction on $r$ does not tighten as quickly as the restriction on the length of the loop. In fact, when $\mathcal{E}$ reaches zero, the total length of the loop must be zero, whereas there is no requirement for the string to be at the bottom of the throat ($r = 0$). From this we argue that, in general, the length of the loop disappears before the internal motion, so it will not be localised at the tip of the throat.

Figure 5.7 shows the effect of the gravitational radiation damping on the simple loop Ansatz (5.1.13). A rather large value of damping, equivalent to setting $G\mu \simeq 10^{-7}$ in (5.2.32), was chosen to highlight the effect, and demonstrates clearly how the

external loop radius, $\rho$, reduces overall more quickly than the internal oscillations. The motion towards the end of the time period becomes more and more noisy as the loop enters more often the sharp valley in the effective potential at $\rho = 0$. We conclude that the emission of gravitational radiation will neither cause the string to be pulled to the tip of the throat nor the motion to become effectively 4D.

## 5.3 Comparison with behaviour in flat extra dimensions

We now discuss the ways in which motion in warped spacetime differs from the case where the extra dimensions are flat (the latter was discussed in Chapter 3).

A flat internal metric allows us to impose the third gauge choice, $\dot{x}^2 = -x'^2$. The equations of motion then become a wave equation, and the solution is simply a sum of left- and right-moving waves,

$$\mathbf{x}(\zeta, t) = \frac{1}{2}\left(\mathbf{a}(t-\zeta) + \mathbf{b}(t+\zeta)\right) . \tag{5.3.35}$$

The functions $\mathbf{a}$ and $\mathbf{b}$ can take any form subject to the constraint $\mathbf{a}'^2 = \mathbf{b}'^2 = 1$. This gives some interdependence between the different directions. Essentially it means that if $\mathbf{a}'$ or $\mathbf{b}'$ is large in one direction, it must be small in another. This is directly related to the conservation of energy, given by the condition: $\mathbf{x}'^2 + \dot{\mathbf{x}}^2 = 1$, which implies that if length or velocity terms are large in one direction, they must be small in another.

In the case of warped spacetime, loop trajectories are no longer periodic (as we see clearly on Figure 5.1, for example). This is essentially due to the presence of two different coupled characteristic frequencies of oscillation: the characteristic frequency of the loop based on its size, and the frequency of oscillation up and down the throat, based on the scale of the throat. These two different frequencies interfere, resulting in non-periodic motion. This effect is particularly noticeable if the frequencies are comparable, which depends on the scale of the loop and the size of $\epsilon$ (which gives the scale of the throat).

In a similar way to the flat space case described above, the length and velocity

terms are still constrained by the conservation of energy, so that if they are large in a particular direction they must be small in another, which is expressed by the following equation:

$$\dot{\mathbf{x}}^2 + h\left(\dot{r}^2 + B^2\dot{\phi}^2\right) + \frac{\mathbf{x}'^2}{E^2 h} + \frac{1}{E^2}\left(r'^2 + B^2\phi'^2\right) = 1.$$

However, there is an additional interaction between the different directions that is not present in flat space. We saw in Section 5.1 that motion in all directions is affected by the radial distance, $r$, of the string from the tip of the warped throat. We saw that if a string is close to the tip of the throat, its total length and velocity are larger, and they are smaller if the string is far from the tip. When the frequency of internal oscillations is much higher than those in the external part of the loop, which is the case for a realistic cosmological scenario, this results in more of an averaged effect (see for example Figure 5.1), but nonetheless an important one.

The fact that some interaction between the internal radial distance and the other directions exists is apparent in the equations of motion, since the equation of motion (5.1.9) for the internal radial distance, $r$, contains terms depending on all the other directions, and the other equations of motion, (5.1.10) and (5.1.8), depend on $r$. On the other hand, without warping, no such dependence appears. This all means that strings in warped spacetime have more interesting and complex motion than those in flat spacetime, and we have seen a few examples of their curious dynamics in this chapter (see for example Figures 5.2 and 5.3). The main conclusion is that the warped geometry will also contain appreciable internal motion which will then impact on the physics of the 4D cosmological network.

In many explorations of cosmic superstrings, the strings are considered to interact with the IIB supergravity fields, in particular the NS-NS 2-form (for the fundamental string) or the RR 2-form (for the D-string), or indeed both (for $(p, q)$ strings). While at low energies these supergravity interactions are not expected to persist, [82], since the exact solution we are using for the throat contains fluxes of both these fields, we briefly discuss the effect of these 2-forms on the motion of the strings.

For a string charged under a 2-form, $B_{MN}$, the Nambu action acquires an addi-

tional term,

$$S \propto -\int d\zeta dt\sqrt{-\gamma} + \int d\zeta dt \epsilon^{ab} x^M_{,b} x^N_{,b} B_{MN} \,. \tag{5.3.36}$$

The equation of motion is then,

$$\begin{aligned} \frac{1}{\sqrt{-\gamma}}\left(\frac{\partial}{\partial t}\left(\frac{\dot{x}^M x'^2}{\sqrt{-\gamma}}\right) + \frac{\partial}{\partial \zeta}\left(\frac{x'^M \dot{x}^2}{\sqrt{-\gamma}}\right)\right) + \frac{1}{\gamma}\Gamma^M_{NP}\left(x'^2 \dot{x}^N \dot{x}^P + \dot{x}^2 x'^N x'^P\right) \\ = (\dot{x}^N x'^P - x'^N \dot{x}^P) H^M_{\ NP} \,. \end{aligned} \tag{5.3.37}$$

The key effect of including charge on the string is that, just as the path of a charged particle is curved in a magnetic field, the charged string will pick up transverse forces coming from the $H_3$ or $F_3$ fluxes. Thus, we do not expect a simple single-angle motion, such as that of the simple Ansatz considered in (5.1.7), and the general motion will be quite complex. However, at least one internal coordinate must have $\zeta$-dependence as well as time-dependence in order for this effect to be apparent, since $B_{MN}$ only has non-zero components in internal directions. So in fact the Ansatz with only time-dependence used in Section 5.1.2 is still a valid solution, if rather specialised.

Since there is no $H^0_{NP}$ component, the quantity $E$ given by the Nambu dynamics is still conserved, so the system still has a conserved energy. In order for the B-field to localise the string at the bottom of the throat, therefore, energy would have to be transferred into the other dimensions. This would require a damping term in the equation of motion for $r$, i.e. a term with opposite sign to $\dot{r}$. Since $H_3$ is antisymmetric, both $N$ and $P$ on the RHS of (5.3.37) must be angular directions when $M = r$, so that there can be no term containing $\dot{r}$ and therefore no damping term. Thus the conclusion that strings are not fixed at the tip of a warped throat is unchanged by the addition of this interaction. In fact, since the interaction with fluxes increases the amount of internal motion, the effect on the external loop motion will be to make it deviate even more from the exact flat-space form, (5.3.35).

## 5.4 Conclusion

In this chapter, we have explored explicitly the motion of a cosmic (super)string on a compactification with warped internal dimensions, using the Klebanov-Strassler

throat as an explicit test geometry. We find that there is no classical geometrical or dynamical mechanism that preferentially damps the motion in the internal dimensions. On the contrary, we observe a general tendency for motion in the internal dimensions either to become or persist in being relevant under a wide range of scenarios.

# Chapter 6

# Quintessence with black holes

In this chapter we motivate and derive an analytic, perturbative solution for a black hole in a quintessence background.

Quintessence was first proposed as an alternative to the cosmological constant in 1998 [35]. It is perhaps the simplest modification of gravity that can explain dark energy, in which a non-interacting scalar field with a potential is included in the gravitational action. Many other modified gravity models also include a scalar field, and we hope that our results will be useful in studying the interaction of general cosmological scalar fields with black holes. Examples of dark energy models with scalar fields include k-essence, where the kinetic term in the action is modified; chameleon fields, which interact with matter; and phantom dark energy, where the kinetic energy is negative, to name a few (see [43, 47] for reviews).

The first section of this chapter reviews relevant work on black hole solutions, scalar fields surrounding black holes, and the quintessence universe. Section 6.2 gives details of the metrics that inspire the final solution. The Schwarzschild-de Sitter spacetime is particularly important here, as we will write the quintessence black hole as a perturbative expansion around this metric. Section 6.3 gives the first order solution for the scalar field, and in Section 6.4, the first order corrections to the metric are given, showing the growth of the black hole as it slowly accretes the scalar field. This is the first time the backreaction of a cosmological scalar field on a black hole has been modelled analytically. The key results of this chapter are also given in [40].

## 6.1 Background

In this section we review work that is relevant to the problem of a black hole in a quintessence universe.

In the first subsection, 6.1.1, we discuss cosmological black hole solutions and the implications of no hair theorems for cosmological scalar fields. Secondly, in Section 6.1.2, we describe the basics of quintessence cosmology. Finally, Section 6.1.3 discusses the effect of an astrophysical black hole on a quintessence field, reviewing work on how the scalar field behaviour may change in the region around a black hole. Here we make use of the large separation between the scale of expansion of the universe and the scale of astrophysical black holes.

### 6.1.1 Cosmological black holes

There is one known exact black hole solution in a dynamical spacetime, known as the McVittie metric. It was found by McVittie in 1933 [119], but has been largely ignored due to difficulties in interpretting its meaning. It appears, on first glance, to describe a black hole in a FRW background with arbitrary scale factor, $a(t)$. It can be written as

$$ds^2 = \left(1 - \frac{r_s}{r} - H(t)^2 r^2\right) dt^2 + \frac{2H(t)r}{\sqrt{1 - r_s/r}} dr dt - \frac{dr^2}{1 - r_s/r} - r^2 d\Omega_{II}^2 \qquad (6.1.1)$$

where $H(t) = \dot{a}/a$. In the limit $H \to 0$, this becomes the Schwarzschild metric, (1.3.9). In the limit $r_s \to 0$, it is the FRW metric, (1.1.1), under the coordinate transformation $r = a(t)\tilde{r}$. However, it turns out that the would-be event horizon, which occurs at the smaller positive root of the function $(1 - r_s/r - H^2 r^2)$ (close to $r = r_s$), is in general singular.

Recently, in [96], the authors thoroughly analysed the structure of the McVittie metric and concluded that it does represent a black hole with a non-singular event horizon for any scale factor that asymptotes to an exponential at large $t$, i.e. in the presence of a cosmological constant. For a quintessence spacetime the asymptotics are very different, so McVittie's metric is not a good model for a black hole in a quintessence spacetime.

There are several problems with the McVittie metric as a description of an astrophysical black hole. Firstly, a "no accretion condition" is enforced, meaning the black hole does not accrete any matter, which is physically unrealistic. The energy-density, $\rho$, is homogeneous, which one expects to lead to accretion on to the black hole since it is surrounded by matter. However, the gravitational attraction of the black hole is balanced by an $r$-dependent negative pressure. This certainly does not model a realistic matter field. This is a case where Einstein's equations have been solved by choosing a metric and working out what the matter content must be in order to solve the equations, (1.2.6). While this can be a useful technique, it may also lead to unphysical solutions.

At this point it is worthwhile mentioning Kiselev's black hole solution [105], especially as it is known as a black hole surrounded by quintessence. Actually the use of the word quintessence here refers to the fact that the matter content of the spacetime has equation of state parameter, $-1 < \omega < -\frac{1}{3}$, which is the case for a cosmological quintessence scalar field. Here the similarity ends, since the spacetime far from the black hole is not a quintessence universe, the energy-momentum tensor is not that of a free scalar field (although the author suggests that it represents a scalar field coupled to cold dark matter), and the black hole again does not accrete any matter.

Exact black hole solutions, therefore, do not offer much insight into the properties of a quintessence black hole. The black hole is expected to accrete some of the quintessence field, and the field itself will somehow be affected by the presence of the black hole. To determine this behaviour it must be realistically modelled.

As discussed in Section 1.3, due to no hair theorems, scalar fields are not expected to have a non-trivial profile around black holes. In fact, on large timescales, it is expected that any excitation of the scalar field will die away, and thus, classically, it must sit at the minimum of its potential in some region around a black hole. No hair theorems are not rigorously proved, nor do they apply to a non-stationary scenario, for example a dynamical, expanding cosmology. However, it is widely believed that their spirit will be upheld, and since cosmological expansion will not have a significant effect on a black hole, it will not have a long-lived scalar field

surrounding it. Evidence to the contrary has been recently found in [17,18], where a massive scalar field surrounds a Schwarzschild black hole on cosmological timescales.

In a quintessence spacetime, no hair theorems are circumvented in a particular way. The quintessence field is a *rolling* scalar field, which means it is a dynamical field moving slowly down a potential. In general such a potential is monotonic, i.e. it has no minimum. Therefore it is impossible for the field to sit at the minimum of its potential in any region, including of course the region around the black hole, and thus the spirit of the no hair theorems cannot be upheld. It is inherently a dynamical field, and while it will not violate the no hair theorems by forming a stationary configuration, it is expected to have a long-lived profile. This is an example that violates the "spirit" of no hair.

### 6.1.2 Quintessence cosmology

In a quintessence cosmology, the accelerated expansion of the universe is driven by a massless scalar field rolling down a potential. Just as for the radiation era or matter era, the metric is taken to be FRW, and the matter content − a scalar field − determines the scale factor, $a(t)$ (see Section 1.1).

We include a scalar in the gravitational action as follows:

$$S = \int d^4x\sqrt{-g}\left(-\frac{R}{2\kappa} + \partial_\mu\phi\partial^\mu\phi - \bar{V}(\phi)\right), \tag{6.1.2}$$

where $\kappa = 8\pi G$ and $\bar{V}$ is a potential for the scalar field. Assuming a flat FRW cosmological metric,

$$ds^2 = dt^2 - a(t)^2(dr^2 - r^2 d\Omega^2) \tag{6.1.3}$$

and a homogeneous scalar field, $\phi$, depending only on $t$, the action gives the following Friedmann equations for the evolution of $\phi(t)$ and the scale factor, $a(t)$, which can be easily solved for simple potentials:

$$\ddot{\phi} = -\frac{1}{2}\bar{V}_{,\phi} - 3\dot{\phi}H, \tag{6.1.4}$$

$$H \equiv \frac{\dot{a}}{a} = \sqrt{\frac{\kappa}{3}}\sqrt{\dot{\phi}^2 + \bar{V}}. \tag{6.1.5}$$

A dot represents differentiation with respect to $t$. We use the potential

$$\bar{V} = M^4\exp(-\beta\phi), \tag{6.1.6}$$

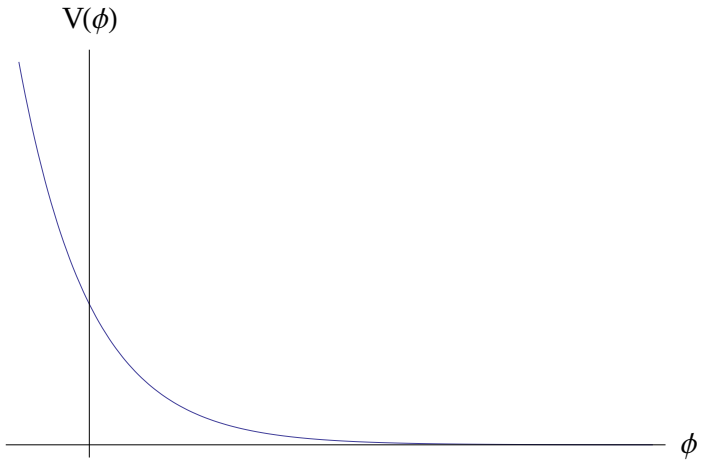


Figure 6.1: A potential, $\bar{V}$, for a rolling quintessence field

where $\beta$ has dimensions of length and $M$ is some mass scale associated with the scalar field. This potential is shown in Figure 6.1.

The potential (6.1.6) gives the solution to (6.1.4) and (6.1.5) as

$$a = \left(\frac{t}{t_0}\right)^k, \tag{6.1.7}$$

$$\phi_{cos} = \frac{2}{\beta}\ln\left(\frac{\beta M^2 t}{2\sqrt{3k-1}}\right), \tag{6.1.8}$$

where $t_0$ is a constant and $k = 4\kappa/\beta^2$. If $k > 1$ there will be an accelerated expansion. In fact we find that to fit within observational bounds, we must have $k \gg 1$. This can be seen by considering the equation of state,

$$\omega = \frac{\dot{\phi}^2 - \bar{V}}{\dot{\phi}^2 + \bar{V}}.$$

Putting in the solution for the scalar field (6.1.8), gives

$$\omega = -1 + \frac{2}{3k}.$$

Since observations constrain the equation of state to be close to $-1$ [109], this implies that $k \gg 1$. We will use this fact later in perturbative expansions.

The scalar field is increasing over time (as $\ln(t)$), moving down the potential in Figure 6.1, which is known as "rolling" down its potential. One can consider the potential energy from the scalar field to be driving the cosmological expansion. Other potentials that give similar behaviour include inverse powers of $\phi$ (for example

$V \sim \phi^{-2}$) and combinations thereof, to name a few. We propose that the exact form of the potential will not have a significant qualitative effect on the results presented in this thesis, and will discuss this further in Section 6.4.2.

The most realistic quintessence models are tracker solutions, in which the quintessence tracks the radiation energy density until the time of matter-radiation equality, at which point it decreases more slowly than matter, and comes to dominate only at late times. These models were proposed in 1999 [159, 182], where it was shown that tracker behaviour has very little dependence on the initial conditions, and gives a natural explanation for the scale of cosmic acceleration. This therefore provides a reasonable solution to the cosmological constant problem. Potentials that give this behaviour include inverse powers, $V \sim \phi^{-\alpha}$.

With an exponential potential, it has been shown that the spacetime cannot be asymptotically flat or asymptotically de Sitter [133], which are the two cases for which black hole no hair theorems have been shown to apply. This additionally supports the idea that no hair theorems do not apply to this system.

### 6.1.3 Quintessence field around a black hole

We will now consider how the presence of black holes in the universe affects the behaviour of a cosmological scalar field. This is a review of work to date, mainly from [91].

The expansion of the universe occurs on large distance- and time-scales relative to that of an astrophysical black hole, at least in the recent universe. Expansion is observed on intergalactic scales ($\mathcal{O}$(Mpc)), whereas a black hole is tiny even on galactic scales ($\mathcal{O}(\mu$pc)). At earlier times, there may not have been such a separation of scales, so in this section we focus on late time black holes.

The separation of scales allows the division of spacetime approximately into three regions:

(i) *Cosmological region:* defined as "far from the black hole", where cosmological expansion is the only significant effect. Here the spacetime should closely resemble the quintessence cosmology, (6.1.3), with (6.1.7) and (6.1.8).

(ii) *Intermediate region:* between intergalactic and subgalactic scales, where both

cosmological expansion and the gravity of the black hole have an extremely small effect. Here the spacetime is essentially flat.

(iii) *Black hole region:* where the spacetime curvature of the black hole is significant. Here we take the metric to be that of a Schwarzschild black hole. The separation of scales justifies ignoring the backreaction of the scalar field in this region.

We will now consider the behaviour of the scalar field in each region.

In region (i) the scalar field will be rolling down its potential (Figure 6.1), and homogeneous in space (for this particular coordinate choice). Its behaviour will be given by (6.1.8).

In region (ii) the scalar field evolution is approximately linear, $\dot{\phi} \simeq const$. The limit in which one obtains a flat metric ($a(t) = const$) is the limit in which the potential, $\bar{V}$ is everywhere zero. Therefore, in region (ii) we must assume the contribution of $\bar{V}$ is small enough to be ignored. The equation for the scalar field, (6.1.4), then becomes simply that of a free scalar field,

$$\ddot{\phi}_{flat} = 0. \tag{6.1.9}$$

By comparison with the cosmological solution we therefore take

$$\phi_{flat} \simeq \phi_0 + \frac{2t}{\beta t_0} \tag{6.1.10}$$

in the intermediate region. $\phi_0$ is a constant, which again from the cosmological solution, (6.1.8), takes the value,

$$\phi_0 = \frac{2}{\beta} \ln \left( \frac{\beta t_0 M^2}{2e\sqrt{3k-1}} \right). \tag{6.1.11}$$

Clearly a linear approximation such as this is valid only on short timescales, and indeed the approximation of spacetime as flat is valid only on timescales for which $a(t)$ does not significantly change. The scale factor is $a(t) = (t/t_0)^k$, and it is therefore approximately constant on a time interval $\Delta t \lesssim t_0$, which is also the region for which the scalar field evolution is approximately linear. Therefore the solution (6.1.10) is valid throughout region (ii).

In region (iii), close to the black hole, we approximate spacetime by the Schwarzschild metric. This is not an exact solution to Einstein's equations in the presence

of the quintessence field, but if the effect of expansion and therefore the scalar field is small on these length scales, it will be a reasonable approximation. Since the Schwarzschild metric is asymptotically flat, we can extend this metric as far as region (ii), and thus match the cosmological and black hole spacetimes together.

The scalar field evolution in region (iii) must also be matched onto the cosmological solution. The behaviour of a scalar field on a Schwarzschild background was derived by Jacobson in 1999 [91]. The equation of motion for $\phi$ is (see (1.3.9) for the Schwarzschild metric):

$$\Box\phi = \frac{\phi_{,tt}}{\left(1-\frac{r_s}{r}\right)} - \left(1-\frac{r_s}{r}\right)\phi_{,rr} - \left(\frac{2}{r}-\frac{r_s}{r^2}\right)\phi_{,r} = -\frac{1}{2}\bar{V}_{,\phi}. \tag{6.1.12}$$

As $r$ becomes large, away from the black hole, we regain the flat space evolution equation, (6.1.9). As before, ignoring the backreaction of the scalar field means the $\bar{V}$ terms must be neglected. At this order, the equation of motion for $\phi$ therefore becomes,

$$\frac{\phi_{,tt}}{\left(1-\frac{r_s}{r}\right)} + \left(1-\frac{r_s}{r}\right)\phi_{,rr} + \left(\frac{2}{r}-\frac{r_s}{r^2}\right)\phi_{,r} = 0. \tag{6.1.13}$$

Clearly the flat space solution from region (ii), equation (6.1.10), solves (6.1.13). The problem is that this solution is not regular on the black hole event horizon, because the coordinate $t$ goes to infinity here. As mentioned, the flat space approximation is only valid in short time intervals, and thus will naturally not be valid where $t$ becomes very large. From [91], if $\phi$ is chosen to depend only on $r$, the solution to (6.1.12) is

$$\phi_{rad} = \ln\left(1-\frac{r_s}{r}\right). \tag{6.1.14}$$

Therefore, a linear combination of $\phi_{rad}$ and $\phi_{flat}$ that approaches $\phi_{flat}$ at large $r$, and is regular on the horizon, will give a physically reasonable first order solution for $\phi$. Since the horizon is a null surface, it is sensible to write the solution in terms of a null coordinate, $v_s$, and $r$ (which is finite on the horizon, $r = r_s$). One example of a null coordinate that is finite on the future event horizon is

$$v_s = t + r_\star = t + r + r_s \ln\left(\frac{r}{r_s} - 1\right). \tag{6.1.15}$$

In this case, the appropriate solution is found to be,

$$\phi = \phi_0 + \dot{\phi}_c\left(t + r_s\ln\left(1-\frac{r_s}{r}\right)\right) = \phi_0 + \dot{\phi}_c\left(v_s - r - r_s\ln\left(\frac{r}{r_s}\right)\right). \tag{6.1.16}$$

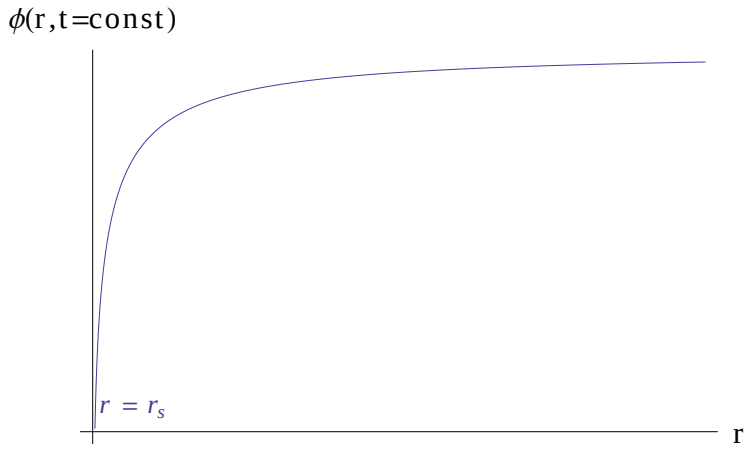


Figure 6.2: $\phi$ at fixed $t$ - field appears "delayed" relative to cosmological case.

A similar solution was also derived by Frolov and Kofman [72]. The solution clearly has the correct properties. The $r$-dependence disappears when $r$ becomes large, and the field is finite on the horizon. Everywhere, $\phi$ increases linearly with $t$, so it is everywhere rolling. If we keep $t$ fixed and look at the $r$-dependence, it appears that the rolling scalar field is "left behind" as one moves to smaller $r$ (i.e. towards the black hole), since the value of $\phi$ is smaller there. Frolov and Kofman refer to this as the "delayed field approximation", and it is shown on Figure 6.2. However, close to the event horizon the coordinate $t$ is no longer very meaningful, since the horizon occurs at infinite $t$. On the horizon itself, (6.1.16) increases linearly with $v_s$. If we keep $v_s$ fixed and look at the $r$-dependence, the value of $\phi$ gets *larger* towards the horizon, so it has effectively rolled *further* down its potential, contrary to the idea that it is left behind. The $r$-dependence at fixed $v_s$ is shown on Figure 6.3. The nature of the spatial dependence of $\phi$ is therefore somewhat ambiguous since it is a coordinate-dependent statement, but it is clear at least that it rolls down its potential in all parts of the spacetime up to and including the event horizon itself.

## 6.2 Metrics

In our study of the fully backreacted system, we take inspiration from various different metrics, and work with particular coordinate systems. This section gives the relevant metrics and coordinate systems, with some discussion of their properties.

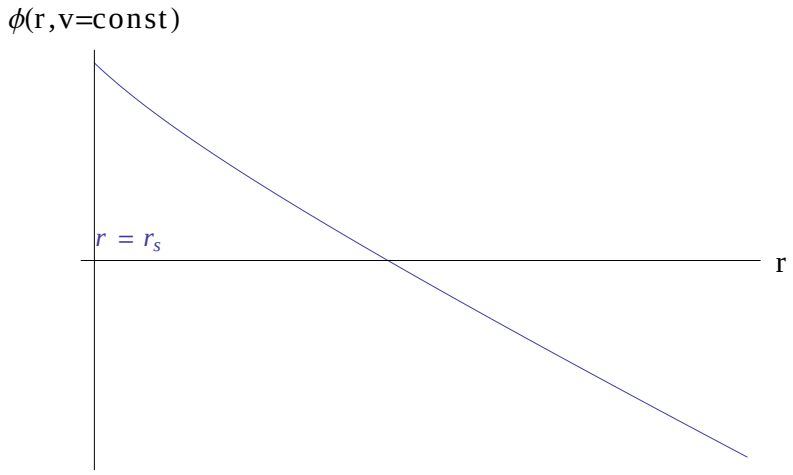


Figure 6.3: $\phi$ at fixed $v_s$ - field appears "ahead" of cosmological case.

Firstly, note that a black hole in a quintessence cosmology may be considered as a 2-dimensional problem by imposing spherical symmetry. The most general spherically symmetric metric may be written as [32]:

$$ds^2 = e^{2\nu}B^{-1/2}4dUdV - Bd\Omega_{II}^2, \tag{6.2.17}$$

where $U$ and $V$ are null coordinates, and $\nu$ and $B$ are two free functions, $\nu(U,V)$ and $B(U,V)$. With the metric written in this form, Einstein's equations become particularly simple. The function $B$ in particular is interesting because it is proportional to the area of 2-spheres, and therefore gives some physical information about the spacetime.

The Schwarzschild metric, (1.3.9), may be written in this form as follows:

$$ds_{schw}^2 = \frac{r_s^2}{-uv}\left(1 - \frac{r_s}{r}\right)4dudv - r^2 d\Omega_{II}^2, \tag{6.2.18}$$

with the coordinate transformation

$$u = -\exp\left(\frac{1}{2r_s}(r^\star - t)\right) \;\; ; \;\; v = \exp\left(\frac{1}{2r_s}(r^\star + t)\right), \tag{6.2.19}$$

where

$$r^\star = r + r_s \ln\left|\frac{r}{r_s} - 1\right|. \tag{6.2.20}$$

This corresponds to

$$t = r_s \ln(-v/u) \;\; ; \;\; r = r(uv), \tag{6.2.21}$$

where the function $r$ must be determined numerically. The coordinates $u$ and $v$ are known as Kruskal coordinates [110], and in these coordinates the metric is finite on the event horizon (the coordinate singularity present in (1.3.9) is eliminated). The event horizon occurs at $u = 0$, where the coordinate $t \to \infty$, and $r^\star \to -\infty$. The singularities in these coordinates "cancel out", meaning that $v$ is finite and runs along the event horizon. Of course, the event horizon is described by a null coordinate because it is a null surface, which is one reason for choosing to work in a null coordinate system.

Now in the following sections we look at some of the spacetimes that are relevant to our problem. There are a total of 4 interrelated metrics. We are searching for a quintessence black hole metric. Far from the black hole (at large $r$), the quintessence black hole should be the same as the cosmological quintessence metric without the black hole (6.1.3). Another pair of metrics with a similar relation is known: the Schwarzschild-de Sitter black hole metric, which is the same as pure de Sitter spacetime in the large $r$ limit. Considering the two spacetimes without a black hole − quintessence cosmology and de Sitter space − we find that we can write one as a perturbative expansion away from the other. Therefore, we hope that on adding a black hole to each of these spacetimes, they may still be perturbatively equivalent. Indeed, we will later write the quintessence black hole as a perturbation away from Schwarzschild-de Sitter spacetime.

In Section 6.2.1 we look at the Schwarzschild-de Sitter black hole and compare it with pure de Sitter space. In Section 6.2.2 we show the relation between the two cosmological metrics (de Sitter and Quintessence).

### 6.2.1 De Sitter space, with and without a black hole

The only known exact metric for a black hole in an expanding universe is the *Schwarzschild-de Sitter metric*. This describes a stationary black hole in a background with a positive cosmological constant, $\Lambda$. Without a black hole, a cosmological constant gives an exponentially expanding cosmology (see Section 1.1), known as de Sitter space. This is when the scale factor $a(t)$ in the FRW metric (1.1.1) is proportional to $e^{Ht}$, where $H^2 = \Lambda/3$. Part of the reason that a black hole can be

added analytically into this spacetime is that the metric can be re-written in static coordinates. Firstly, to avoid confusion, we will now replace the coordinates $t$ and $r$ in the FRW metric with $\tau$ and $\rho$, with $t$ and $r$ coordinates reserved for the static form. So we have

$$ds^2_{dS} = d\tau^2 - a(\tau)^2 \left(d\rho^2 - \rho^2 d\Omega^2_{II}\right), \tag{6.2.22}$$

with $a(\tau) = e^{H\tau}$. The transformation to static coordinates $t$ and $r$ is given by

$$\rho = \frac{re^{-Ht}}{\sqrt{1-H^2r^2}}\,; \quad e^{2H\tau} = e^{2Ht}(1-H^2r^2). \tag{6.2.23}$$

So the metric becomes

$$ds^2_{dS} = \left(1-H^2r^2\right)dt^2 - \frac{dr^2}{1-H^2r^2} - r^2 d\Omega^2_{II}. \tag{6.2.24}$$

The Schwarzschild-de Sitter metric in static coordinates is written as

$$ds^2_{SdS} = \left(1 - \frac{r_s}{r} - H^2r^2\right)dt^2 - \frac{dr^2}{1-\frac{r_s}{r} - H^2r^2} - r^2 d\Omega^2_{II}. \tag{6.2.25}$$

This can be clearly compared with the Schwarzschild metric (1.3.9) and the de Sitter metric (6.2.24) in similar coordinates. At large $r$, the black hole terms ($\propto r_s$) disappear and we regain the de Sitter metric, thus the black hole only has a localised effect. For a realistic cosmology, the black hole length scale, $r_s$, will be much smaller than the cosmological length scale, $1/H$. Therefore we may assume that $Hr_s \ll 1$. This metric then has two coordinate singularities, at the two positive roots of the function $(1 - r_s/r - H^2r^2)$. The smaller root corresponds to the black hole horizon, and the outer one corresponds to the *cosmological horizon*, which is an acceleration horizon. This occurs in an expanding universe because parts of the universe that are sufficiently far away from an observer are moving away so quickly that it is impossible ever to reach them (i.e. they are not within the future lightcone of the observer). Like the black hole horizon, then, the cosmological horizon will be a null surface. In pure de Sitter space, with no black hole, there is a cosmological horizon at $r = 1/H$.

The de Sitter metric may be written in the form (6.2.17), as follows,

$$ds^2_{dS} = \frac{1-H^2r^2}{4H^2UV} 4dUdV - r^2 d\Omega^2_{II}, \tag{6.2.26}$$

where

$$U = -\frac{1}{2H}e^{-H(t-r^\star)} \; ; \quad V = -\frac{1}{2H}e^{-H(t+r^\star)}, \tag{6.2.27}$$

$$r^\star = \frac{1}{2H}\ln\left(\frac{1+Hr}{1-Hr}\right). \tag{6.2.28}$$

The Schwarzschild-de Sitter metric may also be written in the form (6.2.17) in a similar way,

$$ds^2_{SdS} = \frac{R_c^2\left(1-\frac{r_s}{r}-H^2r^2\right)}{UV}4dUdV - r^2d\Omega^2_{II} \tag{6.2.29}$$

with

$$U = R_c e^{\frac{t-r^\star}{2R_c}} \; ; \quad V = R_c e^{\frac{t+r^\star}{2R_c}}; \tag{6.2.30}$$

$$r^\star = R_N\ln(r-r_N) + R_h\ln(r-r_h) + R_c\ln(r_c-r). \tag{6.2.31}$$

Now $r_h$, $r_c$ and $r_N$ are the 3 roots of $(1-r_s/r-H^2r^2)$, corresponding to the black hole event horizon, the cosmological horizon, and a root at negative $r$ which does not appear in the spacetime. The $R_i$ are given by:

$$R_i = \frac{r_i}{1-3H^2r_i^2}. \tag{6.2.32}$$

We have chosen $U$ and $V$ so that the metric is regular at the cosmological horizon. We could instead take coordinates so that it is regular at the black hole horizon (see Section 6.3), but there is no known way to remove both coordinate singularities simultaneously. Assuming that $Hr_s$ is small, we arrive at the following approximations,

$$r_h \simeq r_s\left(1+H^2r_s^2\right) \; ; \; r_c \simeq \frac{1}{H}\left(1-\frac{Hr_s}{2}\right) \; ; \; r_N \simeq \frac{1}{H}\left(-1-\frac{Hr_s}{2}\right) \tag{6.2.33}$$

$$R_h \simeq r_s(1+4H^2r_s^2) \; ; \; R_c \simeq -\frac{1}{2H}(1+Hr_s) \; ; \; R_N \simeq \frac{1}{2H}(1-Hr_s). \tag{6.2.34}$$

Examining these, the relationship between de Sitter and Schwarzschild-de Sitter space in these coordinates is apparent. The factor $R_c^2$ in the metric (6.2.29) is approximately equal to the factor $1/(4H^2)$ in (6.2.26), and similarly the multiplicative factors in the coordinates $U$ and $V$ are the same up to order $Hr_s$. Comparing the two $r$ coordinates, we see that they too are equivalent up to order $Hr_s$. For the de Sitter metric (from (6.2.28)) we have

$$Hr = \tanh(Hr^\star). \tag{6.2.35}$$

Expanding in $Hr_s$, for Schwarzschild-de Sitter we have

$$Hr \simeq \tanh\left(\frac{-r^\star}{2R_c}\right) - Hr_s/2 + \epsilon \tag{6.2.36}$$

where

$$\epsilon = Hr_s \cosh^{-2}\left(\frac{-r^\star}{2R_c}\right) \ln\left(1 + \coth\left(\frac{-r^\star}{2R_c}\right)\right). \tag{6.2.37}$$

At large $r$, $\epsilon \to 0$, and so the two expressions (6.2.35) and (6.2.36) become approximately the same.

### 6.2.2 Comparing cosmological metrics

In this section we show that it is possible to write the cosmological quintessence metric as an expansion around de Sitter space in a small parameter. Inspired by this, we will later write the quintessence black hole as a perturbative expansion around the Schwarzschild-de Sitter black hole.

Quintessence and de Sitter cosmologies are both given by the FRW metric, (6.2.22), but with different scale factors. FRW can in general be written in the form (6.2.17) as follows,

$$ds^2 = a^2(\eta)\left(4dUdV - \rho^2 d\Omega_{II}^2\right), \tag{6.2.38}$$

where $\eta$ is a conformal time coordinate defined so that $ad\eta = d\tau$, and $U$ and $V$ are given by

$$U = \frac{\eta - \rho}{2} \;\; ; \;\; V = \frac{\eta + \rho}{2}. \tag{6.2.39}$$

For quintessence, $a(\eta) = (\eta(1-k)/t_0)^{k/(1-k)}$. For de Sitter space, $a(\eta) = -1/(\eta H)$, where we set $H = k/t_0$ for comparison with the quintessence solution. Comparing (6.2.38) with the general form (6.2.17), we see that the metric functions are

$$B = a(\eta)^2\rho^2 \; ; \quad e^{2\nu} = a(\eta)^3\rho. \tag{6.2.40}$$

The quintessence cosmology has equation of state parameter $\omega = -1 + \frac{2}{3k}$. Since $\omega$ is observed to be close to $-1$, it is reasonable to take $k$ to be large (see Section 6.1.2). This allows us to expand the cosmological spacetime around de Sitter spacetime in a power series in $1/k$. Here we will go up to linear order in $1/k$.

In order to compare the metrics we expand the quintessence scale factor as follows

$$a_{quint} = \left(\frac{\eta(1-k)}{t_0}\right)^{\frac{k}{1-k}} \simeq \left(\frac{-\eta k\left(1-\frac{1}{k}\right)}{t_0}\right)^{-1-\frac{1}{k}}$$

$$\simeq \frac{t_0}{-\eta k}\left(1+\frac{1}{k}\left(1-\ln\left(\frac{-\eta k}{t_0}\right)\right)\right) \equiv -\frac{1}{\eta H}\left(1+\frac{1}{k}\left(1-\ln\left(\frac{-\eta k}{t_0}\right)\right)\right). \quad (6.2.41)$$

Then using (6.2.40), this gives the metric functions as perturbations around de Sitter spacetime,

$$B_{quint} \simeq B_{dS}\left(1+\frac{2}{k}\left(1-\ln\left(\frac{-\eta k}{t_0}\right)\right)\right) \quad (6.2.42)$$

$$e^{2\nu}_{quint} \simeq e^{2\nu}_{dS}\left(1+\frac{3}{k}\left(1-\ln\left(\frac{-\eta k}{t_0}\right)\right)\right). \quad (6.2.43)$$

Subscripts $dS$ and $quint$ denote the de Sitter and quintessence metric functions respectively. Note that this expansion is not valid when $\eta$ is either very small or large, whereupon the log term becomes large. This corresponds to early and late times. Thus, the expansion is valid everywhere in space but not across the whole of time.

In order to check that this expansion solves Einstein's equations from the action (6.1.2) in a consistent manner, we must also approximate the behaviour of the quintessence scalar field, $\phi$. We take $\bar{V}$, the potential for the scalar field, to be exponential as before (giving the power law expansion),

$$\bar{V} = M^4 \exp(-\beta\phi). \quad (6.2.44)$$

For the cosmological solution the scalar field takes the following exact form:

$$\phi = \frac{2}{\beta}\ln\left(\frac{\beta M^2}{2\sqrt{3k-1}}\right) + \frac{2}{\beta(1-k)}\ln(-\eta) + \frac{2}{\beta(1-k)}\ln\left(\frac{k-1}{t_0^k}\right) \quad (6.2.45)$$

which gives

$$\phi \simeq \phi_0 - \frac{2}{\beta k}\ln(-\eta), \quad (6.2.46)$$

where $\phi_0$ is a constant. In the Einstein equations, $\phi_0$ appears only in the potential, $\bar{V}$. We approximate the potential by

$$\bar{V} = \frac{4(3k-1)}{\beta^2}\left(\frac{t_0}{\eta(1-k)}\right)^{\frac{2}{1-k}} \simeq \frac{4(3k-1)}{\beta^2 t_0^2}\left(1+\frac{2}{k}\ln\left(\frac{-\eta k}{t_0}\right)\right)$$

$$\Rightarrow \kappa\bar{V} \simeq H^2\left(3-\frac{1}{k}\left(1-6\ln\left(\frac{-\eta k}{t_0}\right)\right)\right). \quad (6.2.47)$$

Here we use $k = 4\kappa/\beta^2$. Putting this into the Einstein equations along with the perturbative metric functions, (6.2.42,6.2.43), is consistent up to linear order in $1/k$, so the expansion is indeed valid. The Einstein equations are given by equations (6.3.48-6.3.52), and discussed further in the following sections. Note that all of the expansions may be written in terms of the null coordinates $U$ and $V$ using $\eta = (U + V)$ (see (6.2.39)).

## 6.3 First order expansion and solution for the scalar field

To study the full, backreacted quintessence black hole system, we now look at the equations of motion for the metric and scalar field. Using the spherically symmetric form of the metric, (6.2.17), gives the following equations

$$B_{,UV} = 2\left(\kappa\bar{V}(\phi)B^{1/2} - B^{-1/2}\right)e^{2\nu} \tag{6.3.48}$$

$$\nu_{,UV} = \frac{1}{2}\left(\kappa\bar{V}(\phi)B^{-1/2} + B^{-3/2}\right)e^{2\nu} - \kappa\phi_{,U}\phi_{,V} \tag{6.3.49}$$

$$\phi_{,UV} = -\frac{1}{2}\bar{V}_{,\phi}(\phi)B^{-1/2}e^{2\nu} - \frac{1}{2B}\left(B_{,U}\phi_{,V} + B_{,V}\phi_{,U}\right) \tag{6.3.50}$$

$$B_{,VV} = 2\nu_{,V}B_{,V} - 2\kappa B\phi_{,V}^2 \tag{6.3.51}$$

$$B_{,UU} = 2\nu_{,U}B_{,U} - 2\kappa B\phi_{,U}^2. \tag{6.3.52}$$

Here, the final two equations are integrability conditions for the remaining three.

Firstly we will show that the first order contribution of the scalar field acts like a cosmological constant (which we expect since the quintessence cosmology is shown to be de Sitter space to first order) meaning the Schwarzschild-de Sitter metric is a consistent solution at this order. The first order contributions from the scalar field are the potential terms, $\propto \kappa\bar{V}$ in equations (6.3.48,6.3.49). The $\phi$-derivative terms are suppressed by a factor $1/k$ relative to the potential terms:

$$\kappa\bar{V} \simeq 3H^2 = \Lambda \tag{6.3.53}$$

$$\phi_{,U} \sim \phi_{,V} = \mathcal{O}\left(\frac{1}{\beta k}\right) \Rightarrow \kappa(\phi')^2 \sim \frac{1}{k}. \tag{6.3.54}$$

Note that, although in a cosmological setting $H$ will be a small parameter, we do not make any approximation other than the expansion in $1/k$; namely we do not assume that $Hr_s$ is small. Therefore our results will also apply to a situation in which a black hole is a significant fraction of the cosmological horizon size, such as might have been the case in the early universe. With (6.3.53) and assuming the $\phi$-derivative terms are suppressed (6.3.54), the equations for the metric become

$$B_{,UV} = 2\left(3H^2B^{1/2} - B^{-1/2}\right)e^{2\nu} \tag{6.3.55}$$

$$\nu_{,UV} = \frac{1}{2}\left(3H^2B^{-1/2} + B^{-3/2}\right)e^{2\nu} \tag{6.3.56}$$

$$B_{,VV} = 2\nu_{,V}B_{,V} \tag{6.3.57}$$

$$B_{,VV} = 2\nu_{,V}B_{,V}. \tag{6.3.58}$$

These are exactly equivalent to Einstein's equations (1.2.6) with a cosmological constant, $\Lambda = 3H^2$. We therefore take the Schwarzschild-de Sitter metric as the first order in the metric, and write it as

$$ds^2_{SdS} = \frac{R_c^2 N}{UV}4dUdV - r^2 d\Omega^2_{II}, \tag{6.3.59}$$

where

$$N = 1 - \frac{r_s}{r} - H^2r^2. \tag{6.3.60}$$

The equation for $\phi$, (6.3.50), is at a higher order than those for the metric, since $\bar{V}_{,\phi} = -\beta\bar{V}$, and $k = 4\kappa/\beta^2$ is large and therefore $\beta$ is a small parameter, so this equation is suppressed by a factor of $\beta$ relative to the others. This means that we can solve the system perturbatively by first solving this equation for $\phi$, and then putting that solution into the equations for the metric, which gives the next order corrections to the metric. These corrections then give the next order terms in $\phi$, and so forth. This would theoretically allow an expansion to be found to arbitrary order in $1/k$.

We expect the solution for $\phi$ to look like the cosmological solution, (6.2.46), at large $r$, when far from the black hole. Integrating up (6.3.57,6.3.58) gives

$$B = B(F(V) + G(U)), \tag{6.3.61}$$

$$e^{2\nu} = F'(V)G'(U)B'(F+G), \tag{6.3.62}$$

where $F(V)$ and $G(U)$ can be any functions. Here, and in what follows, prime represents differentiation with respect to the argument of a function, whatever this may be. So the $\phi$-equation (6.3.50) becomes

$$\phi_{,UV} = \frac{\beta}{2}\bar{V}_0 B^{-1/2}B'F'G' - \frac{B'}{2B}\left(G'\phi_{,V} + F'\phi_{,U}\right), \tag{6.3.63}$$

where $\bar{V}_0 = 3H^2/\kappa$ is the lowest order term in $\bar{V}$. We see that the following Ansatz will solve this equation:

$$\phi = \phi_0 + (F-G)\phi_1 + \varphi(F+G), \tag{6.3.64}$$

where $\phi_0$ and $\phi_1$ are constants, if

$$\varphi'' = \frac{\beta}{2}\bar{V}_0 B^{-1/2}B' - \frac{B'}{B}\varphi' \Rightarrow (B\varphi')' = \frac{3\beta H^2}{2\kappa}B^{1/2}B' \tag{6.3.65}$$

$$\Rightarrow \varphi = \int\left[\frac{\beta H^2}{\kappa}B^{1/2} + \frac{C}{B}\right]\frac{dB}{B'}. \tag{6.3.66}$$

Now it is necessary to know the general form of $B$, which is obtained by solving equation (6.3.55), giving

$$B'' = 2(3H^2B^{1/2} - B^{-1/2})B' \tag{6.3.67}$$

$$\Rightarrow B' = 4H^2B^{3/2} - 4B^{1/2} + 4r_s \tag{6.3.68}$$

where $4r_s$ is an integration constant, and we have defined it to take this value since this gives the Schwarzschild-de Sitter solution. Defining the $r$ coordinate by $r = \sqrt{B}$ gives $B' \equiv 2rr' = -4rN$, and therefore

$$\varphi = -\frac{1}{2}\int\left[\frac{\beta H^2 r}{\kappa N} + \frac{C}{r^2 N}\right]dr = -\sum_i\left(\frac{\beta H^2}{2\kappa}r_i + \frac{C}{2r_i^2}\right)R_i\ln|r-r_i| + \frac{C}{r_s}\ln r + c. \tag{6.3.69}$$

Here, as before, the $r_i$ are the roots of $N$, and the $R_i$ are defined by equation (6.2.32). $F(V)$ and $G(U)$ may be set as any function by a coordinate transformation of $U$ and $V$. We choose the constants $C$ and $\phi_1$ to ensure that the scalar field is finite both on the black hole event horizon, at $r = r_h$, and on the cosmological horizon, at $r = r_c$. It is possible, as mentioned in Section 6.2.1, to take a coordinate system so that

the metric is finite on either the cosmological horizon or the event horizon, but not both. The metric (6.3.59) uses the coordinates that are finite on the cosmological horizon, which correspond to

$$U = R_c \exp\left(\frac{2G}{R_c}\right) \; ; \quad V = R_c \exp\left(\frac{-2F}{R_c}\right). \tag{6.3.70}$$

The coordinates that are finite on the black hole event horizon are

$$u = -R_h \exp\left(\frac{-2G}{R_h}\right) \; ; \quad v = R_h \exp\left(\frac{-2F}{R_h}\right). \tag{6.3.71}$$

These are equivalent to the Kruskal coordinates for the Schwarzschild metric (6.2.18) in the limit that $H \to 0$. If we write $\phi$ in these two coordinate systems we can find the constraints on $\phi_1$ and $C$ to ensure that it is regular. In the cosmological coordinate system (6.3.70), we impose that $\phi$ is finite at $V = 0$, which corresponds to $r = r_c$, and gives the constraint

$$-\frac{R_c\phi_1}{2} - \left(\frac{\beta H^2 r_c}{2\kappa} + \frac{C}{2r_c^2}\right) R_c = 0. \tag{6.3.72}$$

In the black hole coordinates, (6.3.71), we impose that $\phi$ is regular at $u = 0$ or $r = r_h$, which gives

$$\frac{R_h\phi_1}{2} - \left(\frac{\beta H^2 r_h}{2\kappa} + \frac{C}{2r_h^2}\right) R_h = 0. \tag{6.3.73}$$

Finally, these two conditions give

$$\phi_1 = \frac{\beta}{\kappa}\frac{(r_h - r_c)}{r_h^2 + r_c^2}, \tag{6.3.74}$$

$$C = -\frac{\beta H^2}{\kappa}\frac{r_h^2 r_c^2 (r_h + r_c)}{r_h^2 + r_c^2}. \tag{6.3.75}$$

In order to give an idea of the overall behaviour of the scalar field, Figure 6.4 shows lines of constant $\phi$. On this plot we have compactified all of the spacetime inside the two horizons into a finite box, using the compactification

$$u_c = \frac{1+U}{1-U} \; ; \; v_c = \frac{1+V}{1-V} \tag{6.3.76}$$

for the two axes. $\phi$ becomes larger towards the top of the plot. Close to the event horizon, it is clear that $\phi$ depends only on $V$.

We can now compare the quintessence field in the presence of a black hole with the pure quintessence solution, (6.2.46). On Figure 6.5, the lines of constant $\phi$ for

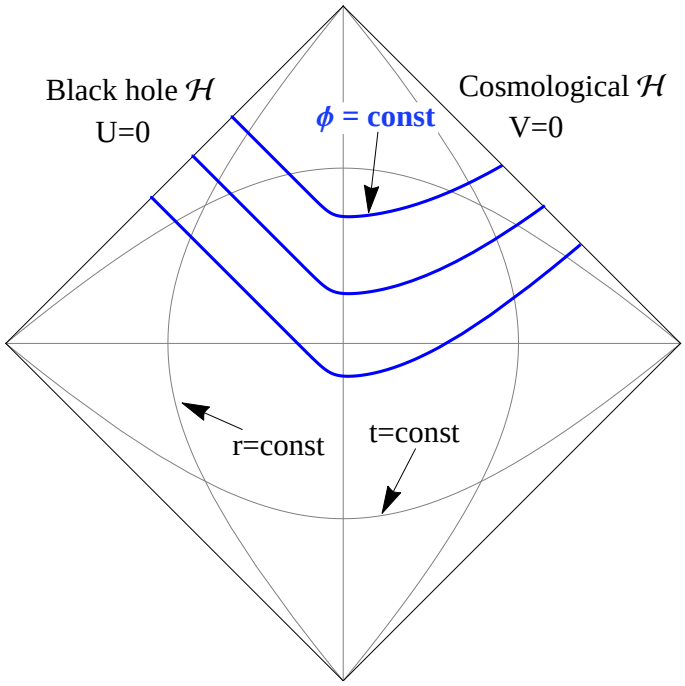


Figure 6.4: Lines of constant $\phi$ on a compactified diagram of the Schwarzschild-de Sitter spacetime, shown in blue. The grey lines show constant surfaces for the static coordinates $t$ and $r$. Here we have taken $H = 1/500$, $r_s = 15$.

the quintessence solution are added to the spacetime diagram from Figure 6.4. These surfaces correspond to $\eta = U + V = const$, since the scalar field solution (6.2.46) depends only on the timelike coordinate $\eta$. We see that the profiles start to deviate at around the line $U = V$, which corresponds to $r^\star = 0$. In pure quintessence, the spacetime doesn't actually extend past this point, so we certainly do not expect the field profiles to match beyond here. The black hole will start to have a large effect on the spacetime beyond $r^\star = 0$, so again it is reasonable that the scalar field behaviour starts to deviate here.

One interesting feature that may be observed in Figure 6.5 is that looking at the field profile along $U + V = const$ surfaces, the scalar field energy is higher near the black hole horizon − it has rolled less far down its potential. This agrees with the "delayed field approximation" of Frolov and Kofman (see Section 6.1.3). We may perhaps consider the scalar field to clump around the black hole. It is difficult, however, to be definitive since this is coordinate-dependent.

The horizon behaviour of the scalar field, $\phi \sim \ln V \sim t + r^\star$ agrees with Jacobson

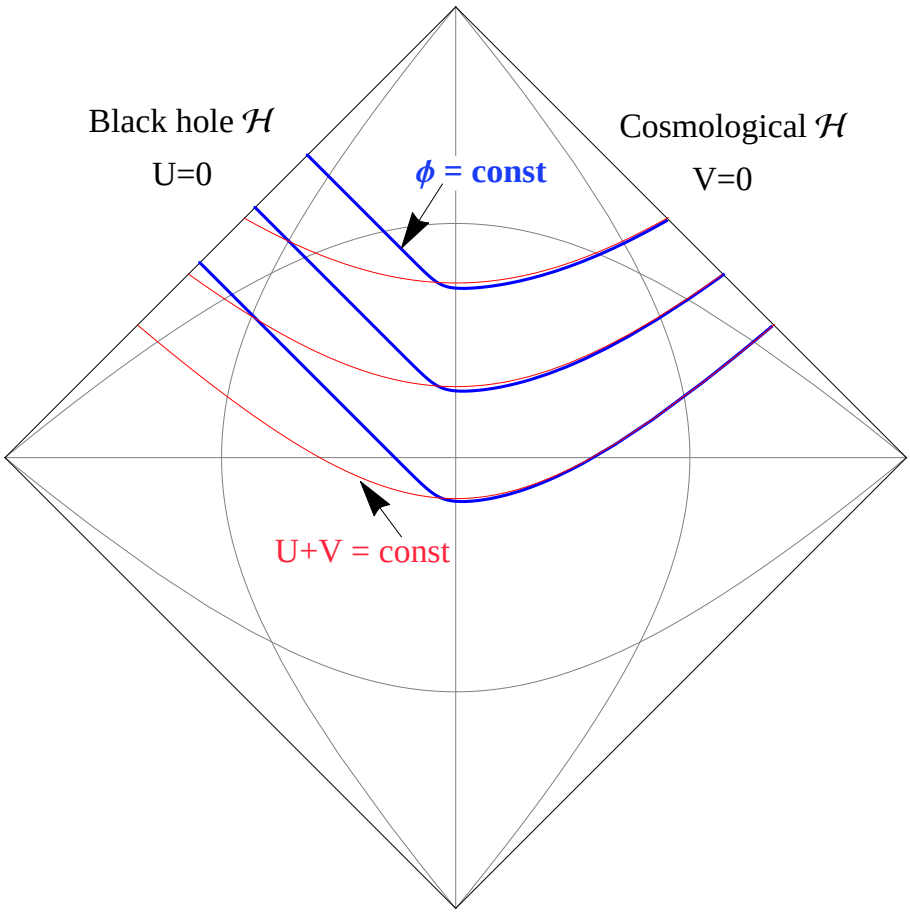


Figure 6.5: Blue lines show surfaces of constant $\phi$ in the Schwarzschild-de Sitter background as in Figure 6.4. Red lines show surfaces of constant $\phi$ for the pure quintessence field, with no black hole, for comparison.

[91] and Frolov and Kofman [72]. Since the field depends only on $V$ here, it is regular, and continues its "rolling" behaviour.

## 6.4 Backreaction

In this section we consider the backreaction of the scalar field solution (6.3.64,6.3.69) on the metric.

Inspired by the expansion of the cosmological quintessence metric around the de Sitter metric, (6.2.42,6.2.43), we write the metric perturbations in the following form,

$$B = r^2\left(1+\frac{\delta_1}{k}\right), \tag{6.4.77}$$

$$e^{2\nu} = \frac{rR_c^2N}{UV}\left(1+\frac{\delta_2}{k}\right). \tag{6.4.78}$$

Now we use the Einstein equations, (6.3.48-6.3.52), to find solutions for $\delta_1(U,V)$ and $\delta_2(U,V)$. Working in the coordinate system that is finite on the cosmological horizon, given by (6.3.70), the metric takes the form (6.3.59), and from the equation for $B'$, (6.3.68), the derivatives are

$$r_{,U} = -\frac{R_cN}{U}\ ; \quad r_{,V} = \frac{R_cN}{V}. \tag{6.4.79}$$

First consider the equations

$$B_{,VV} = 2\nu_{,V}B_{,V} - 2\kappa B\phi_{,V}^2 \tag{6.4.80}$$

$$B_{,UU} = 2\nu_{,U}B_{,U} - 2\kappa B\phi_{,U}^2. \tag{6.4.81}$$

If each equation is divided by $B_{,V}$ and $B_{,U}$, respectively, they can be integrated, giving

$$\ln B_{,U} = 2\nu + 2\kappa\int\frac{UdUr}{2R_cN}\phi_{,U}^2 + F(V), \tag{6.4.82}$$

$$\ln B_{,V} = 2\nu - 2\kappa\int\frac{VdVr}{2R_cN}\phi_{,V}^2 + G(U). \tag{6.4.83}$$

For brevity, define the integrals

$$2\kappa k\int\frac{VdVr}{2R_cN}\phi_{,V}^2 \equiv I_V\ ; \quad 2\kappa k\int\frac{UdUr}{2R_cN}\phi_{,U}^2 \equiv I_U. \tag{6.4.84}$$

Then subtracting (6.4.82) from (6.4.83) gives an equation for $\delta_1$:

$$\frac{-r}{rR_cN}(U\delta_{1,U} + V\delta_{1,V}) = I_U + I_V + \bar{F}(V) - \bar{G}(U) \tag{6.4.85}$$

where

$$F(V) = F_{SdS} + \frac{\bar{F}}{k} \tag{6.4.86}$$

and

$$G(U) = G_{SdS} + \frac{\bar{G}}{k}. \tag{6.4.87}$$

Equation (6.4.85) can be integrated (by $UV$) to give the following form for $\delta_1$:

$$\delta_1 = -\frac{R_cN}{r}\left[\ln(UV)(I_U + I_V) + 2\int \frac{dV\bar{F}}{V} - 2\int \frac{dU\bar{G}}{U} + h(r)\right] \tag{6.4.88}$$

where $h(r)$ is a free function. Now use equation (6.4.82) to give the form of $\delta_2$:

$$\delta_2 = \delta_1 - \frac{rU}{2R_cN}\delta_{1,U} - \bar{F} - I_U. \tag{6.4.89}$$

Alternatively, equation (6.4.83) gives $\delta_2$ as

$$\delta_2 = \delta_1 + \frac{rV}{2R_cN}\delta_{1,V} - \bar{G} + I_V. \tag{6.4.90}$$

Using the solution for $\delta_1$ we can show that these two are equivalent. We now use the following equation to determine the function $h(r)$,

$$B_{,UV} = 2\left(\kappa\bar{V}(\phi)B^{1/2} - B^{-1/2}\right)e^{2\nu}. \tag{6.4.91}$$

On putting the forms of $\delta_1$ and $\delta_2$ into this equation, the $\bar{F}$ and $\bar{G}$ terms cancel out, so these are genuinely free functions. This leaves a second order ODE to determine $h(r)$. Integrating up once gives,

$$h'(r) = \frac{1}{R_cN^2r}\int dr\left[(Nr)'(I_U - I_V) - 24H^2r^2\left(\frac{\kappa\varphi}{\beta} + \chi\right)\right] \tag{6.4.92}$$

where the constant $\chi$ is set by the integration constant, $c$, from $\varphi$ (see equation (6.3.69)). Integrating up again gives $h(r)$. Now the solution still has two free functions, $\bar{F}$ and $\bar{G}$, as well as some integration constants in $h$. For a valid perturbative expansion, $\delta_1$ and $\delta_2$ must be regular on both the cosmological and black hole horizons. We will now show that $\delta_1$ is everywhere regular, and that $\delta_2$ may be made regular by a choice of the functions $\bar{F}$ and $\bar{G}$.

### 6.4.1 Checking the metric perturbations are regular

In order to look at divergence we must write the integrals $I_U$ and $I_V$ more explicitly. In the cosmological coordinate system, (6.3.70), the scalar field, $\phi$, takes the explicit form

$$\phi = \phi_0 - \frac{\phi_1}{2} R_c \ln(UV) + \varphi(r), \tag{6.4.93}$$

where $r$ is defined in terms of $B$ and therefore the function $\varphi$ does not change with the coordinate system. It is given by equation (6.3.69), and therefore, given the form of $r$-derivatives in this coordinate system, (6.4.79), the derivatives of $\phi$ are

$$\phi_{,U} = \frac{R_c}{2U}\left(-\phi_1 + \frac{\beta H^2 r}{\kappa} + \frac{C}{r^2}\right) \; ; \quad \phi_{,V} = \frac{R_c}{2V}\left(-\phi_1 - \frac{\beta H^2 r}{\kappa} - \frac{C}{r^2}\right). \tag{6.4.94}$$

We therefore see that $U\phi_{,U}$ and $V\phi_{,V}$ depend only on $r$, and thus in the integrals $I_V$ and $I_U$ we can replace $dV/V$ with $dr/(R_c N)$ and $dU/U$ with $-dr/(R_c N)$. The integrals therefore become

$$I_U = -\kappa k \int \frac{r dr}{4N^2}\left(-\phi_1 + \frac{\beta H^2 r}{\kappa} + \frac{C}{r^2}\right)^2 = -\int \frac{r dr}{N^2}\left(-\bar{\phi}_1 + H^2 r + \frac{\bar{C}}{r^2}\right)^2 \tag{6.4.95}$$

$$I_V = \kappa k \int \frac{r dr}{4N^2}\left(\phi_1 + \frac{\beta H^2 r}{\kappa} + \frac{C}{r^2}\right)^2 = \int \frac{r dr}{N^2}\left(\bar{\phi}_1 + H^2 r + \frac{\bar{C}}{r^2}\right)^2 \tag{6.4.96}$$

where, since we notice that $\phi_1$ and $C$ have factors of $\beta/\kappa$, we rewrite them as $\bar{\phi}_1 = \kappa\phi_1/\beta$ and $\bar{C} = \kappa C/\beta$.

Now we look at potentially divergent terms in $\delta_1$, equation (6.4.88). The overall factor of $N$ goes to zero as $(r - r_i)$ at the potentially problematic points, that is $r = r_c$ and $r = r_h$. Therefore any term in the brackets that behaves as $\ln(r - r_i)$ is not a problem for $\delta_1$. The only terms that might diverge, then, are terms in $(I_U + I_V)$ that behave as $1/N$ and terms in $h$ that behave as $\ln(r - r_i)/N$, which are the most divergent terms in each of these functions. We will show that these terms exactly cancel at the horizons, and therefore $\delta_1$ is regular everywhere.

The most divergent term in $\ln(UV)(I_U + I_V)$ is

$$-\ln(UV) 4\bar{\phi}_1 \frac{r_s(r - 3r_s) + r^2(2 - 9H^2 r_s^2) + \bar{C}(2r - 6r_s + 9H^2 r_s r^2)}{rN(-4 + 27H^2 r_s^2)}. \tag{6.4.97}$$

This must cancel the most divergent term in $h$, which comes from the term $N' r(I_U - I_V)$ in the integral for $h'$, equation (6.4.92). After some calculation, we find that the

most divergent terms in $h$ may be expressed as

$$4\bar{\phi}_1\left[\sum_i \frac{R_i^3(r_i+\bar{C}-r_s)\ln|r-r_i|}{R_c r_i(r_i-r)}+\frac{2R_c^2\bar{\phi}_1 r_c\ln(r_c-r)}{r_c-r}\right]. \tag{6.4.98}$$

Now, to show that these two divergences cancel requires the following:

- The form of $\bar{\phi}_1 \equiv \kappa\phi_1/\beta$ from equation (6.3.72).
- The fact that, for $V=0$, $\ln(UV)=2\ln(U)+\ln(V/U)=finite+r^\star/R_c\sim\ln(r_c-r)$, and similarly for $U=0$, $\ln(UV)\sim -R_h\ln(r-r_h)$.
- The relation $(1-r_s/r_i-H^2r_i^2)=0$, to rearrange terms.
- The fact that $N\to(r-r_i)/R_i$ as $r\to r_i$ .

Using these, the $\ln|r-r_i|/(r-r_i)$ divergences in (6.4.97) and (6.4.98) are found to cancel on both horizons, and thus $\delta_1$ is finite everywhere.

It remains to examine the divergence in $\delta_2$. We use the form of $\delta_1$ to re-write $\delta_2$ as follows,

$$\delta_2=\delta_1-\frac{R_c}{2}\left[\ln(UV)(N(I_U+I_V))'+(Nh)'\right]+\frac{1}{2}(I_V-I_U)+\frac{R_cN}{2r}(\ln(UV)(I_U+I_V)+h)$$
$$-\bar{F}-\bar{G}-R_cN\left(\frac{N}{r}\right)'\left(\int\frac{dV\bar{F}}{V}-\int\frac{dU\bar{G}}{U}\right). \tag{6.4.99}$$

Here, the terms on the second line are free to be chosen based on the divergences of the first line. Of course the first term, $\delta_1$, is regular. We know the most divergent terms in $(I_U+I_V)$ and in $h$, from above, and therefore conclude that the most divergent terms in the final term, $\frac{R_cN}{2r}(\ln(UV)(I_U+I_V)+h)$, will be logs. The same is also true for the first part of the second term, that is $\ln(UV)(N(I_U+I_V))'$. In the remaining terms, however, there will be $1/N$ divergences. These cannot be cancelled by functions of $U$ and $V$ alone, i.e. $\bar{F}$ and $\bar{G}$ cannot help with these. Therefore we must show that the $1/N$ divergences in the expression

$$-\frac{R_c}{2}(Nh)'+\frac{1}{2}(I_V-I_U) \tag{6.4.100}$$

will cancel out.

The $1/N$-type terms in $(I_V - I_U)$ are given by

$$4\bar{\phi}_1 \left( \frac{2R_c^2 \bar{\phi}_1}{r_c - r} - \frac{r_s(r - 3r_s) + r^2(2 - 9H^2 r_s^2) + \bar{C}(2r - 6r_s + 9H^2 r_s r^2)}{rN(-4 + 27H^2 r_s^2)} \right). \quad (6.4.101)$$

From (6.4.98), the relevant terms in $R_c(Nh)'$ are

$$-4\bar{\phi}_1 \sum_i \frac{R_i^3(r_i + \bar{C} - r_s)N}{r_i(r - r_i)^2} - \frac{8\bar{\phi}_1^2 R_c^3 N r_c}{(r - r_c)^2}. \quad (6.4.102)$$

Using again that $N \to (r - r_i)/R_i$ as $r \to r_i$, and also $1 - r_s/r_i - H^2 r_i^2 = 0$, we can show that these two terms indeed cancel at both horizons. Then in $\delta_2$, the only divergent terms that remain are of the form $\ln|r - r_i|$ and $\ln^2|r - r_i|$. Such divergences can be cancelled by taking $\bar{F}$ and $\bar{G}$ to be of the form,

$$\bar{F} = f_1 + f_2 \ln V \ ; \ \bar{G} = g_1 + g_2 \ln U. \quad (6.4.103)$$

In order to calculate the constants $f_1$, $f_2$, $g_1$ and $g_2$, $\delta_2$ must be calculated more explicitly.

## 6.4.2 Discussion

Showing that the metric perturbations are finite indicates that this expansion, equations (6.4.77,6.4.78), is consistent, and the quintessence black hole will be close to a Schwarzschild-de Sitter spacetime. The expansion is valid everywhere in space (i.e. for all values of the radial coordinate, $r$) and for some portion of time, excluding very early and very late times. Since the two spacetimes have the same causal structure, it is reasonable to assume that the black hole event horizon is still at $U = 0$.

Due to the backreaction of the scalar field, the event horizon area now grows, which we interpret as the accretion of scalar matter by the black hole. The growth of the event horizon is given by the function $B$, which measures the area of 2-spheres. At $U = 0$, $r = r_h$ is a constant, so all $r$-dependent terms in $\delta_1$ (equation (6.4.88)) are constant, and the $\bar{F}$ and $\bar{G}$ terms are zero because they are log terms, so the overall factor of $N$ goes to zero faster than they diverge. This leaves the event horizon behaviour given simply by the $\ln(UV)$ term (removing the $r$-dependent piece),

$$\delta_1 = -\frac{2R_c N}{r} \ln|V|(I_U + I_V) + const. \quad (6.4.104)$$

In order to find the physical behaviour on the event horizon we must use a coordinate system that is finite there, i.e. change the coordinates to $(u, v)$ as given by (6.3.71). Then $\delta_1$ becomes

$$\delta_1 = -\frac{2R_h N}{r}\ln(v)(I_U + I_V) + const. \tag{6.4.105}$$

In fact, only the terms in $(I_U + I_V)$ that behave as $1/N$ will be non-zero at the horizon, and these are given by equation (6.4.97) (without the factor of $\ln(UV)$). This expression simplifies on the event horizon, and we find that

$$B \simeq r_h^2 + \frac{1}{k}\left(8\bar{\phi}_1 R_h^2 \ln(v)(r_h - r_s + \bar{C}) + const\right). \tag{6.4.106}$$

The order of magnitude of $\delta_1$ is $(Hr_s)^2$, if we assume $Hr_s$ is small, which is certainly the case at late times. Thus the event horizon growth is very small indeed,

$$B \sim r_h^2\left(1 + \frac{(Hr_s)^2}{k}\ln(v)\right). \tag{6.4.107}$$

This suggests a horizon growth perhaps of the form

$$B \sim r_h^2 (v)^{(Hr_s)^2/k}. \tag{6.4.108}$$

A small growth rate agrees with [166]. In the early universe, however, $Hr_s$ may not have been small and therefore the accretion rate of scalar field onto a black hole may be much more significant, which could have cosmological implications. This would be interesting to consider in future work.

The results in this chapter are derived assuming a specific form of the scalar field potential, $\bar{V}(\phi) = M^4 \exp(-\beta\phi)$. However, a change of potential should not have a qualitative effect on the results. Since the non-constant terms in $\phi$ are suppressed by a factor of $1/k$ relative to the constant part, $\phi_0$, we may write it as

$$\phi = \phi_0 + \delta\phi, \tag{6.4.109}$$

where $\delta\phi \ll \phi_0$. Then the expansion of the potential that was used when solving Einstein's equations is simply a linearised expansion in $\delta\phi$,

$$\bar{V} \simeq M^4 \exp(-\beta\phi_0)(1 - \beta\delta\phi). \tag{6.4.110}$$

Any potential may be similarly expanded in this general form,

$$\bar{V} \simeq c_1 + c_2\delta\phi. \tag{6.4.111}$$

Although the constants $c_1$ and $c_2$ may be different, this should not dramatically change the result.

# Chapter 7

# Conclusions and future directions

This thesis has presented and set into context some research into a few of cosmology's unsolved problems. The first part focussed on cosmic strings, which are a prediction of many popular models of the early universe, but which have not yet been observed. A detection of cosmic strings would greatly contribute to our understanding of the early universe, and which physical models best describe it. In this work, the effect of extra dimensions on the dynamics and signals of cosmic strings was modelled. We were able to show that the effects would be significant, and therefore a detection of cosmic strings could give information about the existence and even the nature of extra dimensions.

In Chapter 3, exact solutions for cosmic string loops in higher dimensional flat spacetime were derived. Three different solutions were given. Two of these were 2-harmonic solutions, one of which does not exist without extra dimensions, while the other is a higher-dimensional extension of the 3-dimensional solution. In the third solution the string loop winds the internal dimension, which is a new feature allowed by the presence of periodic extra dimensions.

Unlike string loops in 4D flat spacetime, only a zero-measure subset of these solutions contain exact cusps. Some regions of the parameter space were plotted, showing the solutions that contain exact cusps, which, in reality, occur with probability zero. An event close to a cusp, labelled a near cusp event (NCE), however, occurs on a finite proportion of loops. We presented a general argument for the dependence of the proportion of loops on the NCE parameter, $\Delta$ (defining how close

the NCE is to an exact cusp).

We also gave some arguments about self-intersection of cosmic string loops, which has a reduced probability in the presence of extra dimensions. It is suggested that wrapping the extra dimensions enough times will increase the chances to self-intersect sufficiently that it becomes likely to happen, and thus loops will be cut off in some sense "close" to the 4D solutions. This is an area in which further investigation would be useful, since it would better inform the work of Chapter 4.

In this chapter we also showed that winding reduces the average velocity of a string loop. Ideally, in future work, we would also produce plots of the regions of parameter space with self-intersections, given a finite string-width, and of the regions with NCE's for different values of $\Delta$.

In Chapter 4, the gravitational wave signals from cusps on cosmic string loops were calculated. First, the calculation of Damour and Vilenkin [55] was reviewed, and then the higher-dimensional modification was shown. The effect on the gravitational wave signal due to this modification was found to be quite large, reducing the amplitude of the largest gravitational wave bursts that would regularly be recieved on Earth by about an order of magnitude per extra dimension added.

Damour and Vilenkin's calculation shows that cosmic string cusps beam high-frequency gravitational waves in a cone around their direct line of emission. In higher dimensions, only NCE's occur, so cusps will no longer be exact. It can be shown that the effect of deviating from an exact cusp − which means that the left- and right-moving wavevectors do not exactly align − is equivalent to looking in a direction slightly away from the direct line of emission. Therefore the angle of the beaming cone is reduced for an NCE.

The main effect on the overall gravitational wave signal comes from the greatly reduced probability of NCE's. Given the argument of Chapter 3, that loops may be somehow cut off close to 4D solutions, we modelled this effect by restricting the loops to be close to solutions with exact cusps. This makes the reduction in signal less dramatic, but still significant. The restriction on the loop parameter space was modelled only heuristically, and it would be both useful and interesting to investigate how tight this restriction would be in reality and exactly how it is manifest in the

parameter space.

There was also a little ambiguity surrounding the fact that some of the gravitational radiation would be emitted into the internal dimensions, which is worth further consideration.

In Chapter 5, the effect of a warped internal space on the dynamics of cosmic strings was considered. It was found that cosmic string loops are not physically confined to a region near the tip of a warped throat, although they experience an attractive force towards this region. The lack of friction in the system means that having been attracted to the tip of a throat they will simply oscillate back up again. In principle they can travel arbitraily far from the tip, although in practice they rarely do. This tendency for internal motion means that the gravitational wave signal will be reduced by the presence of warped extra dimensions as well as by flat ones.

It was found that because the warp factor, which depends on the internal geometry, multiplies both internal and external parts of the metric, the behaviour of a string in the external 3D space could be dramatically affected by internal motion. As the string moves towards the tip of the throat, either the length or velocity (or both) of the string in the external space significantly increases. If some parts of the string are nearer to the tip of the throat than others, the string in the external space will become distorted (see Figure 5.3). Unlike in flat space, its motion is no longer periodic.

The dynamical effects of cosmological expansion and the emission of gravitational radiation were also considered, and no preferential damping was found in the internal dimensions, thus the presence of internal motion was not affected by these processes. Cosmological expansion has a stretching effect on long, slow-moving strings, increasing their total energy, and a redshifting effect on the velocities of highly relativistic strings, decreasing their total energy. Thus the total energy tends to oscillate back and forth. Once the strings' energy-scale becomes significantly less than the horizon scale, the effects of expansion become negligible.

The main shortcoming in all of this work is that we have not yet observed either cosmic strings or extra dimensions. This means that we cannot know the

exact properties of the cosmic strings for which we are searching, nor the particular nature of extra dimensions, should they exist. The conclusions made in this work are, however, fairly general. The Nambu action, with which we modelled the strings, describes any non-interacting 1-dimensional object, so it can be used to model a variety of different types of cosmic string. A reduction in cusp probability, which has the largest effect on signals, will happen in any higher-dimensional spacetime, since the argument depends only on the dimensionality of the space. Thus the conclusions regarding observational effects apply to a wide range of scenarios. In Chapter 5, we showed that a warped compactification can have distinctive effects on the behaviour of cosmic strings. This is specific to the form of the extra dimensions, suggesting that we cannot make a general conclusion about effects such as these.

The final chapter showed work on black hole solutions in a quintessence universe. The goal was to find a fully general-relativistic solution so that the interaction between a cosmological scalar field and a black hole would be better understood. While no hair theorems may suggest that a scalar field will have neither dynamics nor spatial variation around a black hole (for example it will not form a clump around a black hole), our results showed that in this case it is dynamical, and that it appears to have a non-trivial spatial dependence, resulting in a higher energy-density of scalar field close to the black hole horizon. It was also found that the black hole slowly accretes the scalar field and therefore grows in size.

The black hole was modelled as a perturbative expansion away from a Schwarzschild de Sitter black hole. The perturbative expansion is valid when the power-law cosmological scale factor has a high power, $a \sim t^k$, $k \gg 1$, which is indeed the case according to observations. It is valid in some time interval, but not at very early and late times. It is, however, valid throughout all of space, and for any value of $Hr_s$ (the ratio of the black hole mass scale to the horizon scale). Therefore, it may also be used to describe black holes in the early universe, where they may be a significant fraction of the horizon size. In this case, the rate of accretion of the scalar field onto the black hole could be much higher, and thus have a significant effect on its mass.

There is much work still to be done on this solution now it has been derived, to fully understand its properties and cosmological implications. However, it paves the

way for analytic study of dynamical black hole solutions, which is new in general relativity. Even if no observational consequences arise, it should help futher the understanding of the fundamental theory.

Finally, the outlook for cosmology in the near future is a good one. The results from the Planck satellite [1] have now been released, offering a much more detailed insight into the early universe, which may perhaps overturn many of our current ideas. The first detection of gravitational waves may also happen in the very near future, and several experiments are currently running that could directly detect dark matter [150, 160]. It is also possible that the LHC [3], since it recreates conditions in the early universe, may tell us more about how it all began.

# Bibliography


[1] ESA Science and Technology: Planck. `http://planck.esa.int`.

[2] LAMBDA - Cosmic Background Explorer. `http://lambda.gsfc.nasa.gov/product/cobe/`.

[3] LHC Homepage. `http://lhc.web.cern.ch`.

[4] LIGO - Laser Interferometer Gravitational-Wave Observatory. `http://www.ligo.caltech.edu`.

[5] LISA: Laser Interferometer Space Antenna Project. `http://lisa.nasa.gov`.

[6] Wilkinson Microwave Anisotropy Probe (WMAP). `http://map.gsfc.nasa.gov`.

[7] Andreas Albrecht, Richard A. Battye, and James Robinson. The Case Against Scaling Defect Models of Cosmic Structure Formation. *Phys.Rev.Lett.*, 79:4736–4739, 1997.

[8] Andreas Albrecht and Neil Turok. Evolution of Cosmic String Networks. *Phys.Rev.*, D40:973–1001, 1989.

[9] Bruce Allen and E.P.S. Shellard. Cosmic String Evolution: A Numerical Simulation. *Phys.Rev.Lett.*, 64:119–122, 1990.

[10] A. Avgoustidis. Cosmic String Dynamics and Evolution in Warped Spacetime. *Phys.Rev.*, D78:023501, 2008.

[11] A. Avgoustidis and E.P.S. Shellard. Cycloops: Dark Matter or a Monopole Problem for Brane Inflation? *JHEP*, 0508:092, 2005.

[12] A. Avgoustidis and E.P.S. Shellard. Velocity-Dependent Models for Non-Abelian/Entangled String Networks. *Phys.Rev.*, D78:103510, 2008.

[13] Anastasios Avgoustidis, Sarah Chadburn, and Ruth Gregory. Cosmic Superstring Trajectories in Warped Compactifications. *Phys.Rev.*, D86:063516, 2012.

[14] Anastasios Avgoustidis and Edmund J. Copeland. The Effect of Kinematic Constraints on Multi-tension String Network Evolution. *Phys.Rev.*, D81:063517, 2010.

[15] E. Babichev and M. Kachelriess. Constraining Cosmic Superstrings with Dilaton Emission. *Phys.Lett.*, B614:1–6, 2005.

[16] Luca Baiotti, Ian Hawke, Pedro J. Montero, Frank Loffler, Luciano Rezzolla, et al. Three-dimensional Relativistic Simulations of Rotating Neutron Star Collapse to a Kerr Black Hole. *Phys.Rev.*, D71:024035, 2005.

[17] Juan Barranco, Argelia Bernal, Juan Carlos Degollado, Alberto Diez-Tejedor, Miguel Megevand, et al. Are Black Holes a Serious Threat to Scalar Field Dark Matter Models? *Phys.Rev.*, D84:083008, 2011.

[18] Juan Barranco, Argelia Bernal, Juan Carlos Degollado, Alberto Diez-Tejedor, Miguel Megevand, et al. Schwarzschild Black Holes Can Wear Scalar Wigs. *Phys.Rev.Lett.*, 109:081102, 2012.

[19] Jacob D. Bekenstein. Nonexistence of Baryon Number for Static Black Holes. *Phys.Rev.*, D5:1239–1246, 1972.

[20] J.D. Bekenstein. Novel 'No Scalar Hair' Theorem for Black Holes. *Phys.Rev.*, D51:6608–6611, 1995.

[21] David P. Bennett and Francois R. Bouchet. High Resolution Simulations of Cosmic String Evolution. 1. Network Evolution. *Phys.Rev.*, D41:2408, 1990.

[22] David P. Bennett and Francois R. Bouchet. Constraints on the Gravity Wave Background Generated by Cosmic Strings. *Phys.Rev.*, D43:2733–2735, 1991.

[23] Neil Bevis, Edmund J. Copeland, Pierre-Yves Martin, Gustavo Niz, Alkistis Pourtsidou, et al. Evolution and Stability of Cosmic String Loops with Y-junctions. *Phys.Rev.*, D80:125030, 2009.

[24] Neil Bevis and Paul M. Saffin. Cosmic String Y-junctions: A Comparison Between Field Theoretic and Nambu-Goto Dynamics. *Phys.Rev.*, D78:023503, 2008.

[25] Pijushpani Bhattacharjee and N.C. Rana. Ultrahigh-Energy Particle Flux from Cosmic Strings. *Phys.Lett.*, B246:365–370, 1990.

[26] P. Binetruy, A. Bohe, T. Hertog, and D.A. Steer. Gravitational Wave Signatures from Kink Proliferation on Cosmic (Super-) Strings. *Phys.Rev.*, D82:126007, 2010.

[27] P. Binetruy, A. Bohe, T. Hertog, and Daniele A. Steer. Gravitational Wave Bursts from Cosmic Superstrings with Y-junctions. *Phys.Rev.*, D80:123510, 2009.

[28] P. Binetruy, A. Bohe, T. Hertog, and Daniele A. Steer. Proliferation of Sharp Kinks on Cosmic (Super-)string Loops with Junctions. *Phys.Rev.*, D82:083524, 2010.

[29] Jose J. Blanco-Pillado and Alberto Iglesias. Strings at the Bottom of the Deformed Conifold. *JHEP*, 0508:040, 2005.

[30] Jose J. Blanco-Pillado, Ken D. Olum, and Benjamin Shlaer. Large Parallel Cosmic String Simulations: New Results on Loop Production. *Phys.Rev.*, D83:083514, 2011.

[31] Francois R. Bouchet, David P. Bennett, and Albert Stebbins. Microwave Anisotropy Patterns from Evolving String Networks. *Nature*, 335:410–414, 1988.

[32] Peter Bowcock, Christos Charmousis, and Ruth Gregory. General Brane Cosmologies and their Global Space-Time Structure. *Class.Quant.Grav.*, 17:4745–4764, 2000.

[33] Philippe Brax and Carsten van de Bruck. Cosmology and Brane Worlds: A Review. *Class.Quant.Grav.*, 20:R201–R232, 2003.

[34] Malcolm N. Butler, Robert A. Malaney, and Milan B. Mijic. On the Evolution of a Superconducting Cosmic String Network. *Phys.Rev.*, D43:2535–2541, 1991.

[35] R.R. Caldwell, Rahul Dave, and Paul J. Steinhardt. Cosmological Imprint of an Energy Component with General Equation of State. *Phys.Rev.Lett.*, 80:1582–1585, 1998.

[36] Philip Candelas and Xenia C. de la Ossa. Comments on Conifolds. *Nucl.Phys.*, B342:246–268, 1990.

[37] Sean M. Carroll. Is our universe natural? *Nature*, 440:1132–1136, 2006.

[38] B. Carter. Axisymmetric Black Hole Has Only Two Degrees of Freedom. *Phys.Rev.Lett.*, 26:331–333, 1971.

[39] Sarah Chadburn. Cosmic Strings in Higher Dimensions. Submitted for MSci degree.

[40] Sarah Chadburn and Ruth Gregory. Time dependent black holes and scalar hair. arXiv:1304.6287, 2013.

[41] A.L. Chen, D.A. DiCarlo, and S.A. Hotes. Selfintersections in a Three Parameter Space of Cosmic Strings. *Phys.Rev.*, D37:863, 1988.

[42] Eugene Chudnovsky and Alexander Vilenkin. Strings in the Sun? *Phys.Rev.Lett.*, 61:1043, 1988.

[43] Timothy Clifton, Pedro G. Ferreira, Antonio Padilla, and Constantinos Skordis. Modified Gravity and Cosmology. *Phys.Rept.*, 513:1–189, 2012.

[44] Edmund J. Copeland, D. Haws, M. Hindmarsh, and N. Turok. Dynamics of and Radiation from Superconducting Strings and Springs. *Nucl.Phys.*, B306:908, 1988.

[45] Edmund J. Copeland, Robert C. Myers, and Joseph Polchinski. Cosmic F and D Strings. *JHEP*, 0406:013, 2004.

[46] Edmund J. Copeland and P.M. Saffin. On the Evolution of Cosmic-superstring Networks. *JHEP*, 0511:023, 2005.

[47] Edmund J. Copeland, M. Sami, and Shinji Tsujikawa. Dynamics of Dark Energy. *Int.J.Mod.Phys.*, D15:1753–1936, 2006.

[48] Edmund J. Copeland and N. Turok. The Stability of Cosmic String Loops. *Phys.Lett.*, B173:129, 1986.

[49] Edmund J. Copeland, N. Turok, and M. Hindmarsh. Dynamics of Superconducting Cosmic Strings. *Phys.Rev.Lett.*, 58:1910–1913, 1987.

[50] E.J. Copeland, H. Firouzjahi, T.W.B. Kibble, and Daniele A. Steer. On the Collision of Cosmic Superstrings. *Phys.Rev.*, D77:063521, 2008.

[51] E.J. Copeland, T.W.B. Kibble, and Daniele A. Steer. Constraints on String Networks with Junctions. *Phys.Rev.*, D75:065024, 2007.

[52] Ben Craps. The Cosmological Singularity Problem. 2010.

[53] Jin Dai, R.G. Leigh, and Joseph Polchinski. New Connections Between String Theories. *Mod.Phys.Lett.*, A4:2073–2083, 1989.

[54] Thibault Damour and Alexander Vilenkin. Cosmic Strings and the String Dilaton. *Phys.Rev.Lett.*, 78:2288–2291, 1997.

[55] Thibault Damour and Alexander Vilenkin. Gravitational Wave Bursts from Cusps and Kinks on Cosmic Strings. *Phys.Rev.*, D64:064008, 2001.

[56] Anne-Christine Davis, William Nelson, Senthooran Rajamanoharan, and Mairi Sakellariadou. Cusps on Cosmic Superstrings with Junctions. *JCAP*, 0811:022, 2008.

[57] R.L. Davis and E.P.S. Shellard. Cosmic Vortons. *Nucl.Phys.*, B323:209–224, 1989.

[58] David Delaney, Kimberly Engle, and Xania Scheick. The General Two Harmonic Cosmic String. *Phys.Rev.*, D41:1775, 1990.

[59] Konstantinos Dimopoulos and Anne-Christine Davis. Friction Domination with Superconducting Strings. *Phys.Rev.*, D57:692–701, 1998.

[60] Jean-Francois Dufaux. Cosmic Super-Strings and Kaluza-Klein Modes. *JCAP*, 1209:022, 2012.

[61] Gia Dvali and Alexander Vilenkin. Formation and Evolution of Cosmic D Strings. *JCAP*, 0403:010, 2004.

[62] G.R. Dvali and S.H. Henry Tye. Brane Inflation. *Phys.Lett.*, B450:72–82, 1999.

[63] Damien A. Easson, Ruth Gregory, David F. Mota, Gianmassimo Tasinato, and I. Zavala. Spinflation. *JCAP*, 0802:010, 2008.

[64] Albert Einstein. The Foundation of the General Theory of Relativity. *Annalen Phys.*, 49:769–822, 1916.

[65] Roberto Emparan and Harvey S. Reall. Black Holes in Higher Dimensions. *Living Rev.Rel.*, 11:6, 2008.

[66] Hassan Firouzjahi. Energy Radiation by Cosmic Superstrings in Brane Inflation. *Phys.Rev.*, D77:023532, 2008.

[67] Hassan Firouzjahi, Johanna Karouby, Shahram Khosravi, and Robert Brandenberger. Zipping and Unzipping of Cosmic String Loops in Collision. *Phys.Rev.*, D80:083508, 2009.

[68] Hassan Firouzjahi, Salomeh Khoeini-Moghaddam, and Shahram Khosravi. Cosmic Strings Collision in Cosmological Backgrounds. *Phys.Rev.*, D81:123506, 2010.

[69] D. Forster. Dynamics of Relativistic Vortex Lines and their Relation to Dual Theory. *Nucl.Phys.*, B81:84, 1974.

[70] Andrew R. Frey and Anshuman Maharana. Warped Spectroscopy: Localization of Frozen Bulk Modes. *JHEP*, 0608:021, 2006.

[71] A. Friedmann. On the Possibility of a World with Constant Negative Curvature of Space. *Z.Phys.*, 21:326–332, 1924.

[72] Andrei V. Frolov and Lev Kofman. Inflation and de Sitter Thermodynamics. *JCAP*, 0305:009, 2003.

[73] H. Georgi and S.L. Glashow. Unity of All Elementary Particle Forces. *Phys.Rev.Lett.*, 32:438–441, 1974.

[74] Steven B. Giddings, Shamit Kachru, and Joseph Polchinski. Hierarchies from Fluxes in String Compactifications. *Phys.Rev.*, D66:106006, 2002.

[75] P. Goddard, J. Goldstone, C. Rebbi, and Charles B. Thorn. Quantum Dynamics of a Massless Relativistic String. *Nucl.Phys.*, B56:109–135, 1973.

[76] Tetsuo Goto. Relativistic Quantum Mechanics of One-Dimensional Mechanical Continuum and Subsidiary Condition of Dual Resonance Model. *Prog.Theor.Phys.*, 46:1560–1569, 1971.

[77] III Gott, J. Richard. Gravitational Lensing Effects of Vacuum Strings: Exact Solutions. *Astrophys.J.*, 288:422–427, 1985.

[78] Mariana Grana. Flux Compactifications in String Theory: A Comprehensive Review. *Phys.Rept.*, 423:91–158, 2006.

[79] Ruth Gregory, David Kubiznak, and Danielle Wills. Rotating Black Hole Hair. 2013.

[80] Alan H. Guth. The Inflationary Universe: A Possible Solution to the Horizon and Flatness Problems. *Phys.Rev.*, D23:347–356, 1981.

[81] F.S. Guzman and F.D. Lora-Clavijo. Spherical Non-linear Absorption of Cosmological Scalar Fields onto a Black Hole. *Phys.Rev.*, D85:024036, 2012.

[82] Rhiannon Gwyn, Mairi Sakellariadou, and Spyros Sypsas. Theoretical Constraints on Brane Inflation and Cosmic Superstring Radiation. *JHEP*, 1109:075, 2011.

[83] David Haws, Mark Hindmarsh, and Neil Turok. Superconducting Strings or Springs? *Phys.Lett.*, B209:255, 1988.

[84] Christopher P. Herzog, Igor R. Klebanov, and Peter Ouyang. Remarks on the Warped Deformed Conifold. 2001.

[85] Peter W. Higgs. Broken Symmetries and the Masses of Gauge Bosons. *Phys.Rev.Lett.*, 13:508–509, 1964.

[86] Peter W. Higgs. Broken Symmetries, Massless Particles and Gauge Fields. *Phys.Lett.*, 12:132–133, 1964.

[87] Mark Hindmarsh and P.M. Saffin. Scaling in a $SU(2)/Z_3$ Model of Cosmic Superstring Networks. *JHEP*, 0608:066, 2006.

[88] Mark Hindmarsh, Stephanie Stuckey, and Neil Bevis. Abelian Higgs Cosmic Strings: Small Scale Structure and Loops. *Phys.Rev.*, D79:123504, 2009.

[89] C.J. Hogan and M.J. Rees. Gravitational Interactions of Cosmic Strings. *Nature*, 311:109–113, 1984.

[90] Mark G. Jackson, Nicholas T. Jones, and Joseph Polchinski. Collisions of Cosmic F and D-Strings. *JHEP*, 0510:013, 2005.

[91] Ted Jacobson. Primordial Black Hole Evolution in Tensor Scalar Cosmology. *Phys.Rev.Lett.*, 83:2699–2702, 1999.

[92] Nicholas T. Jones, Horace Stoica, and S.H. Henry Tye. Brane Interaction as the Origin of Inflation. *JHEP*, 0207:051, 2002.

[93] Nicholas T. Jones, Horace Stoica, and S.H. Henry Tye. The Production, Spectrum and Evolution of Cosmic Strings in Brane Inflation. *Phys.Lett.*, B563:6–14, 2003.

[94] Katherine Jones-Smith, Harsh Mathur, and Tanmay Vachaspati. Aharonov-bohm radiation. *Phys. Rev. D*, 81:043503, Feb 2010.

[95] Nick Kaiser and A. Stebbins. Microwave Anisotropy Due to Cosmic Strings. *Nature*, 310:391–393, 1984.

[96] Nemanja Kaloper, Matthew Kleban, and Damien Martin. McVittie's Legacy: Black Holes in an Expanding Universe. *Phys.Rev.*, D81:104044, 2010.

[97] Justin Khoury, Burt A. Ovrut, Nathan Seiberg, Paul J. Steinhardt, and Neil Turok. From Big Crunch to Big Bang. *Phys.Rev.*, D65:086007, 2002.

[98] T.W.B. Kibble. Topology of Cosmic Domains and Strings. *J.Phys.*, A9:1387–1398, 1976.

[99] T.W.B. Kibble. Some Implications of a Cosmological Phase Transition. *Phys.Rept.*, 67:183, 1980.

[100] T.W.B. Kibble. Evolution of a System of Cosmic Strings. *Nucl.Phys.*, B252:227, 1985.

[101] T.W.B. Kibble, George Lazarides, and Q. Shafi. Strings in SO(10). *Phys.Lett.*, B113:237, 1982.

[102] T.W.B. Kibble and Neil Turok. Selfintersection of Cosmic Strings. *Phys.Lett.*, B116:141, 1982.

[103] D.A. Kirzhnits. Weinberg Model in the Hot Universe. *JETP Lett.*, 15:529–531, 1972.

[104] D.A. Kirzhnits and Andrei D. Linde. Macroscopic Consequences of the Weinberg Model. *Phys.Lett.*, B42:471–474, 1972.

[105] V.V. Kiselev. Quintessence and Black Holes. *Class.Quant.Grav.*, 20:1187–1198, 2003.

[106] Igor R. Klebanov and Matthew J. Strassler. Supergravity and a Confining Gauge Theory: Duality Cascades and Chi SB Resolution of Naked Singularities. *JHEP*, 0008:052, 2000.

[107] Theodoros Kolyvaris, George Koutsoumbas, Eleftherios Papantonopoulos, and George Siopsis. A New Class of Exact Hairy Black Hole Solutions. *Gen.Rel.Grav.*, 43:163–180, 2011.

[108] E. Komatsu et al. Five-Year Wilkinson Microwave Anisotropy Probe (WMAP) Observations: Cosmological Interpretation. *Astrophys.J.Suppl.*, 180:330–376, 2009.

[109] E. Komatsu et al. Seven-Year Wilkinson Microwave Anisotropy Probe (WMAP) Observations: Cosmological Interpretation. *Astrophys.J.Suppl.*, 192:18, 2011.

[110] M.D. Kruskal. Maximal Extension of Schwarzschild Metric. *Phys.Rev.*, 119:1743–1745, 1960.

[111] P. Laguna and R.A. Matzner. Numerical Simulation of Bosonic Superconducting String Interactions. *Phys.Rev.*, D41:1751–1763, 1990.

[112] Matthew Lake, Steve Thomas, and John Ward. Non-topological Cycloops. *JCAP*, 1001:026, 2010.

[113] Louis Leblond and S.H. Henry Tye. Stability of D1 Strings Inside a D3-Brane. *JHEP*, 0403:055, 2004.

[114] Georges Lemaitre. A Homogeneous Universe of Constant Mass and Increasing Radius Accounting for the Radial Velocity of Extra-Galactic Nebulae. *Mon.Not.Roy.Astron.Soc.*, 91:483–490, 1931. English translation of paper from 1927.

[115] C.J.A.P. Martins. Scaling Laws for Non-intercommuting Cosmic String Networks. *Phys.Rev.*, D70:107302, 2004.

[116] C.J.A.P. Martins and E.P.S. Shellard. Quantitative String Evolution. *Phys.Rev.*, D54:2535–2556, 1996.

[117] C.J.A.P. Martins and E.P.S. Shellard. Extending the Velocity Dependent One Scale String Evolution Model. *Phys.Rev.*, D65:043514, 2002.

[118] Liam McAllister and Eva Silverstein. String Cosmology: A Review. *Gen.Rel.Grav.*, 40:565–605, 2008.

[119] G.C. McVittie. The Mass-Particle in an Expanding Universe. *Mon.Not.Roy.Astron.Soc.*, 93:325–339, 1933.

[120] Ruben Minasian and Dimitrios Tsimpis. On the Geometry of Nontrivially Embedded Branes. *Nucl.Phys.*, B572:499–513, 2000.

[121] J.N. Moore, E.P.S. Shellard, and C.J.A.P. Martins. On the Evolution of Abelian-Higgs String Networks. *Phys.Rev.*, D65:023503, 2002.

[122] K.J.M. Moriarty, Eric Myers, and Claudio Rebbi. Dynamical Interactions of Flux Vortices in Superconductors. *Phys.Lett.*, B207:411, 1988.

[123] Holger Bech Nielsen and P. Olesen. Vortex Line Models for Dual Strings. *Nucl.Phys.*, B61:45–61, 1973.

[124] N.K. Nielsen. Dimensional Reduction and Classical Strings. *Nucl.Phys.*, B167:249, 1980.

[125] Eimear O'Callaghan, Sarah Chadburn, Ghazal Geshnizjani, Ruth Gregory, and Ivonne Zavala. Effect of Extra Dimensions on Gravitational Waves from Cosmic Strings. *Phys.Rev.Lett.*, 105:081602, 2010.

[126] Eimear O'Callaghan, Sarah Chadburn, Ghazal Geshnizjani, Ruth Gregory, and Ivonne Zavala. The Effect of Extra Dimensions on Gravity Wave Bursts from Cosmic String Cusps. *JCAP*, 1009:013, 2010.

[127] Eimear O'Callaghan and Ruth Gregory. Kinks, Extra Dimensions, and Gravitational Waves. *JCAP*, 1103:004, 2011.

[128] Ken D. Olum and Vitaly Vanchurin. Cosmic String Loops in the Expanding Universe. *Phys.Rev.*, D75:063521, 2007.

[129] H.V. Peiris et al. First Year Wilkinson Microwave Anisotropy Probe (WMAP) Observations: Implications for Inflation. *Astrophys.J.Suppl.*, 148:213, 2003.

[130] Marco Peloso and Lorenzo Sorbo. Moduli from Cosmic Strings. *Nucl.Phys.*, B649:88–100, 2003.

[131] S. Perlmutter et al. Measurements of Omega and Lambda from 42 High Redshift Supernovae. *Astrophys.J.*, 517:565–586, 1999.

[132] R. Plaga. Superconducting Cosmic Strings Near the Electroweak Scale and Cosmic Ray Propagation. *Phys.Rev.*, D47:3635–3638, 1993.

[133] S.J. Poletti and D.L. Wiltshire. The Global Properties of Static Spherically Symmetric Charged Dilaton Space-Times with a Liouville Potential. *Phys.Rev.*, D50:7260–7270, 1994.

[134] A. Pourtsidou, A. Avgoustidis, E.J. Copeland, L. Pogosian, and D.A. Steer. Scaling Configurations of Cosmic Superstring Networks and their Cosmological Implications. *Phys.Rev.*, D83:063525, 2011.

[135] John Preskill. Cosmological Production of Superheavy Magnetic Monopoles. *Phys.Rev.Lett.*, 43:1365, 1979.

[136] Jean M. Quashnock and David N. Spergel. Gravitational Selfinteractions of Cosmic Strings. *Phys.Rev.*, D42:2505–2520, 1990.

[137] Adam G. Riess et al. Observational Evidence from Supernovae for an Accelerating Universe and a Cosmological Constant. *Astron.J.*, 116:1009–1038, 1998.

[138] Christophe Ringeval, Mairi Sakellariadou, and Francois Bouchet. Cosmological Evolution of Cosmic String Loops. *JCAP*, 0702:023, 2007.

[139] H.P. Robertson. Kinematics and World-Structure. *Astrophys.J.*, 82:284–301, 1935.

[140] V.A. Rubakov and M.E. Shaposhnikov. Do We Live Inside a Domain Wall? *Phys.Lett.*, B125:136–138, 1983.

[141] V.C. Rubin, N. Thonnard, and Jr. Ford, W.K. Rotational Properties of 21 SC Galaxies with a Large Range of Luminosities and Radii, from NGC 4605 /R = 4kpc/ to UGC 2885 /R = 122 kpc/. *Astrophys.J.*, 238:471, 1980.

[142] R. Ruffini and J.A. Wheeler. Introducing the Black Hole. *Physics Today*, 24:30, 1971.

[143] Eray Sabancilar. Cosmological Constraints on Strongly Coupled Moduli from Cosmic Strings. *Phys.Rev.*, D81:123502, 2010.

[144] Mairi Sakellariadou. A Note on the Evolution of Cosmic String/Superstring Networks. *JCAP*, 0504:003, 2005.

[145] Mairi Sakellariadou and Horace Stoica. Dynamics of F/D Networks: The Role of Bound States. *JCAP*, 0808:038, 2008.

[146] P. Salmi, A. Achucarro, E.J. Copeland, T.W.B. Kibble, R. de Putter, and D. Steer. Kinematic Constraints on Formation of Bound States of Cosmic Strings: Field Theoretical Approach. *Phys.Rev.*, D77:041701, 2008.

[147] M. Sazhin, Giuseppe Longo, J.M. Alcala', R. Silvotti, G. Covone, et al. CSL-1: A Chance Projection Effect or Serendipitous Discovery of a Gravitational Lens Induced by a Cosmic String? *Mon.Not.Roy.Astron.Soc.*, 343:353, 2003.

[148] M.V. Sazhin, M. Capaccioli, G. Longo, Maurizio Paolillo, and O.S. Khovanskaya. The True Nature of csl-1. 2006.

[149] Robert J. Scherrer, Jean M. Quashnock, David N. Spergel, and William H. Press. Properties of Realistic Cosmic String Loops. *Phys.Rev.*, D42:1908–1914, 1990.

[150] R.W. Schnee. Introduction to Dark Matter Experiments. 2011.

[151] John H. Schwarz. An SL(2,Z) Multiplet of Type IIB Superstrings. *Phys.Lett.*, B360:13–18, 1995.

[152] Karl Schwarzschild. On the Gravitational Field of a Mass Point According to Einstein's Theory. *Sitzungsber.Preuss.Akad.Wiss.Berlin (Math.Phys.)*, 1916:189–196, 1916.

[153] E.P.S. Shellard. Cosmic String Interactions. *Nucl.Phys.*, B283:624–656, 1987.

[154] Warren Siegel. Strings with Dimension-Dependent Intercept. *Nucl.Phys.*, B109:244, 1976.

[155] Xavier Siemens, Jolien Creighton, Irit Maor, Saikat Ray Majumder, Kipp Cannon, and Jocelyn Read. Gravitational Wave Bursts from Cosmic (Super)Strings: Quantitative Analysis and Constraints. *Phys.Rev.*, D73:105001, 2006.

[156] Vesto M. Slipher. Nebulae. *Proc.Am.Phil.Soc.*, 56:403–409, 1917.

[157] David Spergel and Ue-Li Pen. Cosmology in a String Dominated Universe. *Astrophys.J.*, 491:L67–L71, 1997.

[158] Daniele A. Steer and Tanmay Vachaspati. Light from Cosmic Strings. *Phys.Rev.*, D83:043528, 2011.

[159] Paul J. Steinhardt, Li-Min Wang, and Ivaylo Zlatev. Cosmological Tracking Solutions. *Phys.Rev.*, D59:123504, 1999.

[160] T.J. Sumner. Experimental Searches for Dark Matter. *Living Rev.Rel.*, 5:4, 2002.

[161] Hiroyuki Tashiro, Eray Sabancilar, and Tanmay Vachaspati. Constraints on superconducting cosmic strings from early reionization. *Phys. Rev. D*, 85:123535, Jun 2012.

[162] Arthur Christopher Thompson. Dynamics of Cosmic String. *Phys.Rev.*, D37:283–297, 1988.

[163] S.E. Thorsett and R.J. Dewey. Pulsar Timing Limits on Very Low Frequency Stochastic Gravitational Radiation. *Phys.Rev.*, D53:3468–3471, 1996.

[164] Neil Turok. Grand Unified Strings and Galaxy Formation. *Nucl.Phys.*, B242:520, 1984.

[165] S.-H. Henry Tye, Ira Wasserman, and Mark Wyman. Scaling of Multi-tension Cosmic Superstring Networks. *Phys.Rev.*, D71:103508, 2005.

[166] Luis Arturo Urena-Lopez and Andrew R. Liddle. Supermassive Black Holes in Scalar Field Galaxy Halos. *Phys.Rev.*, D66:083005, 2002.

[167] Jon Urrestilla and Alexander Vilenkin. Evolution of Cosmic Superstring Networks: A Numerical Simulation. *JHEP*, 0802:037, 2008.

[168] Tanmay Vachaspati and Alexander Vilenkin. Gravitational Radiation from Cosmic Strings. *Phys.Rev.*, D31:3052, 1985.

[169] A. Vilekin and E. P. S. Shellard. *Cosmic Strings and Other Topological Defects.* Cambridge University Press, 2000.

[170] A. Vilenkin. Cosmic Strings. *Phys.Rev.*, D24:2082–2089, 1981.

[171] A. Vilenkin. Cosmological Density Fluctuations Produced by Vacuum Strings. *Phys.Rev.Lett.*, 46:1169–1172, 1981.

[172] Alexander Vilenkin. Cosmic Strings as Gravitational Lenses. *Astrophys.J.*, 282:L51–L53, 1984.

[173] Graham Vincent, Nuno D. Antunes, and Mark Hindmarsh. Numerical Simulations of String Networks in the Abelian Higgs Model. *Phys.Rev.Lett.*, 80:2277–2280, 1998.

[174] Graham R. Vincent, Mark Hindmarsh, and Mairi Sakellariadou. Scaling and Small Scale Structure in Cosmic String Networks. *Phys.Rev.*, D56:637–646, 1997.

[175] U.F. Wichoski, Jane H. MacGibbon, and Robert H. Brandenberger. High-energy Neutrinos, Photons and Cosmic Ray Fluxes from VHS Cosmic Strings. *Phys.Rev.*, D65:063005, 2002.

[176] Edward Witten. Superconducting Strings. *Nucl.Phys.*, B249:557–592, 1985.

[177] Edward Witten. Bound States of Strings and p-Branes. *Nucl.Phys.*, B460:335–350, 1996.

[178] Mark Wyman, Levon Pogosian, and Ira Wasserman. Bounds on Cosmic strings from WMAP and SDSS. *Phys.Rev.*, D72:023513, 2005.

[179] Ya.B. Zeldovich. Cosmological Fluctuations Produced Near a Singularity. *Mon.Not.Roy.Astron.Soc.*, 192:663–667, 1980.

[180] Ya.B. Zeldovich and M. Yu. Khlopov. On the Concentration of Relic Magnetic Monopoles in the Universe. *Phys.Lett.*, B79:239–241, 1978.

[181] Ya.B. Zeldovich, I. Yu. Kobzarev, and L.B. Okun. Cosmological Consequences of the Spontaneous Breakdown of Discrete Symmetry. *Zh.Eksp.Teor.Fiz.*, 67:3–11, 1974.

[182] Ivaylo Zlatev, Li-Min Wang, and Paul J. Steinhardt. Quintessence, Cosmic Coincidence, and the Cosmological Constant. *Phys.Rev.Lett.*, 82:896–899, 1999.